NTNU – Trondheim
Norwegian University of
Science and Technology

Feasibility Study on Active Wave Compensation of ROV

Modelling, Analysis and Simulation

Hilde Christine Hagen

Marine Technology
Submission date: December 2014
Supervisor: Asgeir Johan Sørensen, IMT
Co-supervisor: Per Rundtop, Sintef Fiskeri og havbruk AS
Mauro Candeloro, IMT

Norwegian University of Science and Technology
Department of Marine Technology

NTNU
Norwegian University of
Science and Technology

Master Thesis

Feasibility Study on Active Wave Compensation of ROV

Hilde Christine Hagen

Department of Marine Technology
Marine Cybernetics
December 30, 2014

NTNU Trondheim
Norwegian University of Science and Technology
Department of Marine Technology

MASTER THESIS IN MARINE CYBERNETICS

FALL 2014

FOR

STUD. TECH. Hilde Christine Hagen

Feasibility Study on Active Wave Compensation for Remotely Operated Vehicles

Modelling, simulation and analysis

Work description

Today, most salmon farms are located in areas exposed to winds, currents and waves, as appose to farms at more sheltered locations. It is essential to find out what the limitations with regards to these forces are. How much exposure can the netpen, the bottom ring chain and operations and maintenance of the farm endure? In this thesis the topic of maintenance by ROV's will be the main focus. Operation of aquaculture sites demands that the net is surveyed on a regular basis. The nets will experience sea fouling, which needs to be cleaned to ensure a healthy environment for the fish. Fish escape due to net damage is also important to consider. These tasks are currently performed by Remotely Controlled Vehicles (ROVs) and divers. In these exposed areas there are many challenges related to time-consuming surveys of the net. As the surrounding environment changes, the ROV must adapt to the net, avoid damaging it and maintain good maneuvering.
This thesis will propose a design of a small size ROV for investigating net integrity. Metocean data will be used to simulate the ROV in the wave zone and to determine the wave loads. Control strategy for active wave compensation will be developed and tested through simulations.

Scope of work

1. Review relevant literature on ROV control systems and operations. In particular DP operations in the wave zone are of interest.

2. Propose a ROV design and develop hydrodynamic models including coefficients of the ROV for three sizes (600, 200 and 50 kg) using DNV GL's Sesam software package. Assess thrust capability and thrust loss in the wave zone, for the proposed ROV design.

3. Define relevant simulation cases and MetOcean data (sea state) for the simulation study. Include wind and waves.

4. Run frequency-domain simulations in Wadam and time-domain simulations in SIMO to analyse ROV motions subject to sea and wind loads operating the ROV at different depth in the wave-zone.

5. Propose and develop control strategies for wave compensation and wave filtering.

6. Run simulations in SIMO or NTNU ROV simulator to study the performance of the controllers for different tuning.

7. All results to be discussed and reported.

8. Develop state observer to estimate sea state and fluid velocity from on-board ROV sensors.

The report shall be written in English and edited as a research report including literature survey, description of mathematical models, description of control algorithms, simulation results, model test results, discussion and a conclusion including a proposal for further work. Source code should be provided on a CD with code listing enclosed in appendix. It is supposed that Department of Marine Technology, NTNU, can use the results freely in its research work, unless otherwise agreed upon, by referring to the student's work. The thesis should be submitted in three copies within December 22nd.

Advisers: PhD Candidate Mauro Candoloro and Per Rundtop, Sintef.

Professor Asgeir J. Sørensen
Supervisor

Preface

The work in this thesis is an extension of two papers written as a part of the specialization topics *Underwater robotics in safe and autonomous subsea operations* and *Advanced model-based design and testing of marine control systems* at the Department of Marine Technology during the fall of 2014.

The objective of this thesis has been to investigate active wave compensation for ROVs performing maintenance and diverse monitoring tasks in the wave zone for exposed aquacultural sites. Three ROVs of different sizes has been analysed and a controller has been tested on the models for various exposure degrees on the sea states and different depth of the models. The topic was presented to me by researcher Per Rundtop from SINTEF Fisheries and Aquaculture and I wish to thank him both for proposing it and for his guidance along the way.

This thesis presents the final work carried out in my Master's degree at Norwegian University of Science and Technology. The Department of Marine Technology has been a safe and exciting place to learn and to live these five years. I would like to thank my supervisor Asgeir Sørensen for his guidance and for encouraging me to specialize in marine cybernetics, which I am positive will be one of the most exciting and innovative areas to be a part of in the forthcoming years.

I am grateful to my advisor PhD candidate Mauro Candeloro, for all the times he has helped me with subject and project related topics. I would like to acknowledge the girls in office A2.011 for tremendous support through courses, projects and my Master thesis.

My family and friends are hereby greatly acknowledged for tremendous support every single day.

Hilde Christine Hagen
December 30, 2014, Trondheim.

Abstract

The aquaculture industry is using remotely operated vehicles (ROVs) for maintenance tasks on fish farms. These tasks include, among others, washing of the netpen and visual inspections. These are tedious tasks, and it would be an advantage if the ROVs were controlled automatically instead of manually. Such systems exist in the industry today, but the systems are often designed to operate in deep water.

In this thesis the focus lies with Salmon fish farms. These farms are today located at exposed areas to improve the growth environment for Salmon. Exposed locations require more robust maintenance systems as the locations itself are more prone to bad weather and large wave and current loads. When working in the wave zone, the large and highly varying first order wave loads are dominant. To be able to withstand these loads three small sized ROVs will be proposed and investigated. The ROVs are 600 kg, 200 kg and 50 kg.

The ROVs are analysed in Wadam to determine the kinetic properties of the designs. Dynamic positioning systems for the ROVs are suggested and time domain simulations are perfomed in SIMO. Weather data from Rataran fish farm is used to set up the simulation cases. Some alterations was necessary to use the results from Wadam in SIMO, as Wadam assumes surface vessels.

The results illustrate that an operational window for the three ROVs is set by a limiting significant wave height H_s of 2.0 m and a peak period T_p no less than 5 s should be operated in. However, H_s and T_p must be evaluated simultaneously. As some of the simulated cases illustrate, small significant wave heights or larger peak periods can also cause wave loads that are impossible to operate in.

Sammendrag

Oppdrettsnæringen bruker fjernstyrte undervannsfarkoster (ROVer) for å utføre vedlikehold på oppdrettsanlegg. Vedlikehold utført av ROVer inkluderer blant annet visuell inspeksjon av nøtene og vasking av dem. Dette er tidskrevende oppgaver, og det ville vært fordelaktig å kontrollere ROVene automatisk heller enn manuelt. Slike systemer finnes i dag, men systemene er ofte designet for å operere på dypt vann.

I denne oppgaven er fokuset lagt til lakseoppdrett. Disse oppdrettsanleggene er ofte lagt til områder som er eksponert for hardt vær. En eksponert lokasjon krever mer robuste vedlikeholdssystemer. De dominerende lastene som påvirker ROVene er første ordens bølgekrefter. Tre ROVer med størrelse 600 kg, 200 kg og 50 kg er blitt foreslått og undersøkt.

ROVene er analysert i Wadam for å finne de hydrodynamiske egenskapene. Dynamiske posisjoneringssystem har blitt foreslått for ROVene og tidssimuleringer blitt utført i SIMO. Værdata fra Rataren oppdrettsanlegg er brukt i simuleringene.

Resultatene illustrerer et operasjonsvindu for alle tre ROVer. H_s bør ikke overskrive 2.0 meter og topp perioden bør være større enn 5.0 sekunder. Det er viktig å evaluere disse parameterne sammen.

Nomenclature

AUV	Autonomous Underwater Vehicle
CB	Centre of buoyancy
CFD	Computational Fluid Dynamics
CG	Centre of gravity
CO	Centre of origin
DOF	Degrees of freedom
DP	Dynamic Positioning
DVL	Doppler Velocity Log
FEM	Finite Element Method
HF	High Frequency
HIL	Hardware-in-the-Loop
HiPAP	High precision acoustic positioning system
LF	Low Frequency
LP	Low Pass
NED	Reference frame referring to North, East and Down position on the surface of the Earth
PID	Proportional, integral and derivative
TF	Transfer Function
UTM	Universal transverse mercator
WF	Wave Filter

Contents

List of Figures

List of Tables

Chapter 1

Introduction

1.1 Background and Motivation

The workspace of Remotely operated vehicles (ROVs) normally lie below the wave zone and, they are designed for deep water operations. But - their functionality is applicable in the entire marine environment.

One industry interested in improving the ROV maneuverability is the aquaculture fish farming industry. This applies in particular for operations of exposed farming sites. On the occasion of bad weather, people are not permitted on the sites. Consequences can be immense if the bad weather continues, especially economically. The survival rate can be largely decreased if no automatic feeding system is in place or if the food is not delivered to the site. Also, the probability of adverse events increases. Standards (NS 9415, 2009) require frequent inspections - daily if possible and particularly inspections in the aftermath of a storm.

The inspections under water are usually executed by an ROV. The ROV is used as a platform for both visual inspections and maintenance like cleaning the net. These are tedious tasks, and it would be beneficial to control the ROV automatically. It is, however, unsure if it is possible for the thrusters of an ROV to counteract the wave loads, as they are large and highly varying wave loads, which are normally filtered out when performing stationkeeping of an ROV.

In this thesis a 600 kg, a 200 kg and a 50 kg ROV, thruster-design and controllers is evaluated for performance of these tasks. The work in this thesis is an extension of two papers written during the fall of 2014 (Hagen, 2014a,b).

The ROV will be modelled in the DNV GL Sesam package software *Wadam* which uses potential theory to solve the equations of motions established for harmonic motion of rigid body systems (DNV Software, 2014b). Some necessary alterations will be done to the results from Wadam. These alterations, the control system and the results from Wadam will be implemented to *SIMO*, also a part of the Sesam package, and time domain simulations will be performed.

1.1.1 The Beginning of ROVs

It is not certain exactly when the history of ROV's started. However, some claim that it started with Dimitri Rebikoff's POODLE (Christ and Wernli Sr., 2011; Michel et al., 1999b; ROV Committee of The Marine Technology Society, 2014). This was the first tethered unmanned vehicle, and it was built to aid in archaeological research in 1953. In the years to come it was not underwater archaeology that drove the development of ROVs forward. It was the US Navy - they needed to recover torpedoes that were lost at sea, in a safe and secure manner.

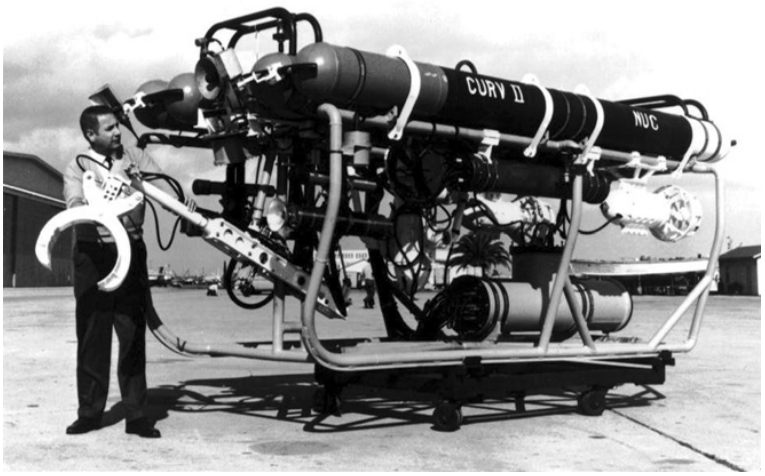

Figure 1.1: The Navy's second edition CURV vehicle (Christ and Wernli Sr., 2011)

Nine years later, the CURV was developed, a Cable-Controlled Underwater Research Vehicle and then came the PIV, a Pontoon Implacement Vehicle. Development was in other words, slow. Huge challenges had to be solved for the first time and the ROV's advantages over manned underwater vehicles and divers had not yet been recognized.

By 1974 only 20 vehicles existed, with 17 of them being governmentally funded. But now the ROV's became more advanced and more sensors was fitted on them. In addition the electrical industry helped with minimizing and improving reliability of the on board electrical systems.

In the following eight years the offshore industry in North America took on ROV designs and soon over 500 ROV's had been built. Due to the offshore oil industry growth in the North Sea the ROV development that had started in the US continued mostly in the UK. The demand for advanced vehicles to go to deep seas increased and using offshore divers became impossible with depths exceeding 3000 meters. Today, underwater vehicles have reached the bottom of the deepest trench in the sea. This point lies in the Challenger Deep in the Mariana trench at 10,911 meters depth (Kyo et al., 1995).

It is not easy to estimate how many ROVs exist at this moment in time, but it was estimated in the end of the 1990's by Michel et al. (1999a) that the number was at least 3000.

1.1.2 Inspection Tasks for the Aquaculture Industry

A marine fish farm's main components is the netpen to hold the fish, the floating collar to provide buoyancy and structural stiffness, the mooring system to keep the fish farm in the desired position and the raft. The raft is a floating work station with all technical equipment needed to execute tasks connected to fish farming - for example feeding, crewing, monitoring, storage and so on. Norwegian Standard for Marine fish farms - "Requirements for site survey, risk analysis, design, dimensioning, production, installation and operation" (NS 9415, 2009) explains the inspection tasks required, and the information in this section is collected from this standard.

Inspection of the marine fish farm after installation is the first inspection to be performed by for instance an ROV. The focus of this inspection is to check that the entire fish farm is installed as planned and that the main components have not been damaged during installation. The ROV will investigate the entire farm, from the attachment of the mooring all the way up along the netpen.

After installation, routine maintenance of a fish farm require special attention to tightening attachment points, surface treatment, lubrication, cleaning and removal of fouling and removal of destroyed equipment. An ROV would typically be used for visual inspection of the fish farms, looking for damages to the net or the mooring, and for cleaning and removing of fouling.

1.1.3 Exposed Salmon Farming

Normally marine fish farms are situated in areas sheltered from wind and the enormous forces of the ocean. This is crucial when dimensioning a fish farm. Today we are witnessing a change in location of these sites, especially with salmon farming. They are placed in more open water, where larger currents and waves occur. This area of aquaculture is referred to as *exposed farming*.

Exposed farming can be defined as "farming sites that are more vulnerable to waves, currents and / or wind than most sites today" (Sandberg et al., 2012). Another way of defining the degree of exposure is demonstrated in table 1.1 (NS 9415, 2009).

Wave Class	H_s [m]	T_p [s]	Designation
A	0.0-0.5	0-2.0	Little exposure
B	0.5-1.0	1-6-3.2	Moderate exposure
C	1.0-2.0	2.5-5.1	Substantial exposure
D	2.0-3.0	4.0-6.7	High exposure
E	>3.0	5.3-18.0	Extreme exposure

Table 1.1: Definition of locations and their exposure (NS 9415, 2009).

Although some operations and maintenance of the farming site can become more difficult and more prone to bad weather, higher currents and larger waves introduce multiple advantages for the fish. High exchange of water increases the quality of the water. It also leads to better reduced ecological effects on the sea floor through increased waste

dispersion and better growth conditions. This will - in theory - result in higher production rates (SINTEF Fisheries and Aquaculture, 2014).

1.2 Outline of Thesis

Chapter 1 is the introduction, where the background for writing this thesis is summarised. Relevant software to be used in the modelling, analysis and simulation will be presented. Some main aspects of the ROV history is outlined and a short introduction to the aquacultural industry and ROV maintenance tasks will be explained. The environment in which the simulations will be performed is finally presented.

Chapter 2 is devoted to the mathematical modelling of a small sized submerged vehicle. Some of the theory concerning wave loads and statistics in Chapter 2 has been inspired by a previously written project report in the subject TMR4160 Computer methods for marine applications performed in the fall of 2012. The models will be presented in both the time domain and the frequency domain.

Chapter 3 provides three proposed ROV designs, including the thrust configuration. The models will be implemented to GeniE, and this procedure will be explained here.

Chapter 4 explains the steps that are performed to analyse the models in the potential theory program Wadam. The results from these analysis will be assessed and presented here.

Chapter 5 shows the implementation and alterations of the Wadam results in to SIMO. A control system will be suggested and implemented. Results from the time domain will finally be provided.

Chapter 6 contains a discussion of the results from Wadam and the results from SIMO. In addition a discussion of the assumptions made and the proposed ROV designs will be presented.

An outline of the Appendix in found on page i, following the Bibliography.

1.3 Contributions

The contributions in this thesis include:

Chapter 1 : Relevant simulation cases are suggested to be able to determine a window of operation for the vehicles to be evaluated. The cases are inspired by wave data provided from an exposed salmon fish farm location.

Chapter 2 : The models from T. I. Fossen (2011) are presented in an applicable manner, that suits both the mathematical modelling theory in Wadam and SIMO.

Chapter 3 : Three ROV designs have been proposed in this chapter. The designs include dimensions, materials, thrust capacities and thrust configuration. The designs have been implemented to GeniE.

Chapter 4 : Different analysis approaches in Wadam have been suggested and evaluate to investigate the kinetics of the three ROV designs. The most important results include added mass, potential damping and transfer functions for first order wave loads and motions.

Chapter 5 : Simulation cases, Wadam results and condition sets have been set up in SIMO. This chapter also includes suggestions to alter and improve results from Wadam. A DP control system has been set up and tuned to avoid filtering first order wave induced motions. An evaluation of the results is presented.

Appendix A.1 Readings of significant wave height and peak periods from a buoy at Rataren fish farm has been presented to reveal the frequency distribution and the rate of occurrence for each sea state observed from May 1, to December 1, 2013.

1.4 Previous Work

1.4.1 ROV Minerva

ROV Minerva is a SUB-fighter 7500, designed and delivered by Sperre AS to NTNU in 2003 (Technical Specifications, 2014).The ROV was delivered with both auto depth and auto heading functions implemented in a low level controller. Minerva is frequently used by scientists for biological and archaeological research, testing equipment and software as well as being an important demonstration tool in many courses within the Department of Marine Technology. The ROV is assumed passively stable in pitch and roll, so it has 4 DOF's (surge, sway, heave and yaw). Minerva's dimensions will be further detailed in table 3.1.

Thrusters

Minerva is equipped with five thrusters. The thruster configuration can be seen in the following figures.

Table 1.2 describes the maximum thrust Minerva can produce as found in a bollard pull test performed in the main towing tank of MARINTEK (Ludvigsen and Ødegaard, 2004). Minerva has had many alterations since the test was performed in 2003 and 2004. She now carries more sensors, meaning more weight. Also this changes her geometry

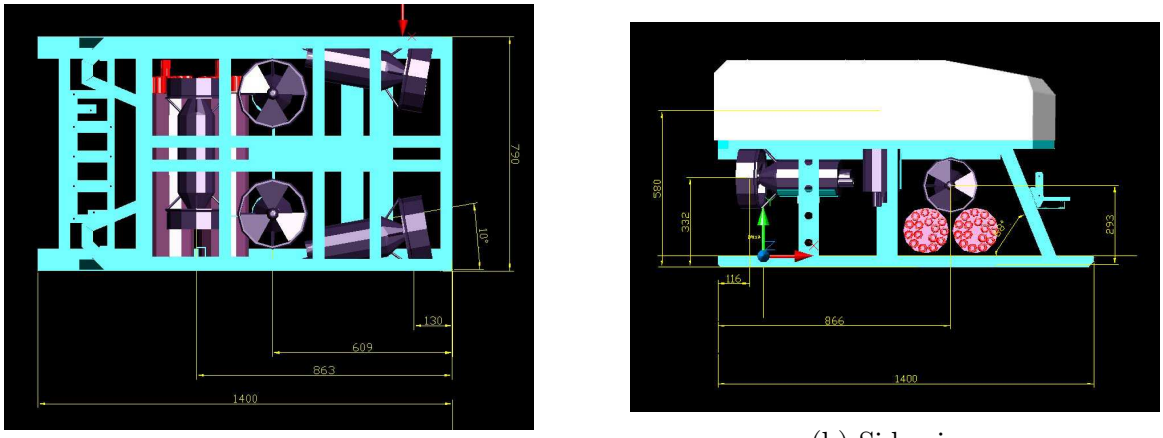

(a) Top view

(b) Side view

Figure 1.2: Thruster configuration ROV Minerva (Svendby, 2007)

which influences the thrusters' capabilities. Additional buoyancy elements have also been appended to give her positive buoyancy.

DOF	Thrust [N]
Surge	478
Sway	195
Heave	389

Table 1.2: Thrust capacity of Minerva

Control System

On and off, the control system has been developing since 2003. The control system utilized today is called Njord and was developed by Espen Tolpinrud based on the work of (among others) Marianne Kirkeby. He also developed a graphical user interface which was named Frigg (Kirkeby, 2010; Tolpinrud, 2012).

Both Frigg and Njord was originally developed for another ROV owned by NTNU, the ROV 30k, and then customized for Minerva. The DP-system consists of a signal processing block, an observer block, controller, a guidance system block and thrust allocation block.

The system has been implemented to LabView (Instruments, 2014) and is frequently HIL tested with a CompactRIO (cRIO). Hardware-in-the-loop (HIL) testing adds the complexity of the plant to be controlled to the test platform and makes it possible to see how the control plant behaves together with the hardware. It has altitude control and terrain following included in its DP system. The developments and results from simulation and sea trials demonstrating the performance is described in Dukan and Sørensen (2012) and Dukan and Sørensen (2013).

Sensors

Minerva is fitted with three CCD cameras and three regular ROV cameras. The ROV has two manipulators, a 5-function arm and a 1-function arm. It has scanning sonar that can be used to map the seabed. For positioning the ROV is fitted with an altimeter, which measures the altitude, a high precision acoustic positioning system (HiPAP) and a Doppler Velocity Log - DVL. The HiPAP consist of a transducer mounted on the deployment vessel of Minerva; R/V Gunnerus that measures the position relative to the vessel. It is integrated with the vessels GPS and MRU through navigation software to yield the UTM coordinates of the ROV. The DVL is a sensor that is used to measure the ROVs velocity either through water or over the sea floor, as well as the altitude. It applies acoustics to determine the vertical distance to the sea floor with four acoustic beams. The ROV communicates through an umbilical cable that is 600 meters long. Gunnerus has an auto function that lets the ship follow the ROV if it needs a larger work area.

1.5 Relevant Software

The software connected to the work that will be performed, is shortly presented here.

DNV GLs *Sesam* software is a product for complete strength assessment and operational management of ships, risers and offshore structures (DNV GL, 2014). Sesam is an abbreviation of Super Element Structural Analysis Modules and has been developed for aiding engineers. It consists of nine different modules, GeniE, GeniE Lite, HydroD, CAESES, DeepC, Marine, Pipeline, Wind and Probability, whereof three will be utilised in this thesis. The modules offer tools for analysing strength and fatigue of structures, stability, computing hydrodynamics, optimisation, risk assessment of operations and performing probabilistic analyses. First, GeniE will be used to build a finite element model (FEM) of the proposed ROV designs. Secondly, the FEM models will be analysed in Wadam, which is a part of HydroD. The hydrodynamical results will lastly be imported to SIMO, a part of the DeepC package.

Sesam GeniE

GeniE is, according to DNV Software (2014c) a tool for "Concept design and analysis of offshore structures". It uses beams and plates to build the structures. In this thesis a command JavaScript-file (file extensions .js) will be read in to GeniE. In this command file the dimensions of the ROV will be given. Then, analysis to create a mesh of the plates will be performed, resulting in a FEM file.

Sesam HydroD

As implicated by this modules name, the Sesam HydroD software compute hydrodynamic and hydrostatic analysis of vessels. It uses Wadam to calculate interaction between waves and fixed or floating structures, given by one or multiple FEM files. In Wadam, Airy wave theory and linear potential theory is applied, presenting results as complex transfer functions. Wasim is used for vessels with forward speed, and produce results in the time

domain that can be transformed by Fourier to the time domain. The HydroD software has two more modules, Waveship and Postresp. Further information can be found in DNV GL (2014).

Sesam Marine

Sesam Marine consists of modules Sima, Simo and Riflex. The objective of this package is to enable risk management of marine operations through visualization of operations, run "what-if" analyses, with dynamic positioning and reduce risk of marine operations. Sima, is the graphical interface, pre-processor and post-processor to SIMO and Riflex. These two programs can perform analysis and simulation for marine operations (SIMO), and for riser systems (Riflex). SIMO will be used in this work to model the environment given by sea state and to simulate the ROVs within this environment. A built in system for dynamic positioning (DP) will be applied to the system. The results are given in time domain, see section 5.6.

Additional Software

In addition to the software mentioned Microsoft Excel Starter (2010) will be used for simple non-matrix-computations. This includes calculations of optimal ROV dimensions and evaluation of environmental data from Rataren fish farm. For matrix calculations and producing representation of the results, MATLAB (R2013b) will be used. Microsoft Starter Word (2011), Paint and Notepad are also used for creating figures and small scripts.

1.6 Environment - Rataren Fish Farming Site

Rataren fish farm, in Frøya kommune in Sør-Trøndelag, Norway, is a great example of an exposed farming site, see fig. 1.3, as well as the picture on the cover. It is situated 300 meters off the coast and has been classified as a site of substantial/high exposure in a study performed for SINTEF Fisheries and Aquaculture Ltd. by Sandberg et al. (2012). Rataren is owned and operated by SalMar and used as a test location for AquaCulture Engineering (ACE). Recent MetOcean-data provided from this location by AquaCulture Engineering (2013) suggest that at times the exposure is as large as extreme with an average peak period T_p of 12 meters. The measured data is from May to December 2013 with the average significant wave height, H_s, at 0.6 meters. This data will be used to determine the depth of the ROVs and the sea states used in simulation.

The environmental conditions simulated are given in table 1.3. The most relevant cases to investigate are determined from using frequency- and probability distribution, see tables A.1 and A.2 in Appendix A.1. The entries in table A.1 contains the count of the occurrences of T_p and H_{m0} values ranging from the area given in the table. For instance it counts how many times a sea state with T_p between 13 and 14 seconds and H_{m0} between 1 and 1.5 meters has occurred (7 times). In table A.2 the same values are shown, but in percent, thus it says something about the probability of each sea state occurring. In other

Figure 1.3: Rataren fish farm in Frøya kommune. Rataren I to the left and Rataren II can be seen to the right (ACE Project, 2014).

words, the tables summarize the distribution of sea states from May 1, to December 1 in 2013 on Rataren fish farm.

1.6.1 Simulation Cases

The first case is given by the sea state with the largest occurrence (11.8 %), $T_p > 24$ s and $H_{m0} < 0.5$ m. Case 2 will be given by the sea state with the largest occurrence after Case 2, see Appendix A.1. The next five cases will consist of sea states that are more extreme, but still likely to happen. Case 8 is set to be calm sea. See table below.

Case	H_s class [m]	T_p class [s]	P [%]
1	0.0 - 0.5	24 - 25	11.82
2	0.0 - 0.5	9 - 10	9.67
3	0.5 - 1.0	10 - 11	3.44
4	0.5 - 1.0	3 - 4	0.96
5	1.0 - 1.5	12 - 13	1.79
6	1.5 - 2.0	17 - 18	0.06
7	2.0 - 2.5	7 - 8	0.39
8	Calm water		

Table 1.3: Simulation cases given by sea state.

The chosen envelope for this thesis includes the area of the net because this thesis' main focus lies on the day-to-day tedious maintenance tasks and the investigations related to storms and installation tasks where the area is the entire fish farm. The net at Rataren

goes down to about 27-28 meters (AquaCulture Engineering, 2013) and the deepest point in the area of the entire farm is about 45 meters below the surface. A bathymetric map has been provided by AquaCulture Engineering (2013) and illustrates the depth in the area of Rataren. See appendix A.2.

The ROV will thus be simulated at depths 10 and 20 meters.

Chapter 2

Modelling of Small Size ROV

In the following section a general model for small size ROVs will be presented. The model will be described in the vectorial notations of Fossen (2011) and SNAME (1950). Mainly, all equations and formulation have been taken from Fossen (2011). Exceptions are emphasised when other references are cited.

2.1 Kinematics

The ROV kinematics considers the geometry of the vessel motion. The vessel model will be developed for 6 DOF as described in table 2.1.

DOF	Name	Description	Position	Velocity	Force
1	Surge	Motion in direction of x-axis	x	u	X
2	Sway	Motion in direction of y-axis	y	v	Y
3	Heave	Motion in direction of z-axis	z	w	Z
4	Roll	Rotation about the x-axis	ϕ	p	K
5	Pitch	Rotation about the y-axis	θ	q	M
6	Yaw	Rotation about the z-axis	ψ	r	N

Table 2.1: Notation for motion of marine vessels as set by SNAME (1950)

.

2.1.1 Reference Frames

Three reference frames will be used to describe the motion of the vehicle:

- The NED-frame {n}, the North-East-Down frame. This is assumed to be an *inertial* frame, i.e. a frame where all physical laws take their simplest form. The NED frame has its origin at the surface of the earth with the x-axis pointing toward North, y-axis pointing towards east and the z-axis pointing downwards. The position of the ROV is given in the NED-frame as

$$\boldsymbol{\eta} = [\boldsymbol{p}^n_{b/n}, \boldsymbol{\Theta}_{nb}]^\top = [N, E, D, \phi, \theta, \psi]^\top \tag{2.1}$$

- The BODY frame {b}. It is fixed to the body with the x-axis pointing forwards, y-axis to the vehicles starboard side and the z-axis pointing downwards. The body-fixed velocity is given as:

$$\boldsymbol{\nu} = [\boldsymbol{v}^b_{b/n}, \boldsymbol{\omega}^b_{b/n}]^\top = [u, v, w, p, q, r]^\top \tag{2.2}$$

- The seakeeping frame {s}. This frame is also considered to be inertial, and is fixed to the vehicles equilibrium state. When the vehicle is affected by waves, the seakeeping frame will oscillate compared to the body as the body is disturbed from its equilibrium position. The seakeeping coordinates are described as perturbations, i.e. disturbances:

$$\delta\boldsymbol{\eta} = [\boldsymbol{r}^s_{b/s}, \boldsymbol{\Theta}_{sb}]^\top, \delta\boldsymbol{\nu} = [\boldsymbol{v}^b_{b/s}, \boldsymbol{\omega}^b_{b/s}]^\top \tag{2.3}$$

  The perturbation and velocity in the seakeeping frame is commonly expressed:

$$\boldsymbol{\xi} = \delta\boldsymbol{\eta}, \qquad \dot{\boldsymbol{\xi}} = \delta\boldsymbol{\nu} \tag{2.4}$$

  Moreover, the position in the seakeeping frame is denoted $\boldsymbol{\xi} = [\xi_1, \xi_2, \xi_3, \xi_4, \xi_5, \xi_6]^\top$.

2.1.2 Transformation Between Frames

Using Euler angle transformation, the relationship between the velocity, $\dot{\boldsymbol{\eta}} \in \mathbb{R}^3 \times \mathcal{S}^3$, of the ROV in {n} and velocity, $\boldsymbol{\nu} \in \mathbb{R}^6$, given in {b} is found by using rotation matrices:

$$\dot{\boldsymbol{\eta}} = \begin{bmatrix} \boldsymbol{R}^n_b(\boldsymbol{\Theta}_{nb}) & \boldsymbol{0}_{3\times3} \\ \boldsymbol{0}_{3\times3} & \boldsymbol{T}_\Theta(\boldsymbol{\Theta}_{nb}) \end{bmatrix} \boldsymbol{\nu} = \boldsymbol{J}_\Theta(\boldsymbol{\Theta})\boldsymbol{\nu} \tag{2.5}$$

where $\boldsymbol{R}^n_b \in SO(3)$ in the transformation matrix $\boldsymbol{J}_\Theta \in \mathbb{R}^{6\times6}$ is given as:

$$\boldsymbol{R}^n_b(\boldsymbol{\Theta}_{nb}) = \begin{bmatrix} c\phi c\theta & -s\psi c\theta + c\psi s\theta s\phi & s\psi s\phi + c\psi c\phi s\theta \\ s\psi c\theta & s\psi c\phi + c\phi s\theta s\psi & -c\psi s\phi + s\theta s\psi c\phi \\ -s\theta & c\theta s\phi & c\theta c\phi \end{bmatrix} \tag{2.6}$$

where $c(\cdot)$, $s(\cdot)$ and $t(\cdot)$ are the trigonometrical functions $\cos(\cdot)$, $\sin(\cdot)$ and $\tan(\cdot)$. $\boldsymbol{T}_\Theta \in \mathbb{R}^{3\times3}$ is defined as:

$$\boldsymbol{T}_{\boldsymbol{\Theta}}(\boldsymbol{\Theta}_{nb}) = \begin{bmatrix} 1 & s\phi t\theta & c\phi t\theta \\ 0 & c\phi & -s\phi \\ 0 & s\phi/c\theta & c\phi/c\theta \end{bmatrix}, c\theta \neq 0 \tag{2.7}$$

$\boldsymbol{T}_{\boldsymbol{\Theta}}$ has a singularity at $\cos\theta \neq 0$. However, we are assuming that the ROV is stable in pitch (and roll), thus the ROV wil never experience pitch angles of $\pm$ 90 °.

The same concept applies to transformation between {b} and {s} and the relationship is written accordingly:

$$\delta\dot{\boldsymbol{\eta}} = \begin{bmatrix} \boldsymbol{R}^s_b(\boldsymbol{\Theta}_{sb}) & \boldsymbol{0}_{3\times3} \\ \boldsymbol{0}_{3\times3} & \boldsymbol{T}_\Theta(\boldsymbol{\Theta}_{sb}) \end{bmatrix} \delta\boldsymbol{\nu} = \boldsymbol{J}_\Theta(\delta\boldsymbol{\eta})\delta\boldsymbol{\nu} \tag{2.8}$$

2.2 Kinetics

The ROV kinetics deal with the relationship between the motions (the kinematics) and the forces and moments causing the motions.

2.2.1 Rigid Body Forces and Moments

Newtonian mechanics is used to determine the kinetics. This is referred to as *Rigid-Body* kinetics and describes the motion related to the forces and torques acting on the body:

$$\boldsymbol{\tau} = [\boldsymbol{f}, \boldsymbol{m}]^\top = [X, Y, Z, K, M, N]^\top \tag{2.9}$$

The motion of rigid bodies together with the hydrostatics (hs) and hydrodynamics (hyd) of a marine craft constitute the equations of motions. The rigid body forces are generalized in the vector $\boldsymbol{\tau}_{RB} \in \mathbb{R}^6$ and can be expressed as follows (Fossen, 1991):

$$\boldsymbol{M}_{RB}\dot{\boldsymbol{\nu}} + \boldsymbol{C}_{RB}(\boldsymbol{\nu})\boldsymbol{\nu} = \boldsymbol{\tau}_{RB} \tag{2.10}$$

$$\boldsymbol{\tau}_{RB} = \boldsymbol{\tau}_{hyd} + \boldsymbol{\tau}_{hs} + \boldsymbol{\tau}_{wind} + \boldsymbol{\tau}_{wave} + \boldsymbol{\tau}_{control} \tag{2.11}$$

relating the forces with the vessels rigid body mass and inertia, $\boldsymbol{M}_{RB}$, as well as the Coriolis and centripetal forces, $\boldsymbol{C}_{RB}$, caused by the body frames rotation about {n}. The rigid body motions in {s} are accordingly:

$$\boldsymbol{M}_{RB}\ddot{\boldsymbol{\xi}} + \boldsymbol{C}_{RB}(\dot{\boldsymbol{\xi}})\delta\dot{\boldsymbol{\eta}} = \delta\boldsymbol{\tau}_{RB} \tag{2.12}$$

$$\delta\boldsymbol{\tau}_{RB} = \boldsymbol{\tau}_{hyd} + \boldsymbol{\tau}_{hs} + \boldsymbol{\tau}_{ext} \tag{2.13}$$

where $\boldsymbol{\tau}_{ext}$ is the external force vector. The rigid body Coriolis and centripetal forces is caused by the rotation of {b} about {n} in equation (2.10) and about {s} in equation (2.12). The rigid body mass and Coriolis matrices can in general be expressed as:

$$\boldsymbol{M}_{RB} = \begin{bmatrix} m\boldsymbol{I}_{3\times3} & -m\boldsymbol{S}(\boldsymbol{r}_g^b) \\ m\boldsymbol{S}(\boldsymbol{r}_g^b) & \boldsymbol{I}_b \end{bmatrix} \in \mathbb{R}^{6\times6} \tag{2.14}$$

$$\boldsymbol{C}_{RB} = \begin{bmatrix} m\boldsymbol{S}(\boldsymbol{\omega}) & -m\boldsymbol{S}(\boldsymbol{\omega})\boldsymbol{S}(\boldsymbol{r}_g^b) \\ m\boldsymbol{S}(\boldsymbol{\omega})\boldsymbol{S}(\boldsymbol{r}_g^b) & -\boldsymbol{S}(\boldsymbol{I}_b\boldsymbol{\omega}) \end{bmatrix} \in \mathbb{R}^{6\times6} \tag{2.15}$$

Here $\boldsymbol{I}$ is the identity matrix, m is the vessels mass (in air), $\boldsymbol{r}_g^b$ is the vector from the centre of origin (CO) and the centre of gravity (CG), $\boldsymbol{I}_b$ is the inertia matrix and $\boldsymbol{S}(\boldsymbol{\cdot}) \in \mathbb{R}^{3\times3}$ is a skew-symmetric matrix representing the cross-product:

$$\boldsymbol{S}([\boldsymbol{x}, \boldsymbol{y}, \boldsymbol{z}]^\top) = \begin{bmatrix} 0 & -z & y \\ z & 0 & -x \\ -y & x & 0 \end{bmatrix} \tag{2.16}$$

If the mass matrix is defined as:

$$\boldsymbol{M}_{RB} = \begin{bmatrix} \boldsymbol{M}_{11} & \boldsymbol{M}_{12} \\ \boldsymbol{M}_{21} & \boldsymbol{M}_{22} \end{bmatrix} \tag{2.17}$$

Then, the Coriolis matrix can be determined from the rigid body mass matrix as:

$$\boldsymbol{C}_{RB} = \begin{bmatrix} \boldsymbol{0}_{3\times3} & -\boldsymbol{S}(\boldsymbol{M}_{11}\boldsymbol{\nu}_1 + \boldsymbol{M}_{12}\boldsymbol{\nu}_2) \\ -\boldsymbol{S}(\boldsymbol{M}_{11}\boldsymbol{\nu}_1 + \boldsymbol{M}_{12}\boldsymbol{\nu}_2) & -\boldsymbol{S}(\boldsymbol{M}_{21}\boldsymbol{\nu}_1 + \boldsymbol{M}_{22}\boldsymbol{\nu}_2) \end{bmatrix} \tag{2.18}$$

2.2.2 Hydrodynamic Forces and Moments

Hydrodynamical forces and moments are caused by the fluids motions surrounding a vessel. The forces will be explained in the sections to come and they will be represented both in the time- and the frequency domain. In time domain, with regards to {n}-frame they are:

$$\boldsymbol{\tau}_{hyd} = -\boldsymbol{M}_A\dot{\boldsymbol{\nu}} - \boldsymbol{C}_A(\boldsymbol{\nu})\boldsymbol{\nu} - \boldsymbol{D}(\boldsymbol{\nu})\boldsymbol{\nu} + \boldsymbol{\mu} \tag{2.19}$$

Hydrodynamic Added Mass

Added mass is a force that must be taken into account when an object is moving in higher-density-fluids, i.e. it is usually omitted when operating in air. In water this is a large contribution to the equations of motions as added mass represents the added forces necessary to move the fluid surrounding the vehicle. Furthermore it comes into the equations of motions s because the fluid and the vehicle cannot occupy the same space at the same time. In matrix form in {b} it is expressed as $\boldsymbol{M}_A \in \mathbb{R}^{6\times 6}$:

$$\boldsymbol{M}_A = \begin{bmatrix} \boldsymbol{A}_{11} & \boldsymbol{A}_{12} \\ \boldsymbol{A}_{21} & \boldsymbol{A}_{22} \end{bmatrix} \tag{2.20}$$

Hydrodynamic Damping

Damping forces on a vehicle can be of both linear and non-linear terms. It is expressed as (Fossen, 2011):

$$\boldsymbol{D}(\boldsymbol{\nu}_r) = \boldsymbol{D}_L + \boldsymbol{D}_{NL}(\boldsymbol{\nu}_r) \tag{2.21}$$

Damping is caused by: *skin friction*, *wave drift damping*, *potential damping* and *damping due to vortex shedding*.

Added Coriolis and Centripetal Forces

The hydrodynamical Coriols and centripetal matrix is $\boldsymbol{C}_A = -\boldsymbol{C}_A \in \mathbb{R}^{6\times 6}$ is determined as in (2.18) :

$$\boldsymbol{C}_A = \begin{bmatrix} \boldsymbol{0}_{3\times 3} & -\boldsymbol{S}(\boldsymbol{A}_{11}\boldsymbol{\nu}_1 + \boldsymbol{A}_{12}\boldsymbol{\nu}_2) \\ -\boldsymbol{S}(\boldsymbol{A}_{11}\boldsymbol{\nu}_1 + \boldsymbol{A}_{12}\boldsymbol{\nu}_2) & -\boldsymbol{S}(\boldsymbol{A}_{21}\boldsymbol{\nu}_1 + \boldsymbol{A}_{22}\boldsymbol{\nu}_2) \end{bmatrix} \tag{2.22}$$

Frequency Domain Representation of Hydrodynamical Forces

In frequency domain added mass and damping coefficients are expressed as $\boldsymbol{A}(\omega)$ and $\boldsymbol{B}(\omega)$. They are usually computed from hydrodynamic potential theory programs that integrate the pressure of the fluid over the wetted surface of the vehicle. It is beneficial to determine the zero frequency and infinite frequency added mass and potential damping matrices, as they can simplify the equations of motions in both the time and the frequency domain with the help of the retardation functions. This is presented in section 2.4.2.

Fluid Memory Effects

The fluid memory effects are functions that correspond to the waves caused by the vehicle continuing "at all subsequent times". The effects can be found from *Cummins's equation*, see Cummins (1962). The equation relates the radiation induced hydrodynamic forces to the frequency depended added mass and potential damping and results from Ogilvie (1964) yields the hydrodynamic forces in the time domain with regards to the {s}-frame:

$$\boldsymbol{\tau}_{hyd} = -\bar{\boldsymbol{A}}\ddot{\boldsymbol{\xi}} - \int_0^t \bar{\boldsymbol{K}}(t-\tau)\dot{\boldsymbol{\xi}}(\tau)d\tau \tag{2.23}$$

where $\bar{\boldsymbol{A}} = \boldsymbol{A}(\infty)$ is the potential added mass and the potential damping, $\boldsymbol{B}_{total}(\omega)$, is included in the *retardation functions* are defined as:

$$\bar{\boldsymbol{K}}(t) = \frac{2}{\pi}\int_0^\infty \boldsymbol{B}_{total}(\omega)\cos(\omega t)d\omega \tag{2.24}$$

2.2.3 Hydrostatic Forces and Moments

The hydrostatic forces can be expressed in the time domain in terms of the {n}-frame as:

$$\boldsymbol{\tau}_{hs} = -\boldsymbol{g}(\boldsymbol{\eta}) \tag{2.25}$$

The hydrostatic forces consists of gravitational force $\boldsymbol{f}_g^n$ and buoyancy forces $\boldsymbol{f}_b^n$, as stated by Archimedes (287-212 BC). They act in the vertical plane of {n}, through the CG and centre of buoyancy, CB. The vectors from the CO to CG and CB are denoted $\boldsymbol{r}_g^b$ and $\boldsymbol{r}_b^b$, respectively. The hydrostatic forces given in {b} will be:

$$\boldsymbol{f}_g^b = \boldsymbol{R}_b^n(\boldsymbol{\Theta})^{-1}\boldsymbol{f}_g^n \tag{2.26}$$
$$\boldsymbol{f}_b^b = \boldsymbol{R}_b^n(\boldsymbol{\Theta})^{-1}\boldsymbol{f}_b^n \tag{2.27}$$

where $\boldsymbol{R}_b^n(\boldsymbol{\Theta})$ is the rotation matrix, in eq.(2.6).

The hydrostatic forces and moments in the body frame are commonly called the *restoring forces and moments* and are expressed in the restoring vector $\boldsymbol{g}$. The 6 DOF restoring forces for a submerged vessel are:

$$\boldsymbol{g}(\boldsymbol{\eta}) = -\begin{bmatrix} \boldsymbol{R}_b^n(\boldsymbol{\Theta})^{-1}(\boldsymbol{f}_g^n + \boldsymbol{f}_b^n) \\ \boldsymbol{r}_g^b \times \boldsymbol{R}_b^n(\boldsymbol{\Theta})^{-1}\boldsymbol{f}_g^n + \boldsymbol{r}_b^b \times \boldsymbol{R}_b^n(\boldsymbol{\Theta})^{-1}\boldsymbol{f}_b^n \end{bmatrix} \tag{2.28}$$

To establish the hydrostatic forces we must know about the vessels- and the fluids properties. m is the mass of the vessel in air, g is the gravitational constant, ρ is the density of sea water for a vessel operating at sea and ∇ is the volume displacement of the vessel, i.e. its total submerged volume. For an ROV operating below the surface, totally submerged, the volume displacement will equal its entire volume. Thus, the gravitational force in the

NED frame is equal to the vessels weight $W = mg$, and the buoyancy force is $B = \rho g \nabla$. And so, the restoring forces are written:

$$\boldsymbol{g}(\boldsymbol{\eta}) = \begin{bmatrix} (W-B)s\theta \\ -(W-B)c\theta s\phi \\ -(W-B)c\theta c\phi \\ -(y_g W - y_b B)c\theta c\phi + (z_g W - z_b B)c\theta s\phi \\ (z_g W - z_b B)s\theta + (x_g W - x_b B)c\theta cc\phi \\ -(x_g W - x_b B)c\theta s\phi - (y_g W - y_b B)s\theta \end{bmatrix} \tag{2.29}$$

Vessels in the Surface

The restoring forces of a vehicle in the surface is linearly dependent on its displacement, so it is easily described with respect to {s} as:

$$\boldsymbol{\tau}_{hs} = -\bar{\boldsymbol{C}}\boldsymbol{\xi} \tag{2.30}$$

Where $\bar{\boldsymbol{C}} = \boldsymbol{C}(\boldsymbol{\infty}) = \boldsymbol{C}$ can be found through potential theory, and is constant in the frequency domain. In the {n} frame it is commonly expressed as:

$$\boldsymbol{\tau}_{hs} = -\boldsymbol{G}\boldsymbol{\eta} \tag{2.31}$$

For a surface vessel $\boldsymbol{G}$ and $\boldsymbol{C}$ are:

$$\boldsymbol{C} = \boldsymbol{G} = \begin{bmatrix} 0 & 0 & 0 & 0 & 0 & 0 \\ 0 & 0 & 0 & 0 & 0 & 0 \\ 0 & 0 & \rho g A_{wp}(0) & 0 & 0 & 0 \\ 0 & 0 & 0 & z_g W - z_b B & 0 & 0 \\ 0 & 0 & 0 & 0 & z_g W - z_b B & 0 \\ 0 & 0 & 0 & 0 & 0 & 0 \end{bmatrix} \tag{2.32}$$

Where A_{wp} is the water plane area of the vessel.

2.3 External Forces

2.3.1 Environmental Forces and Moments

First Order Wave Loads

In the wave zone wave loads caused by swell sea and wind generated sea are dominant and are calculated individually and added together, by assuming the principle of superposition is valid. The loads are collected in the generalized vector:

$$\boldsymbol{w} := \boldsymbol{\tau}_{wind} + \boldsymbol{\tau}_{swell} \in \mathbb{R}^6 \tag{2.33}$$

To decrease computational time current is not taken in to account. For this feasibility study current forces will be small compared to the first order loads, and also, they are slowly varying. The performance of the ROV in current can be compared to its performance in long waves, as described in for instance in Case 1 (24-25 s) and 5 (17-18 s).

The Wave Spectra

The wave spectra is determined from energy relations. The energy in a linear wave (per wave front area) is:

$$E_n = \frac{1}{2}\rho g \zeta_{An}^2 \tag{2.34}$$

So, for an irregular sea state, the total energy is expressed as the sum of the energy of all the regular waves that build up the irregular sea state. The relationship between the spectra energy and the wave energy is:

$$\frac{1}{2}\zeta_{An}^2 = S(\omega_n)\Delta\omega \tag{2.35}$$

When the direction of the waves is also considered, the new wave spectrum is expressed:

$$S(\omega, \phi) = S(\omega)D(\phi, \omega) \tag{2.36}$$

The total energy in the wave spectrum can be found by taking the integral over all frequencies and directions in the sea state:

$$\frac{E_{tot}}{\rho g} = \int_0^\infty \int_0^{2\pi} S(\omega, \phi) d\phi d\omega \tag{2.37}$$

Where the peak period T_p is:

$$T_p = \frac{2\pi}{\omega_p} \tag{2.38}$$

And significant wave height H_s is

$$H_s = H_{m0} = 4\sqrt{m_0} \tag{2.39}$$

The ROVs will operate in the North Sea. Standard wave spectra, like the JONSWAP (Joint North Sea Wave Project) as described by Myrhaug (2007) will be used. This is based on observations from the North Sea which is relatively shallow and close to shore. The sea state is said to be not fully developed sea states and is a good estimate for wind generated sea within a certain area given by the significant wave height and peak period. Equations and theory about the JONSWAP spectra, as well as statistics are retrieved from the same book (Myrhaug, 2007).

The JONSWAP wave spectra can be expressed as:

$$S(\omega) = \frac{5}{32\pi} H_s^2 T_p (\frac{\omega_p}{\omega})^5 e^{\frac{-5}{4}(\frac{\omega_p}{\omega})^4} (1 - 0.287 ln\gamma) \gamma^{e^{(-\frac{(\frac{\omega}{\omega_p}-1)^2}{2\sigma^2})}} \tag{2.40}$$

where $\sigma = 0.7, \omega \leq \omega_p$ and $\sigma = 0.9, \omega > \omega_p$, and the spectra moments are:

$$m_n = \int_0^\infty \omega^n S(\omega) d\omega, n = 0, 1, 2... \tag{2.41}$$

γ is the peakedness parameter which can be determined from H_s and T_p:

$$T_p \geq 5\sqrt{H_s} \rightarrow \gamma = 1.0 \tag{2.42}$$

$$T_p \leq 3.6\sqrt{H_s} \rightarrow \gamma = 5.0 \tag{2.43}$$

For values in between these areas, γ is given by figure 2.10 in Myrhaug (2007).

Wave Motion

Superposition The principle of superposition will be used to build up an irregular sea state. The superposition principle for a linear system claims that a problem can be divided into different sub problems, which each has their own solution. The solution of the whole problem is then taken as the sum of the solutions of the sub problems. So, if multiple wave components with wave amplitude ζ_{ai} and frequency ω_i are super posed on each other, the result will be an irregular wave.

From hydrodynamics (Pettersen, 2007; Faltinsen, 1993) we know that the total motion of a wave consisting of n wave components can be described from the following velocity potential:

$$\Phi(x,y,z,t) = \sum_{i=1}^{n} \frac{\zeta_{ai} g e^{k_i z}}{w_i} \frac{\cosh k(z+h)}{\cosh kh} \cos(\omega_i t - k_i x - k_i y + \epsilon_i) \tag{2.44}$$

Where h is the water depth, ϵ is the phase angle of the wave, ζ_{ai} is the wave amplitude and ω_i is the wave frequency.
The waves amplitude can be derived from the wave spectra:

$$\zeta_{ai} = \sqrt{2S(\omega_i)d\omega} \tag{2.45}$$

$$\vec{U}(x,z,t) = \frac{\partial \phi}{\partial x}\vec{i} + \frac{\partial \phi}{\partial y}\vec{j} + \frac{\partial \phi}{\partial z}\vec{k} \tag{2.46}$$

To compute the wave motion, the kinematic boundary condition is used:

$$\zeta g + \frac{\partial \Phi}{\partial t}|_{z=0} = 0 \tag{2.47}$$

Which yields:

$$\zeta(x,t) = \sum_{i=1}^{n} -\zeta_{ai} cos(\omega_i t - k_i x + \epsilon_i) \tag{2.48}$$

The First-Order Wave Excitation Force

The wave force is calculated in the time domain as:

$$\boldsymbol{\tau}_{exc} = \frac{1}{4\pi^2} \int_{-\infty}^{\infty} \int_{-\infty}^{\infty} \boldsymbol{H}(\omega) e^{-i\omega\tau} d\omega \zeta(t-\tau) d\tau \tag{2.49}$$

where $\boldsymbol{H}(\omega)$ is the first order transfer function between the excitation force and wave elevation.

Power Density of a Regular Wave at Deep Sea

Equation (2.34) is an expression for the mean wave energy per area, i.e. the energy density of a wave. It is possible to find the power of a wave if considering the velocity of the wave, which is called the group velocity. Deep water is assumed for simplicity:

$$c_g = \frac{g}{2\omega} \tag{2.50}$$

The power thus becomes:

$$P_w = \frac{1}{2}\rho g \zeta_{An}^2 \frac{g}{2\omega} = \frac{\rho g \zeta_{An}^2 g^2}{4\omega} = \frac{\rho g \zeta_{An}^2 g^2 T}{8\pi} \tag{2.51}$$

Equation (2.51) is an expression that relates energy to both the wave height and the wave frequency/period of the wave.

2.3.2 Actuator Forces and Moments

The configuration of thrusters for an ROV with the size of MaxiROV is usually 4 vectored/horizontal thrusters and 1 or 2 vertical thrusters. Sub-Atlantic produces hydraulic propulsors for ROVs, and thruster dynamics and characteristics is available online (Sub-Atlantic, 2014).

Thruster Characteristics

The characteristics of a propulsor are usually described with these equations (Sørensen, 2013):

$$T_a = \text{sign}(n) K_T \rho D^4 n^2 \tag{2.52}$$

$$Q_a = \text{sign}(n) K_Q \rho D^5 n^2 \tag{2.53}$$

where n is the shaft speed velocity, K_T and K_Q is the thrust and torque-coefficients, usually found from tests and D is the diameter of the thruster.

Thrust Capability

The resulting thrust for the ROV can be expressed as:

$$\boldsymbol{\tau} = \boldsymbol{T}_{conf} \boldsymbol{\eta}_{thrust} \boldsymbol{K} \boldsymbol{u} \tag{2.54}$$

where $\boldsymbol{T}_{conf}(\boldsymbol{\alpha}, \boldsymbol{a}) \in \mathbb{R}^{6\times n}$ is the thrust allocation matrix and n is the number of thrusters. $\boldsymbol{T}_{conf}$ represents the relationship between the forces in the 6 DOF and the individual thrust produced in the reference frame of the individual thrusters. $\boldsymbol{T}_{conf}$ can be calculated from the thruster configuration expressed by the thrusters angular displacement $\boldsymbol{\alpha} \in \mathbb{R}^n$ and the thrusters positions $\boldsymbol{a}$.

$\boldsymbol{\eta}_{thrust} \in \mathbb{R}^{n\times n}$ represents the thrust loss. It is a diagonal matrix, where the trust loss of each thruster is accounted for. The desired force and moments in each DOF is the vector $\boldsymbol{\tau} = [\tau_{\text{surge}}, \tau_{\text{sway}}, \tau_{\text{heave}}, \tau_{\text{roll}}, \tau_{\text{pitch}}, \tau_{\text{yaw}}]^\top \in \mathbb{R}^6$. The thruster characteristics in (2.52) are represented by $\boldsymbol{K}\boldsymbol{u}$, where $\boldsymbol{u} = \text{sign}(n)n^2$ and the thrust produced by each thruster is $\boldsymbol{T}_D = \boldsymbol{\eta}_{thrust}\boldsymbol{K}\boldsymbol{u}$.

2.3.3 The Umbilical

The umbilical provides the communication and power between the mother vessel and the ROV. In other words, it connects the ROV to the mother vessel. Loads caused by the

umbilical are hence dependent on the position of the mother vessel and the position of the ROV. Umbilicals will commonly be designed to have neutral buoyancy to reduce any impacts it may have on the ROV. Still, in deep water operations the drag forces on the umbilical will affect the ROV. These loads will be dependent on the path the ROV has taken down to the operation site. However, in the wave zone, at depths of maximum 30 meters, the loads are negligible and are accordingly not included in this analysis.

2.4 Resulting Models

The mathematical modelling of a small size ROV has been described both in the frequency domain and in the time domain. Moreover, the time domain has been discussed in both the seakeeping frame and the NED. Hence, *three* resulting models will be acknowledged in this section:

2.4.1 Frequency Domain Model

Adding all the kinetics and kinematics described so far, the resulting frequency domain model becomes:

$$[-\omega^2(\boldsymbol{M}_{RB} + \boldsymbol{A}(\omega)) + i\omega\boldsymbol{B}(\omega) + \boldsymbol{C}]\boldsymbol{\xi}(i\omega) = \boldsymbol{\tau}_{exc}(i\omega) \tag{2.55}$$

where $\boldsymbol{\xi}(i\omega)$ is the complex response variable and $\boldsymbol{\tau}_{exc}(i\omega)$ is the complex excitation variable. Only the potential damping is taken into account and the rigid body Coriolis matrix is omitted due to the assumption of linear theory. If viscous damping is included, the damping term is referred to as $\boldsymbol{B}_{total}(\omega) = \boldsymbol{B}(\omega) + \boldsymbol{B}_v(\omega)$.

2.4.2 Time Domain Models

The resulting time domain model in {s} frame is given by:

$$\dot{\boldsymbol{\xi}} = \boldsymbol{J}_\Theta(\delta\boldsymbol{\eta})\dot{\boldsymbol{\xi}} \tag{2.56}$$

$$(\boldsymbol{M}_{RB} + \boldsymbol{A}(\infty))\ddot{\boldsymbol{\xi}} + \boldsymbol{B}_{total}(\infty)\dot{\boldsymbol{\xi}} + \boldsymbol{\mu} + \boldsymbol{C}\boldsymbol{\xi} = \boldsymbol{\tau}_{wave} + \delta\boldsymbol{\tau} \tag{2.57}$$

where the fluid memory effects $\boldsymbol{\mu}$ is given by:

$$\boldsymbol{\mu} = \int_0^t \boldsymbol{K}(t-\tau)\dot{\boldsymbol{\xi}}(\tau)d\tau \tag{2.58}$$

$$\boldsymbol{K}(t) = \frac{2}{\pi}\int_0^\infty [\boldsymbol{B}_{total}(\omega) - \boldsymbol{B}_{total}(\infty)]\cos(\omega t)d\omega \tag{2.59}$$

where the retardation functions, $\boldsymbol{K}(t)$, is represented. Adding all the known contributions from the time domain with all the kinetics and kinematics described so far, the resulting time domain model with respect to the {n} frame is:

$$\dot{\boldsymbol{\eta}} = \boldsymbol{J}_{\Theta}(\boldsymbol{\Theta})\boldsymbol{\nu} \tag{2.60}$$

$$\boldsymbol{M}\dot{\boldsymbol{\nu}} + \boldsymbol{C}(\boldsymbol{\nu})\boldsymbol{\nu} + \boldsymbol{D}(\boldsymbol{\nu})\boldsymbol{\nu} + \boldsymbol{\mu} + \boldsymbol{g}(\boldsymbol{\eta}) = \boldsymbol{\tau}_{wave} + \boldsymbol{\tau} \tag{2.61}$$

where $\boldsymbol{M} = \boldsymbol{M}_{RB} + \boldsymbol{M}_A$, $\boldsymbol{C}(\boldsymbol{\nu}) = \boldsymbol{C}_{RB}(\boldsymbol{\nu}) + \boldsymbol{C}_A(\boldsymbol{\nu})$ and $\boldsymbol{D}(\boldsymbol{\nu}) = \boldsymbol{D}_L + \boldsymbol{D}_{NL}(\boldsymbol{\nu})$ and where $\boldsymbol{\mu}$ is:

$$\boldsymbol{\mu} = \int_0^t \boldsymbol{K}(t-\tau)\delta\boldsymbol{\nu} d\tau \tag{2.62}$$

(2.61) is a so-called *unified* model where seakeeping theory, maneuvering theory, non-linear effects and fluid memory effects have merged into one model (Fossen, 2011, p. 103).

The rigid body mass is easily computed from (2.14). M_A can be found from the infinite frequency added mass.

Chapter 3

ROV Design and Modelling in *GeniE*

A design for small- sized ROV's will be suggested and modelled in *GeniE*, which is a part of the Sesam package software (DNV Software, 2014c). It will further be analysed in *HydroD*, where a *Wadam*-analysis will be performed in the frequency domain (see Chapter 4). Thrust capacity and configuration of thrusters for the three ROVs will also be proposed in this section.

3.1 Proposed ROV Design

The designed ROVs is henceforth named MaxiROV, MidiROV and MiniROV, ranging from largest to smallest in weight and size. Dimensions and materials are chosen from comparison with multiple existing designs. These include the ROV introduced in Section 1.4.1, Minerva (see fig. 1.2), and three other ROVs. Their dimensions, weight and thrust capacity are given in table 3.1. The additional ROVs are:

- A Sub-Atlantic 340 kg ROV named Mohican, see fig. 3.1a.
- A Sub-Atlantic 165 kg ROV named Mohawk, see fig. 3.1b.
- A Sub-Atlantic 85 kg ROV named Mojave, see fig. 3.1c.

Minerva is about 500 kg and has an aluminium frame (Technical Specifications, 2014). To simplify the study, decrease computational time and to ease validation of results, the shape of the proposed models will be a box. Minerva's body consists of a buoyant box on the top and sensors and equipment situated under the box, yielding an estimated vertical CG of 12 cm (Kirkeby, 2010). The volume of the three boxes will be determined from their desired mass. See appended calculations in Appendix E.4. In addition, the determined volume will provide the ROVs of a positive buoyancy of about 7 kg for the medium sized ROV (MaxiROV) and about 0.5 kg for the small sized ROVs (Midi- and MiniROV), as recommended by Christ and Wernli Sr. (2011). The proposed designs will all have a shorter height than normal for ROVs. This is due to the fact that all ROVs have open spaces inside their metal frames for equipment, as can be seen for the existing ROVs in figures 1.2 and 3.1. For instance will a uniform box with the same dimensions

(a) Mohican

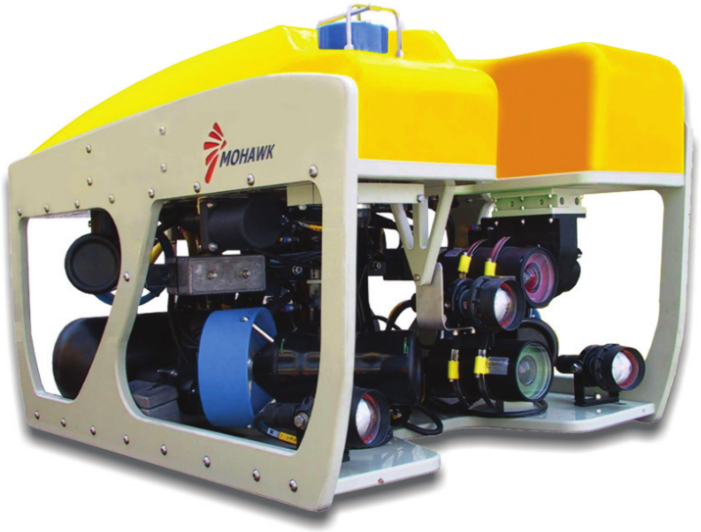

(b) Mohawk

(c) Mojave

Figure 3.1: Sub-Atlantic Observation Class ROVs.

Size	Minerva	Mohican	Mohawk	Mojave
Weight [kg]	500	340	165	85
Length [m]	1.44	1.1	0.98	1.0
Beam [m]	0.82	0.8	0.77	0.63
Height [m]	0.8	1.0	0.6	0.5
Thrust capacity				
Surge [N]	478	1080	785	520
Sway [N]	195	1080	685	520
Heave [N]	389	735	590	255

Table 3.1: Dimensions, weight and thrust capacity of ROVs used for comparison (FORUM Energy Technology, 2013).

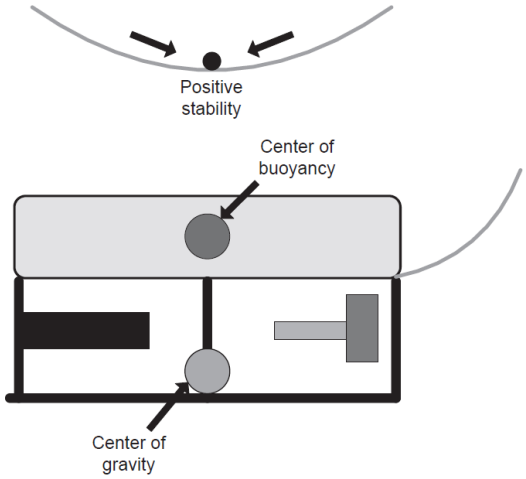

Figure 3.2: ROV with positive stability (Christ and Wernli Sr., 2011)

as Minerva have a substantially larger volume than the real Minerva and thus larger buoyancy. Consequently, an *equivalent height* - $H_{eq.}$ is introduced.

The equivalent height represents the actual height of the ROV if all the mass was pressed together in to a box. For Minerva the equivalent height was set to be 15 percent larger than the height of the buoyant material. The equivalent height makes it possible to estimate the total volume of the frame, thrusters and tools. The box-shaped ROVs therefore has a top layer of buoyant material (Divinycell, MatWeb (2014)) and a bottom layer of a higher density metal - stainless steel, to obtain a desired centre of gravity. The layers thickness are referred to as H_{div} and H_{ss}, respectively. The centre of gravity will be chosen to ensure stability of the ROVs and is estimated as a percentage of the ROVs entire height, H. A submerged vessel must have a higher centre of buoyancy (CB) than the centre of gravity (CG). This will also provide stability in roll and pitch, as the ROVs will naturally return to zero angular displacement when effected by a disturbance. To illustrate, see fig. 3.2.

3.1.1 Resulting Design

The resulting dimensions can be seen in table 3.2 and figs. 3.3a to 3.3c on page 27. As the mass distribution is determined, the rigid body mass matrices are computed according to

eq. (2.14) and the results are appended in appendix B.1. The off-diagonal terms are due to the non-zero z-component of r_g.

		MaxiROV	MidiROV	MiniROV
W	kg	600	200	50
L	mm	1400	1000	800
B	mm	900	650	500
H	mm	860	630	430
$H_{eq.}$	mm	470	300	120
$r_{g,z}$	mm	-170	-120	-50
H_{div}	mm	267	85	21
H_{ss}	mm	56	37	16

Table 3.2: Dimensions of Minerva versus MaxiROV.

3.1.2 Implementation to GeniE

IMT Software Wiki (2011) offers sample models for use in GeniE. It is possible to generate a model for a barge, a simple circular cylinder (spar buoy) or a simplification of an Aker H3 semi-submersible rig. The barge is shaped as a box, and hence will be used to generate command files for GeniE to model the three ROVs. The contents of these command files will be changed to construct only one fourth of the models. This is to ensure XY and XZ-symmetry for the models in Wadam. Moreover, the file establishes a dummy load case that identifies the wet surface of the model. After running the command file, the entire mesh is exported as a FEM file to Wadam.

3.2 Thrust Capacity and Thruster Configuration

3.2.1 Capacity

For MaxiROV an estimate of the thrust capacity can be found using the methodology of model-scaling as described in Steen (2011). Each ROV could be compared to one of the existing ROVs listed in table 3.1, where one will be the "model" and one would be the "full-scale" ROV. To illustrate, Minerva is smaller than MaxiROV in height, weight and beam, and would accordingly be the "model". Then, a scale factor λ could be found as the ratio between the length, beam or height. For MidiROV and MiniROV, Minerva would reversely be the full scale model.

According to this method model scaling is a possibility if the following is true for the model and the full scale vessel:

Similarity in geometry

Similarity in kinematics

Similarity in dynamics

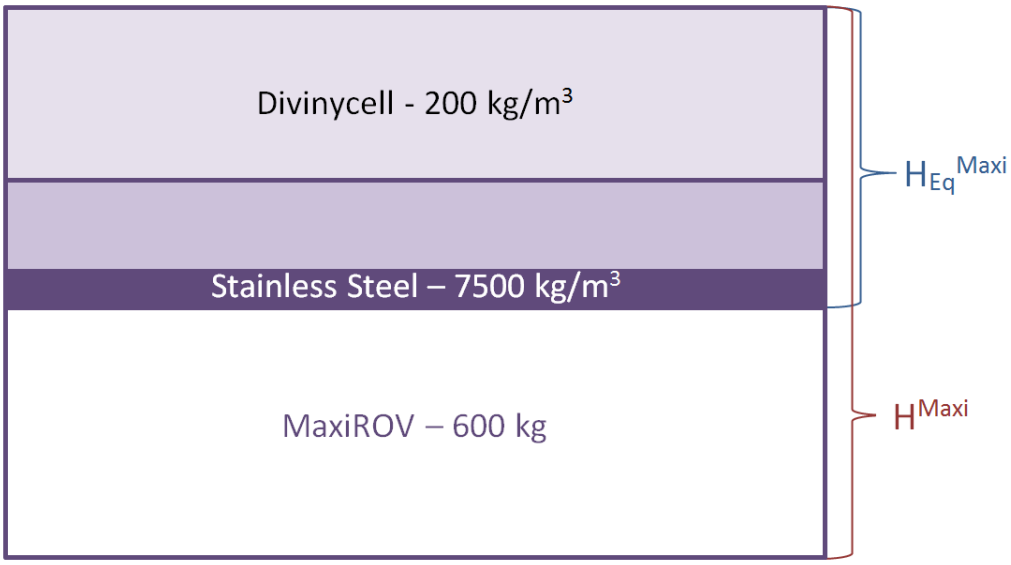

(a) MaxiROV

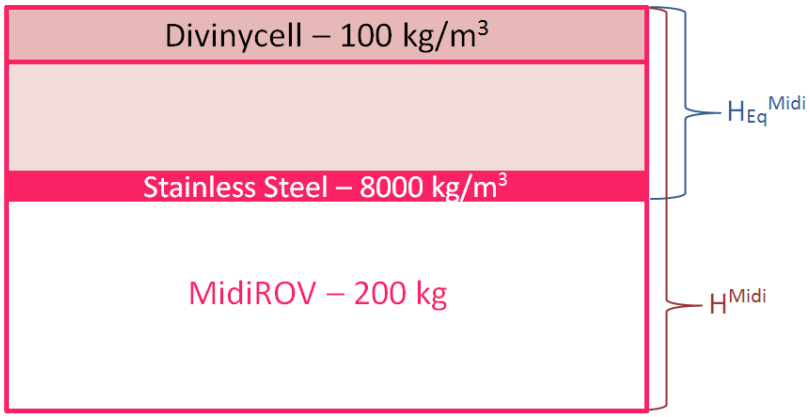

(b) MidiROV

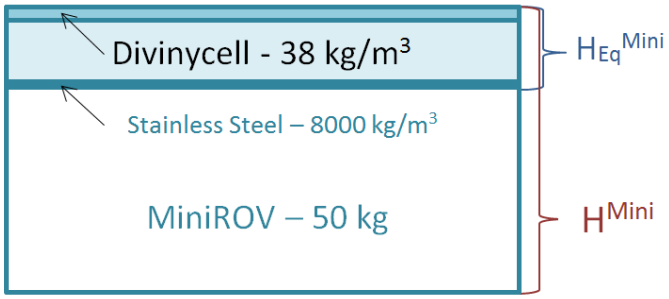

(c) MiniROV

Figure 3.3: Scaled sketches of proposed dimensions and design of ROVs. Side view.

As the ROVs dimensions are determined from the existing design, some similarity in geometry is present. However, the existing ROVs are not boxes. Nevertheless, the ROVs are meant to represent existing designs, thus model-scaling will result in more realistic thrust capacity. Kinematic similarity implies that the fluid's velocity field around both the model and the full scale vessel has vectors of same direction. This is assumed similar for the ROVs. Dynamic similarity means that for instance Reynolds number, $R_N = VL/\nu$, or Froude number, $F_n = V/\sqrt{gL}$, for the model and for the full scale vessel is equal. V is the velocity of the vessel, L is the length, ν is the kinematic viscosity and g is the gravitational acceleration.

By assuming Froude-scaling, the relationship between forces affecting the "model" ROV and the "full scale" ROV is:

$$F_s = \lambda^3 F_m, \qquad \lambda_L = \frac{L_s}{L_m}, \qquad \lambda_B = \frac{B_s}{B_m}, \qquad \lambda_H = \frac{H_s}{H_m} \tag{3.1}$$

During full scale tests by Ludvigsen and Ødegaard (2004) the thrust capacity of Minerva was determined by performing a bollard pull test. The results showed that the achieved thrust was less than the thrust specified by the ROV producer. This indicates that the thruster might have experienced some thrust loss. The thrust capacity available for ROVs Mohican, Mohawk and Mojave is provided by the producers of the ROVs. The producers have probably included some thrust loss effects; however, as showed in the tests of Minerva, these effects are sometimes underestimated. Consequently, the thrust capacity for Minerva will be taken as the estimate for all three ROV designs. All three scale factors are computed, see table 3.3.

ROV	λ_L	λ_B	λ_H	$\boldsymbol{\lambda}$
MaxiROV	1.029	1.098	1.076	*1.098*
MidiROV	1.440	1.262	1.278	*1.262*
MiniROV	1.800	1.640	1.806	*1.640*

Table 3.3: Scale factor, λ for MaxiROV, MidiROV and MiniROV

When Minerva is set as the mode the largest scale factor is used and vice versa. So, for MaxiROV the largest factor is chosen, and for MidiROV and MiniROV the smallest factor is chosen, see the last column in table 3.3. The estimated capacity is calculated using eq. (3.1) and the results are presented in table 3.4.

ROV	Surge $[N]$	Sway$[N]$	Heave $[N]$
Minerva	478	195	389
MaxiROV	632	258	514
MidiROV	238	97	194
MiniROV	143	58	117

Table 3.4: Thrust capacity of Minerva and MaxiROV

3.2.2 Configuration

The thrusters will be added to the model in the time domain when simulating in SIMO. SIMO only provides the possibility to add thrusters in the horizontal plane, consequently there is no option to specify thrusters to provide provide neither thrust in the z-direction, nor moments in pitch and roll. For this reason the system has only three DOFs to control: surge (1), sway (2) and yaw (6). As mentioned in section 2.3.2, it is common to have four thrusters in the horizontal plane. The thruster configuration of the three ROVs is inspired by the Sub-Atlantic ROV, Mohican, see figure 3.1a (FORUM Energy Technology, 2013).

In SIMO the four thrusters are modelled as fixed ducted thrusters, and positioned in a similar manner as the Mohican thrusters are. Their positions are decided to be symmetrical. The configurations are summarized in table 3.5. The thrust direction, α, is relative to the x-axis.

Thruster	X pos. $[m]$	Y pos. $[m]$	α [°]
MaxiROV			
Tfp	0.560	0.297	140
Tfs	0.560	-0.297	-140
Tbp	-0.560	0.297	35
Tbs	-0.560	-0.297	-35
MidiROV			
Tfp	0.400	0.215	140
Tfs	0.400	-0.215	-140
Tbp	-0.400	0.215	35
Tbs	-0.400	-0.215	-35
MiniROV			
Tfp	0.320	0.165	140
Tfs	0.320	-0.165	-140
Tbp	-0.320	0.165	35
Tbs	-0.320	-0.165	-35

Table 3.5: Thruster configuration where f = front, b = back, p = port and s = starboard.

As the controller will output a control vector, $\boldsymbol{\tau}_c$, in the degrees of freedom that are to be controlled, this can be translated into thrust settings for each separate thruster of the ROV through the configuration matrix, $\boldsymbol{T}_{conf}$. $\boldsymbol{T}_{conf}$ is found using trigonometry. The relation between the control vector $\boldsymbol{\tau}_c \in \mathbb{R}^3$ and the produced thrust of the ROVs, $\boldsymbol{T}_D$ is:

$$\boldsymbol{\tau}_c = \begin{bmatrix} \tau_{\text{surge}}[\text{N}] \\ \tau_{\text{sway}}[\text{N}] \\ \tau_{\text{yaw}}[\text{Nm}] \end{bmatrix} = \mathbf{T}_{3\times 4}(\boldsymbol{\alpha})\mathbf{T}_d \tag{3.2}$$

$$= \begin{bmatrix} \cos\alpha_{fp} & \cos\alpha_{fs} & \cos\alpha_{bp} & \cos\alpha_{bs} \\ \sin\alpha_{fp} & \sin\alpha_{fs} & \sin\alpha_{bp} & \sin\alpha_{bs} \\ -l\cos(\beta - 180 + \alpha_{fp}) & l\cos(\beta - 180 - \alpha_{fs}) & l\cos(\beta - \alpha_{bp}) & -l\cos(\beta + \alpha_{bs}) \end{bmatrix} \begin{bmatrix} T_{fp} \\ T_{fs} \\ T_{bp} \\ T_{bs} \end{bmatrix} \tag{3.3}$$

where l is the distance from CO to each thruster (equal length for all thrusters) and β is the angle between a line through the origin of the thruster, parallel to the y-axis, and the line between the CO of the ROV to the origin of the thruster:

$$l = \sqrt{{X_{pos}}^2 + {Y_{pos}}^2}, \quad \beta = \tan^{-1} \frac{Y_{pos}}{X_{pos}}$$

By using the MATLAB function `pinv` to calculate the Moore-Penrose pseudoinverse $\mathbf{T}^{+}_{4\times3}(\boldsymbol{\alpha}, \boldsymbol{a})$ of $\mathbf{T}_{3\times4}(\boldsymbol{\alpha}, \boldsymbol{a})$, eq. (3.3) can be rewritten as.

$$\mathbf{T}_d = \mathbf{T}^{+}_{4\times3}(\boldsymbol{\alpha}, \boldsymbol{a})\boldsymbol{\tau}_c \tag{3.4}$$

Equation (3.4) shows how thrust can be *allocated* to each thruster. The resulting thruster configuration matrix and the thruster allocation matrix for the three ROVs is placed in Appendix B.2.

Now that the thruster allocation is established in eq. (3.4), it is possible to determine the thrusters capacity and hence the thrust limits linked to the individual thrusters. The surge thrust capacity in table 3.4 will be used with eq. (3.4) to calculate the limits. See table 3.6 for the results.

Thruster	Max thrust[N]	Min thrust [N]
MaxiROV		
Tfp	192	-192
Tfs	192	-192
Tbp	206	-206
Tbs	206	-206
MidiROV		
Tfp	72	-72
Tfs	72	-72
Tbp	78	-78
Tbs	78	-78
MiniROV		
Tfp	44	-44
Tfs	44	-44
Tbp	47	-47
Tbs	47	-47

Table 3.6: Thruster capacity, where f = front, b = back, p = port and s = starboard.

Using the thrust capacity in sway instead, which have lower limits, will yield the following thruster capacities:

MaxiROV: [104 N, -104 N] for front thrusters and [108 N, -108 N] for back thrusters.

MidiROV: [39 N, -39 N] for front thrusters and [41 N, -41 N] for back thrusters.

MiniROV: [24 N, - 24 N] for front thrusters and [25 N, -25 N] for back thrusters.

These values are almost half the values in table 3.6. However, the limits in table 3.6 will be used. This will be justified in sections 5.6.4 and 6.3.1.

Chapter 4

Analysis of Model in *Wadam*

The three ROV designs will be analysed in *Wadam*. Wadam uses potential theory and Morison theory to determine hydrodynamic properties and solve the equations of motions in the frequency domain. This is possible by assuming that the problem can be linearised and that it is steady state (Faltinsen, 1993). Assuming linearisation means assuming that the body motion amplitude is proportional to the incident wave amplitude and excitation amplitude. Steady state implies that all transient effects are due to initial conditions.

Wadam assumes structures and vehicles that penetrate the water surface. This is not true for the ROVs subject of this thesis. Several attempts will be performed to avoid this problem. The different approaches will be described in the section below. Results from these attempts will determine which approach(es) is (are) most convenient. Results from Wadam will be presented and explained in the remainder of this chapter. Some parts of the results can be found in Appendix C.

4.1 The Wadam Model

As mentioned, the Wadam results are found in the frequency domain, using potential theory (Fossen, 2011, Chapter. 5.). The theory is explained in Chapter 2 of this report. According to the Wadam user manual (DNV Software, 2014b) the 6 DOF equations of motions in the frequency domain are presented as:

$$[-\omega^2(\boldsymbol{M}+\boldsymbol{A}(\omega))+i\omega(\boldsymbol{B}_p(\omega)+\boldsymbol{B}_v)+\boldsymbol{C}+\boldsymbol{C}_e]\boldsymbol{X}(\omega,\beta)=\boldsymbol{F}(\omega,\beta) \tag{4.1}$$

where $\boldsymbol{M}$ is the inertia body matrix, $\boldsymbol{A}(\omega)$ is the frequency dependent added mass matrix, $\boldsymbol{B}(\omega)_p$ is the frequency dependent potential damping matrix, $\boldsymbol{B}_v$ is the linearised viscous damping matrix, $\boldsymbol{C}$ is the hydrostatic restoring matrix and $\boldsymbol{C}_e$ is an optional external restoring matrix. $\boldsymbol{X}(\omega,\beta)$ and $\boldsymbol{F}(\omega,\beta)$ is the resulting (complex) motion and exciting force vector. ω is the frequency and β is the heading angle of the wave. Equation (4.1) is similar to the classical frequency domain model in eq. (2.55), except the damping term is split in a different matter. This is not uncommon because the damping terms are challenging to identify and there is more than one way to determine them. Also, the restoring term is split in to two parts and the heading angle β is taken into account.

4.2 Wadam Analysis

As explained, several analysis approaches will be examined. A Wadam analysis is easily set up by a *Wadam Wizard*, and different Wizards create different analyses. The wizard prompts the user for information about:

a Type of model: panel, dual or composite.

b Direction set: direction of incoming waves.

c Frequency set: frequency/period/wavelength of the waves to investigate.

d Location: depth of location, density and viscosity of water and air.

e Hydro model: floating or fixed.

f The model itself: FEM file(s) from GeniE.

g Loading condition: trim angle, heel angle or waterline.

h Mass model: given by mass, volume/buoyancy, radius of gyration and desired centre of gravity or the entire mass matrix.

A panel model is a model built up by plates divided into panels determined by a mesh-density. A dual model and a composite model consist of a panel model and a Morison model (DNV Software, 2014b). The Morison model is used for computing Morison drag by strip theory and will be modelled as a beam of length L (equal to the ROVs lengths) with the same cross section as the ROVs fronts, namely a square of dimensions $B \times H$.

In a dual model, the panel and Morison model cover the exactly same area, whereas in a composite model, they can cover different parts (useful for slender parts which only provide structural stiffness and additional drag forces). Figures 4.1a to 4.1c show the panel models of the three ROVs.

Using a Morison model should be considered, as it provides additional drag which affects the ROVs performance a great deal. Hence an analysis will be performed with a dual model, where the panel model and Morison model completely covers each other. This additional drag can also be added later in SIMO, and for this reason the panel model alone is also investigated.

The direction set (**b**) includes all directions between 0 and 360 degrees with a jump of 15 degrees from direction i to the next direction $i + 1$. The frequency set (**c**) includes periods varying from 1 second to 200 seconds, where the step size varies between 0.5 seconds for small periods to 10 seconds for large periods. The location (**d**) is given by data from Rataren, where the depth is 45 meters (see appendix A.2) and the fluid is sea water. When attempting to use the loading condition (**g**) to put the model at the desired depth, this yields negative metacentric height of the model, thus the loading condition is always set to zero. The depth is instead set by translating the input model(s) when defining them (**f**). The Mass model (**h**) is determined by the rigid body mass computed in section 3.1, see appendix B.1. Options **b**, **c**, **d**, **g** and **h** will be kept constant for all analyses.

The list below will explain different approaches to analyse MaxiROV, MidiROV and MiniROV, where type of model, the hydro model and the model files are varied (**a**, **e**

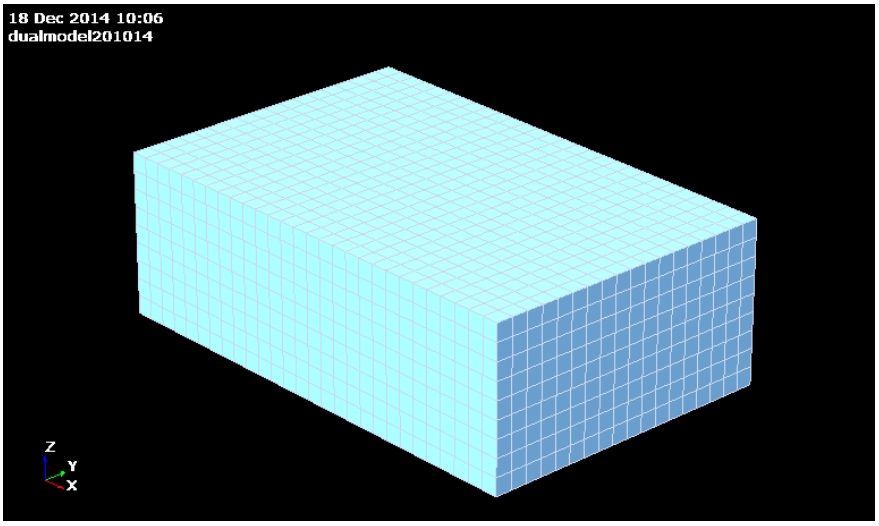

(a) Screenshot of MaxiROV from HydroD (V4.7-01).

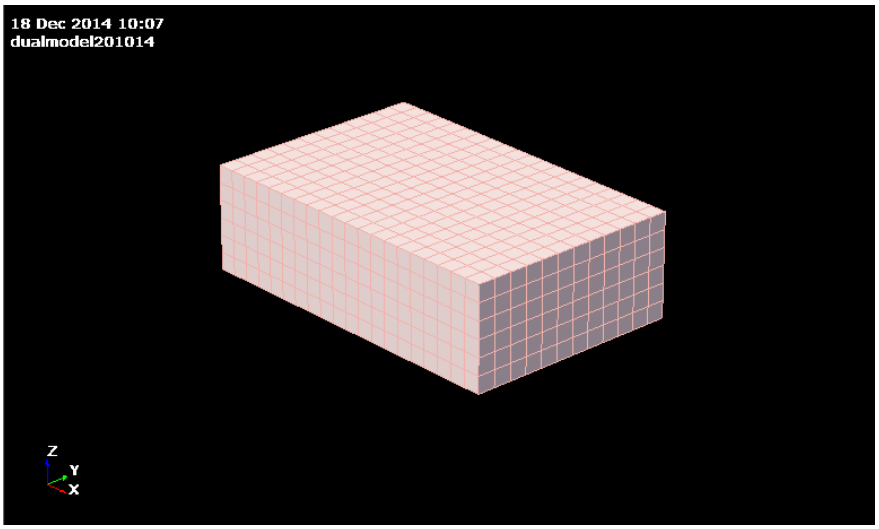

(b) Screenshot of MidiROV from HydroD (V4.7-01).

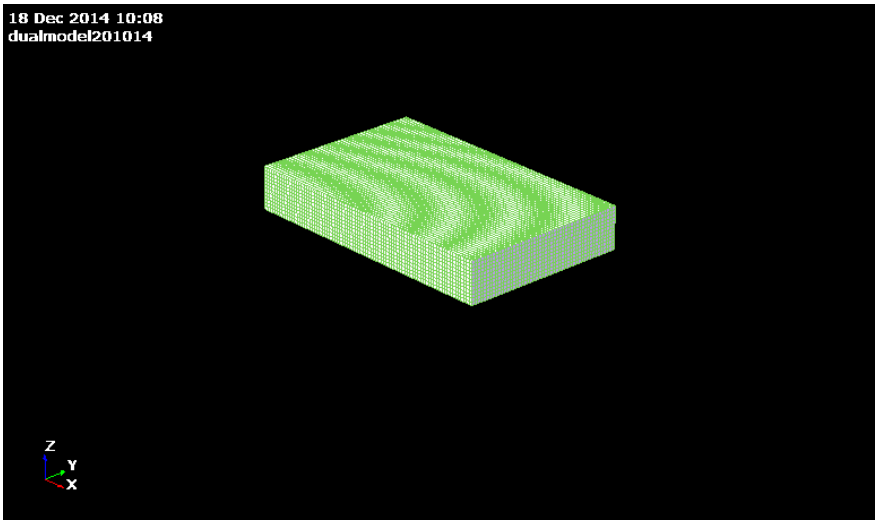

(c) Screenshot of MiniROV from HydroD (V4.7-01).

Figure 4.1: The panel models in HydroD (V4.7-01).

and **f**). That is, the panel models are always constant, but in some analyses a Morison model is also used. The input coordinate system of the panel- and Morison-models lie in the centre of the waterline, thus having its origin, which aligns with the CB of the panel model, at the global CO, $x, y, z = \mathbf{0}$. The analyses are set up as follows:

1 Dual model, floating and translated to correct depth.

2 Panel model, floating and translated to correct depth.

3 Panel model, translated to the correct depth and fixed.

4 Panel model with no excessive buoyancy, translated to the correct depth.

5 Panel model, floating and translated to barely penetrate the water surface.

4.3 Results from Wadam

Going forwards, the analyses will be accepted or rejected. Rejection will mainly be done based on investigations of the ROV behaviour in the time domain. This is possible through SIMO (Simulation of Marine Operations).

Analysis 1 : The Morison drag is computed by using strip theory. Strip theory assumes long and slender bodies, which is not true for the designed ROVs. Thus, this analysis method is omitted.

Analysis 2 and 4 : Yield nonphysical behaviour of the models in SIMO. The vehicles were observed floating up in the air and also sinking through the sea bottom, both also displaying pendulum motions. The reason for this might be that SIMO or Wadam interprets the models as both penetrating the water surface and having their CG at approximately 10 and 20 meters below the water surface. These results are not usable, and the method is rejected.

Analysis 3 : No radiation forces (caused by energy carried away by generated waves) is calculated as the model is fixed. Added mass and potential damping does constitute important contributions. These contributions are considered valuable for this thesis, and the analysis is therefore rejected.

Analysis 5 : At last it is decided that analysis 5 will be used, as the kinetics found gives usable results in SIMO. The ROVs are analysed barely penetrating the water surface and will be translated to the correct depths in SIMO.

Results from analysis 5 follow in the next pages. The results are given as a function of frequency, $\omega = 2\pi/T$. The periods are input from 1 s to 200 s, and so, the frequency is ranging from $\omega = 2\pi/200s = 0.03rad/s$ to $\omega = 2\pi/1s = 6.28rad/s$.

The results include damping forces, added mass, restoring and transfer functions for first order wave loads and first order motions. The results will be explained by investigating energy relations in section 2.3.1 and asymptotic values.

The frequency dependent damping and added mass results are presented in figures 4.2 and 4.3. The transfer function (TF) for the first order wave forces represents the relationship between the amplitude of the forces and the wave amplitude of the incident wave. The

TF for MaxiROV when the incident wave heading was set to 0°, 45°, 90°, 135° and 180° is presented in figs. 4.4 to 4.8. The transfer function for the body motion, also known as the response amplitude operator (RAO), represents the amplitude of the body motion response per wave amplitude. The results for MaxiROV are presented in figs. 4.9 to 4.13. Figures C.1 to C.20 in Appendix C presents the results for MidiROV and MiniROV. The restoring terms are presented in section 4.3.3.

Results from Pinkster (1980) is used for comparison to evaluate the results that vary with frequency. This PhD thesis shows an accurate consistency between analytical and computed results for $\boldsymbol{A}(\omega)$, $\boldsymbol{B}(\omega)$, first order wave force TF and motion TF in surge and in heave. These results are given in figures V-2 to V-7 in his thesis.

The results given below in sway can be verified by studying the surge results, especially as both beam and head sea have been analysed. The amplitudes of the sway results should however be larger than in surge, because the waves encounter a larger area of the ROV when β is 90 degrees ($H \times L$) than when β is 0 degrees ($B \times H$).

4.3.1 Damping Forces

Linearised Viscous Damping

For MaxiROV the linearised viscous damping calculated by Wadam is:

$$\boldsymbol{B}_v = \begin{bmatrix} 0 & 0 & 0 & 0 & 0 & 0 \\ 0 & 1.8e-01 & 0 & 0 & 0 & 0 \\ 0 & 0 & 0 & 0 & 0 & 0 \\ 0 & 0 & 0 & 1.8e-02 & 0 & 0 \\ 0 & 0 & 0 & 0 & 3.8e-03 & 0 \\ 0 & 0 & 0 & 0 & 0 & 9.8e-02 \end{bmatrix} \tag{4.2}$$

For MidiROV it is:

$$\boldsymbol{B}_v = \begin{bmatrix} 1.4e-01 & 0 & 0 & 0 & 0 & 0 \\ 0 & 2.0e-01 & 0 & 0 & 0 & 0 \\ 0 & 0 & 0 & 0 & 0 & 0 \\ 0 & 0 & 0 & 1.9e-03 & 0 & 0 \\ 0 & 0 & 0 & 0 & 1.5e-02 & 0 \\ 0 & 0 & 0 & 0 & 0 & 4.9e-01 \end{bmatrix} \tag{4.3}$$

For MiniROV the viscous damping terms are:

$$\boldsymbol{B}_v = \begin{bmatrix} 1.5e-03 & 0 & 0 & 0 & 0 & 0 \\ 0 & 2.0e-03 & 0 & 0 & 0 & 0 \\ 0 & 0 & 0 & 0 & 0 & 0 \\ 0 & 0 & 0 & 8.7e-06 & 0 & 0 \\ 0 & 0 & 0 & 0 & 3.7-e04 & 0 \\ 0 & 0 & 0 & 0 & 0 & 3.8e-02 \end{bmatrix} \tag{4.4}$$

These results are fairly small compared to the potential damping. Quadratic damping will be added in the time domain simulations in SIMO, see section 5.1.

Frequency Dependent Potential Damping

The potential damping results are given below. A dampers effect on a system is that it limits the system, or rather, the vehicles motion and act against this motion. Section 2.3.1 explains that under certain assumptions it is possible to see a simplified relationship between energy and the frequency/period of a wave. For very long waves (large period), with close to zero frequency a vehicle will slowly be dragged along with the wave in the waves direction. And so, potential damping is not present. As stated in Fossen (2011) the potential damping should be zero when $\omega = 0$. The results in fig. 4.2 correspond with these statements. It should be noted that in reality the total damping is not zero for very long waves, but this is caused by other damping terms (viscous/friction).

Compared to the results in (Pinkster, 1980, fig. V-4,V-5), $B_{11}(\omega)$ and $B_{33}(\omega)$ have very similar shape. They both increase in magnitude as ω increases, B_{11} more swiftly than B_{33}. The end frequency of the plots in fig. 4.2 is 6.3 rad/s, so the results extending this value can not be investigated here; however, a wave with period less than 1 s is not likely to occur, so these results are hence of little interest.

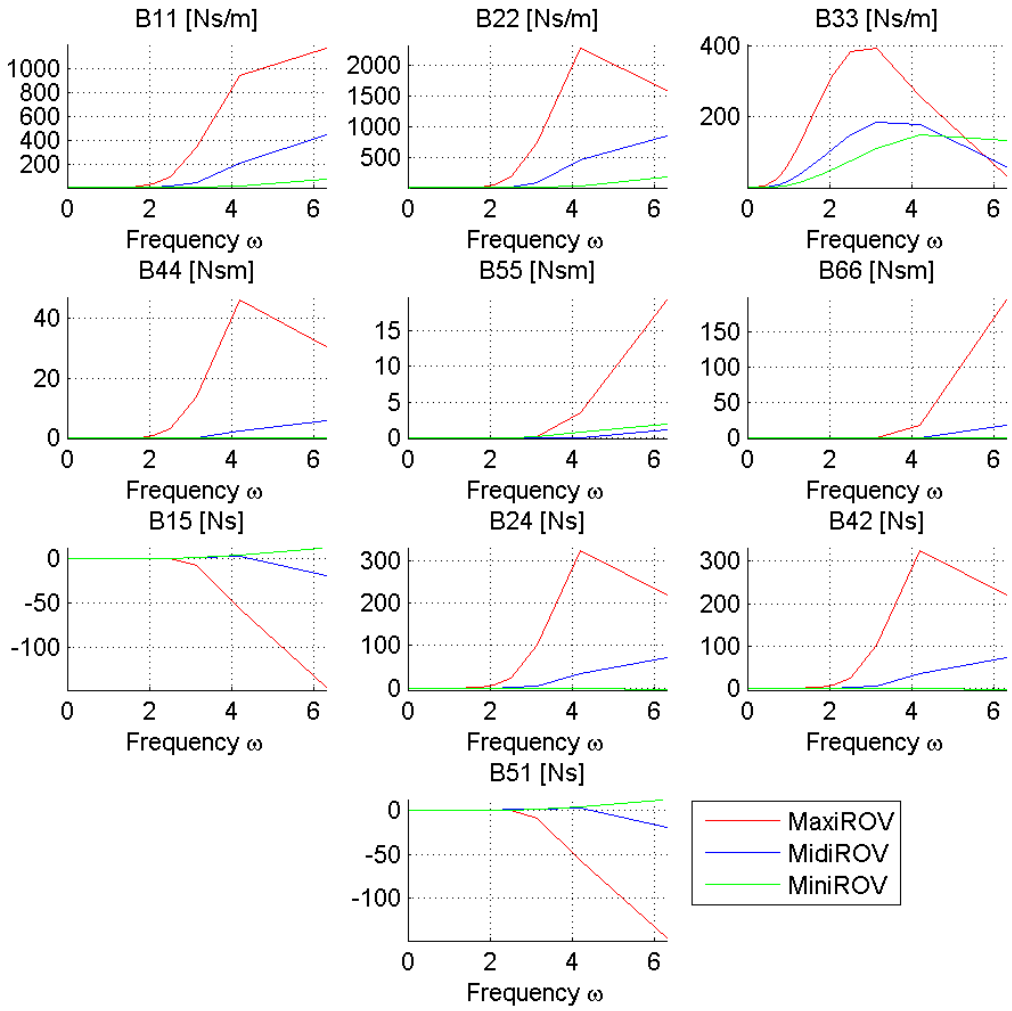

Figure 4.2: The frequency dependent potential damping $\boldsymbol{B}(\omega)$ for MaxiROV, MidiROV and MiniROV.

4.3.2 Frequency Dependent Added Mass

The frequency dependent added mass for all three ROVs and matrix $\boldsymbol{A}(\infty)$ for MaxiROV are presented here. $\boldsymbol{A}(\infty)$ for MidiROV and MiniROV can be found in Appendix C. To evaluate the results, some properties of frequency dependent added mass from Fossen (2011) will be repeated here. Below the wave zone, $\boldsymbol{A}(\omega)$ should not vary with frequency. The results obtained here do show that the vehicle most certainly is in the wave zone, as it does vary. When comparing the amplitudes of the added mass functions with results obtained from a conventional ship in Fossen (2011), they are in general much smaller, as they should be due to the size of the ROVs being a lot less than the size of a conventional ship. In fig. 4.3 the amplitudes are also decreasing with the size of ROV.

Further evaluation when comparing to Pinkster's results show that $A_{11}(\omega)$ and $A_{33}(\omega)$ have equal shape. Also, $A_{22}(\omega)$ is almost equal to $A_{11}(\omega)$ but of larger magnitude, as

expected.

$$\boldsymbol{A}(\infty) = \begin{bmatrix} 153 & 0 & 0 & 0 & -20 & 0 \\ 0 & 268 & 0 & 50 & 0 & 0 \\ 0 & 0 & 483 & 0 & 0 & 0 \\ 0 & 50 & 0 & 23 & 0 & 0 \\ -20 & 0 & 0 & 0 & 43 & 0 \\ 0 & 0 & 0 & 0 & 0 & 35 \end{bmatrix} \tag{4.5}$$

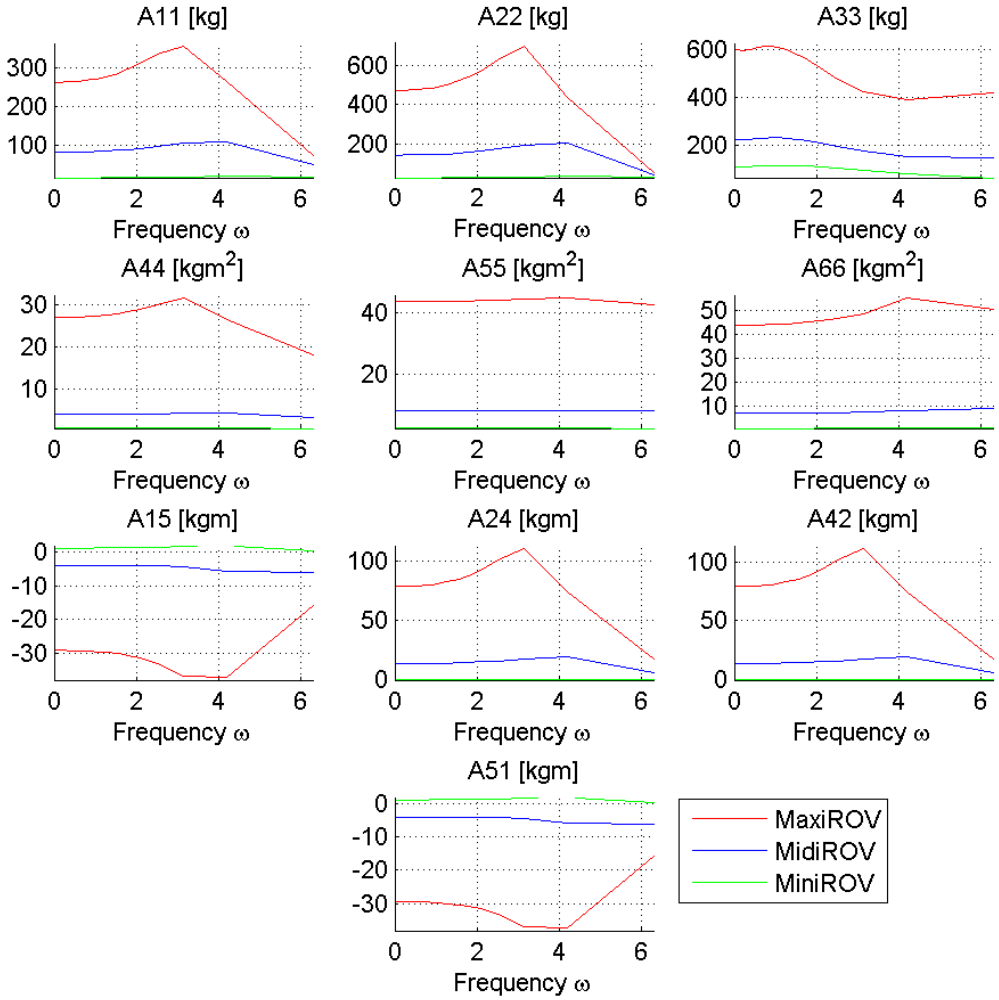

Figure 4.3: The frequency dependent added mass $\boldsymbol{A}(\omega)$ for MaxiROV, MidiROV and MiniROV.

4.3.3 Restoring

The restoring coefficients from Wadam are consistent with eq. (2.32), which is applicable for surface vehicles. These terms will also be altered in section 5.1. Results are given for

all three ROVs:

MaxiROV

$$\boldsymbol{C} = \begin{bmatrix} 0 & 0 & 0 & 0 & 0 & 0 \\ 0 & 0 & 0 & 0 & 0 & 0 \\ 0 & 0 & 12665 & 0 & 0 & 0 \\ 0 & 0 & 0 & 1855 & 0 & 0 \\ 0 & 0 & 0 & 0 & 3068 & 0 \\ 0 & 0 & 0 & 0 & 0 & 0 \end{bmatrix} \tag{4.6}$$

MidiROV

$$\boldsymbol{C} = \begin{bmatrix} 0 & 0 & 0 & 0 & 0 & 0 \\ 0 & 0 & 0 & 0 & 0 & 0 \\ 0 & 0 & 6533 & 0 & 0 & 0 \\ 0 & 0 & 0 & 384 & 0 & 0 \\ 0 & 0 & 0 & 0 & 699 & 0 \\ 0 & 0 & 0 & 0 & 0 & 0 \end{bmatrix} \tag{4.7}$$

MiniROV

$$\boldsymbol{C} = \begin{bmatrix} 0 & 0 & 0 & 0 & 0 & 0 \\ 0 & 0 & 0 & 0 & 0 & 0 \\ 0 & 0 & 4020 & 0 & 0 & 0 \\ 0 & 0 & 0 & 105 & 0 & 0 \\ 0 & 0 & 0 & 0 & 236 & 0 \\ 0 & 0 & 0 & 0 & 0 & 0 \end{bmatrix} \tag{4.8}$$

4.4 First Order Wave Force Transfer Function for MaxiROV from Wadam

In the following pages plots of the first order wave force transfer function can be seen.

4.4.1 Comparison of TF for Wave Force

The TF of wave force in heave matches the results in (Pinkster, 1980, fig. V-3) well, both in amplitude and in phase. In fig. V-2 of the surge wave force, the TFs have fairly different shapes in amplitude and shape. Otherwise, the amplitude in surge at 0° is lower than the amplitudes in sway at 90°. The amplitude results in surge and sway at 45° lie between the results for head and beam sea and all DOFs experience exciting wave loads when the waves come form this angle. Due to symmetry, results for 135° are very similar to the 45° results. However, some of the phase plots in both cases have shifted 180° (surge, pitch

and yaw). The results when $\beta = 180°$ are almost equal in amplitude as the results at head sea. Again, there are some phase shifts.

4.4.2 0 °, Head Sea

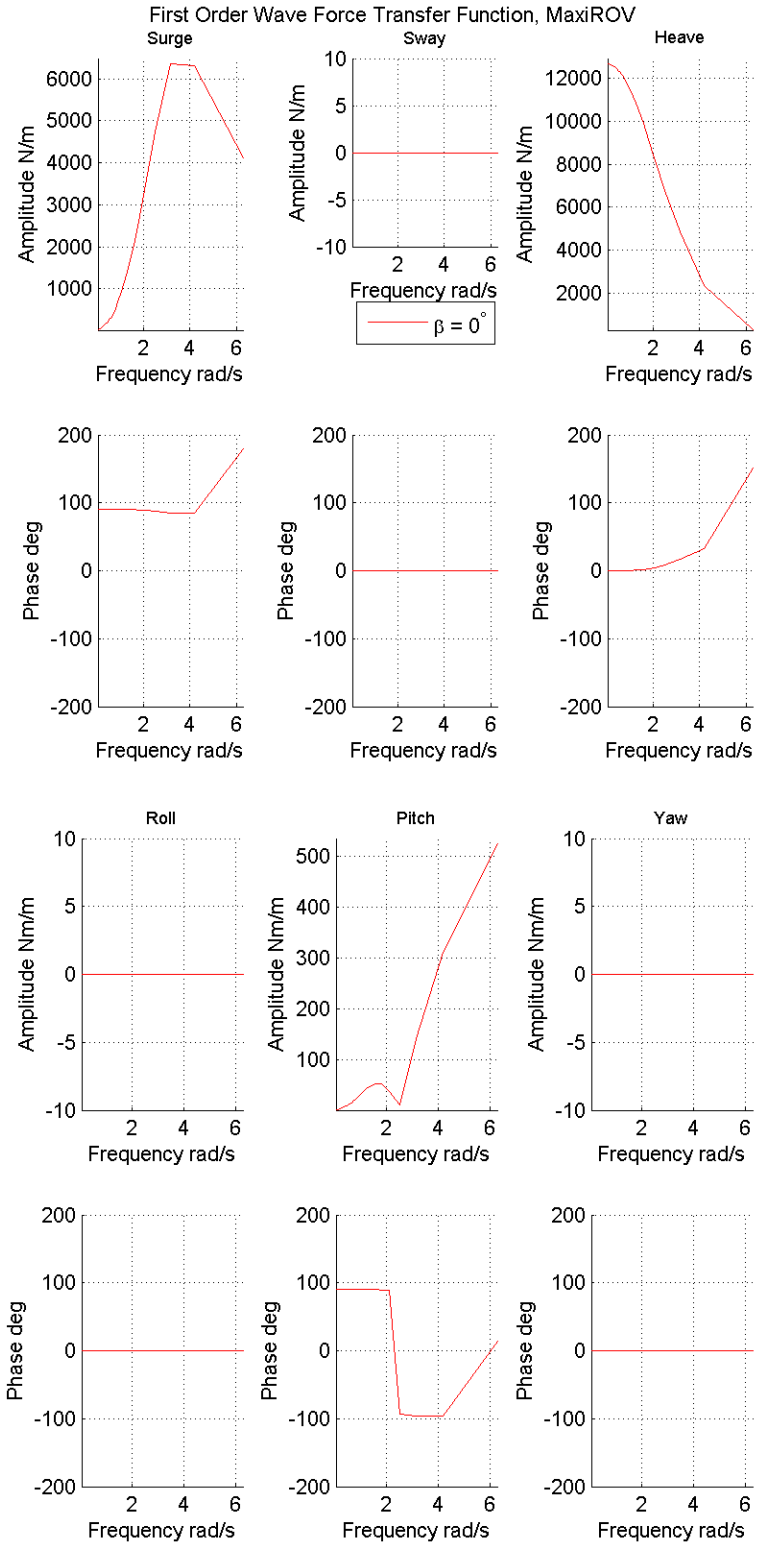

Figure 4.4: The first order wave force transfer function for 0 °, MaxiROV.

4.4.3 45 °

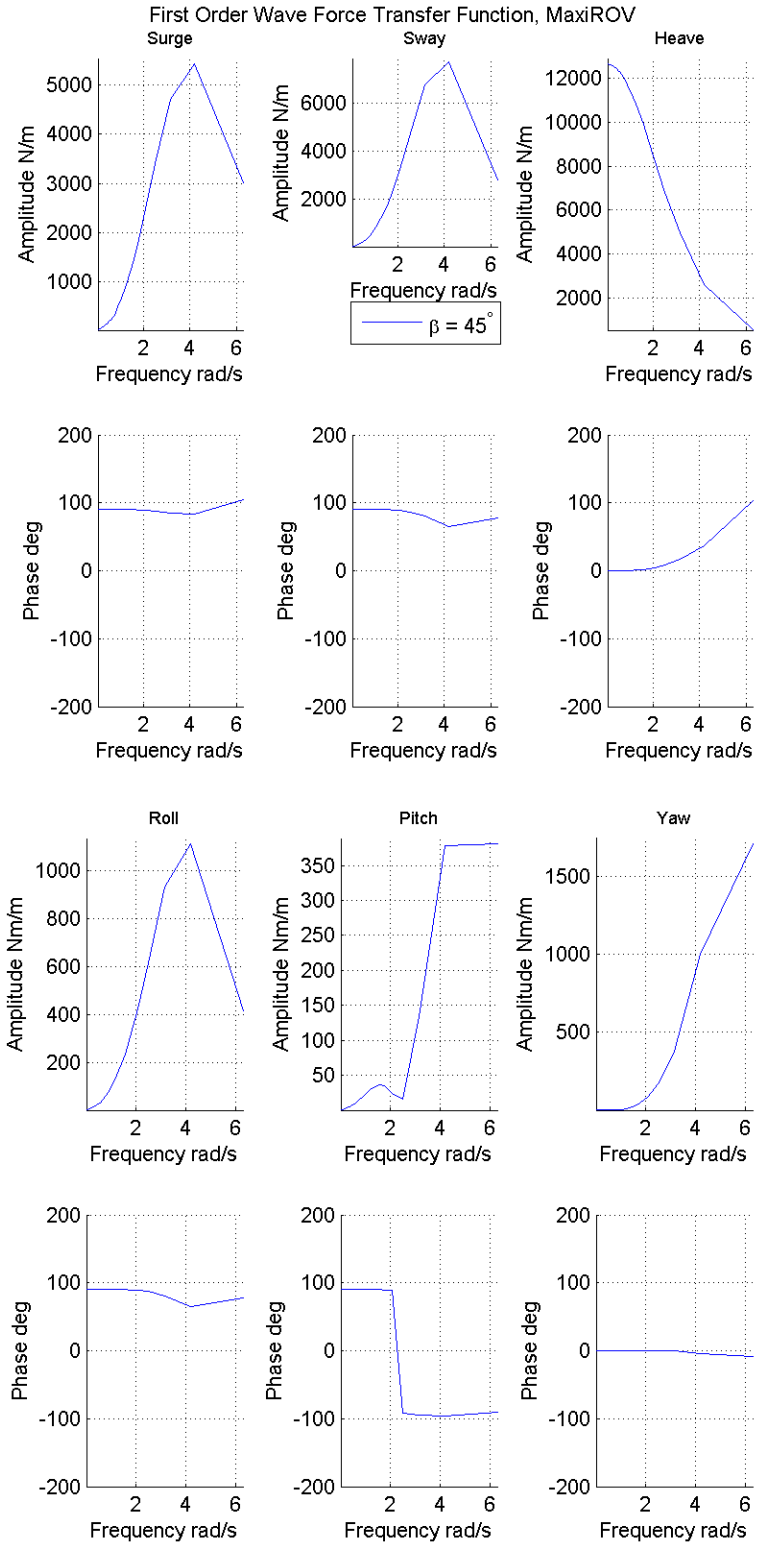

Figure 4.5: The first order wave force transfer function for 45 °, MaxiROV.

4.4.4 90 °, Beam Sea

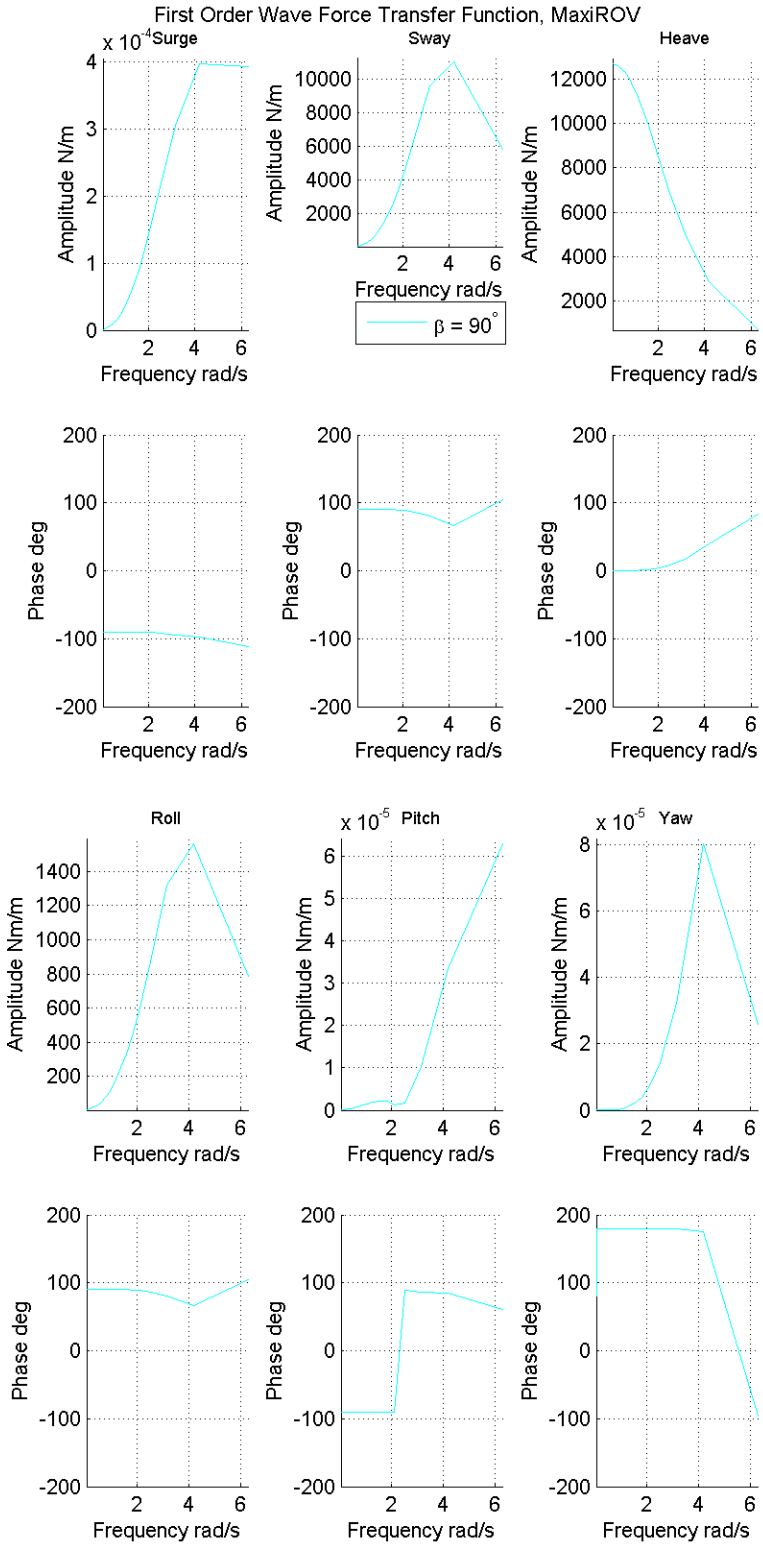

Figure 4.6: The first order wave force transfer function for 90 °, MaxiROV.

4.4.5 135 °

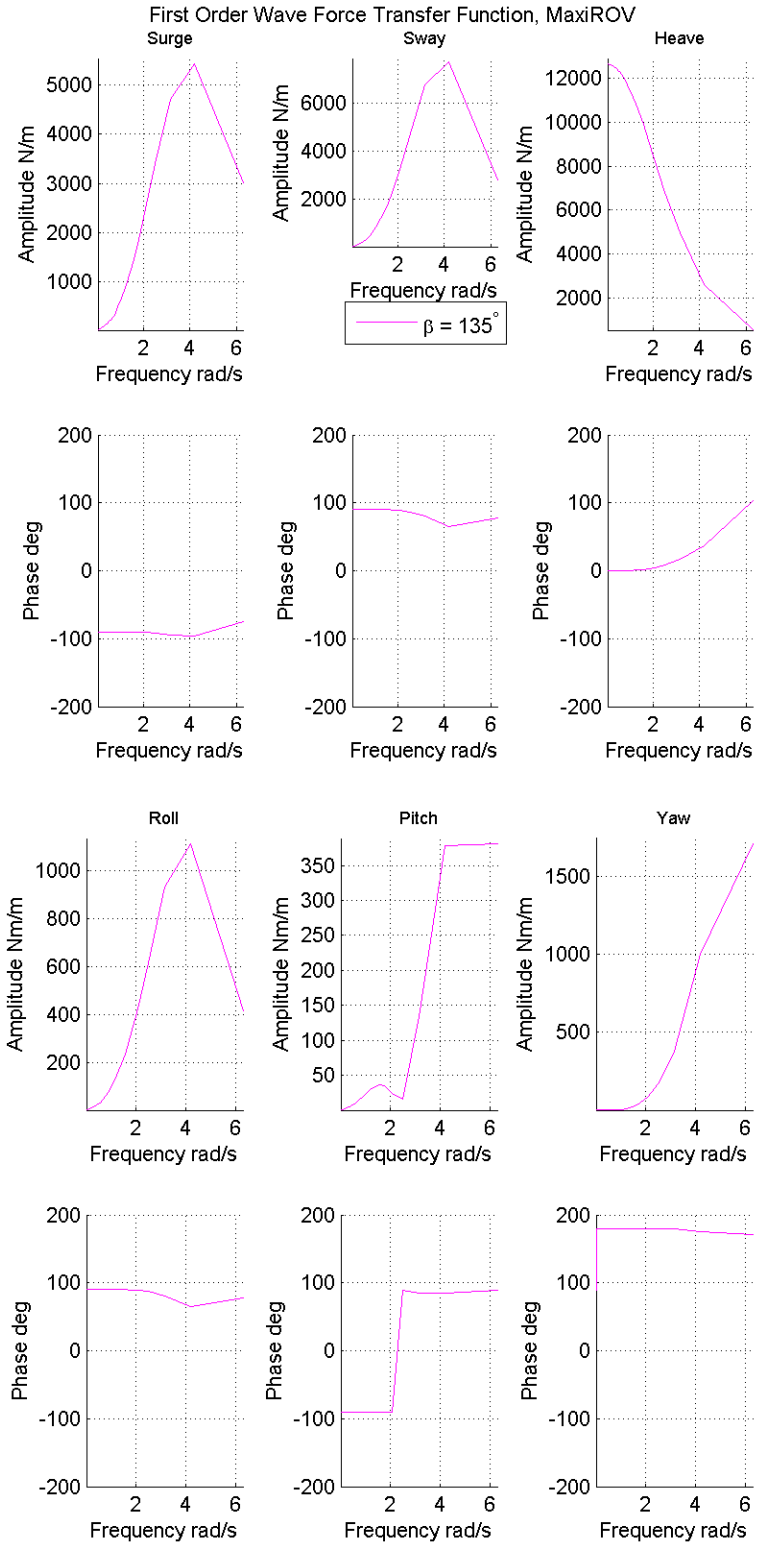

Figure 4.7: The first order wave force transfer function for 135 °, MaxiROV.

4.4.6 180 °

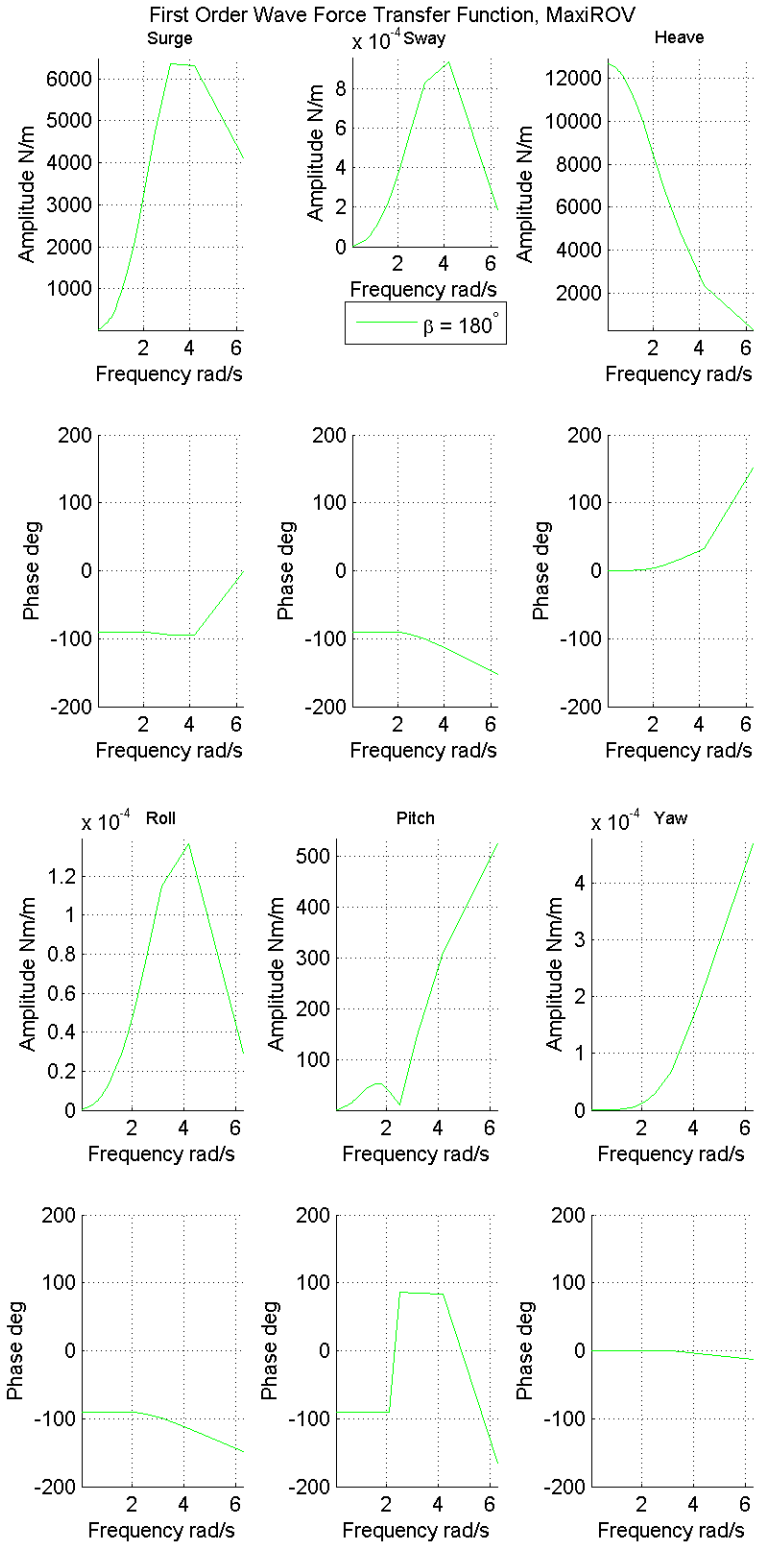

Figure 4.8: The first order wave force transfer function for 180 °, MaxiROV.

4.5 First Order Motion Transfer Function for MaxiROV and MiniROV from Wadam

In the following pages plots of the first order motion transfer function can be seen.

4.5.1 Comparison of TF for Wave Force

From (Pinkster, 1980, Figs. V-6,V-7) the first order surge and heave motion transfer function is plotted, both the TFs amplitude and frequency. The surge TF for MaxiROV at 0° is similar in shape, except for a large increase as $\omega \to 0$ and a small jump when $\omega = 2$ rad/s. These two phenomena are not present in Pinkster's results. For the heave TFs, the results are consistent. The amplitudes both start at value 1 m/m and then increase before the amplitudes decrease towards zero. The phase plots are also similar in shape.

Again, the analogy of head versus beam sea is stressed. The motion amplitude in surge when experiencing head sea, is of equal shape as the amplitude of the sway TF when experiencing beam sea. In the reverse case, the amplitudes are zero. The TFs when β is 45° have magnitudes of values in between the results for head sea and beam sea. Results for 45° and 135° are again very similar. As are the results for 0° and 180°.

4.5.2 0 °, Head Sea

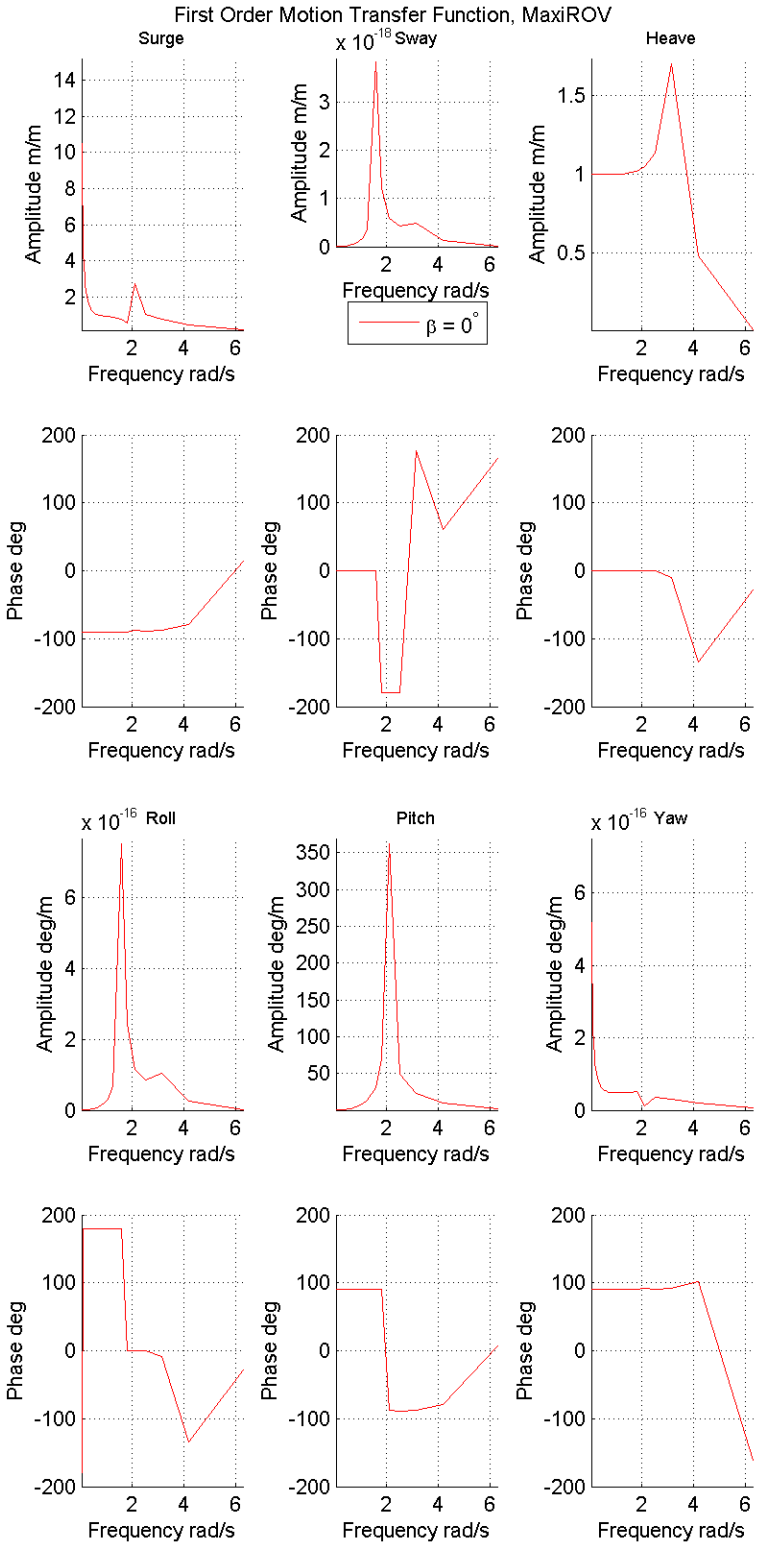

Figure 4.9: The first order motion transfer function for 0 °, MaxiROV.

4.5.3 45 °

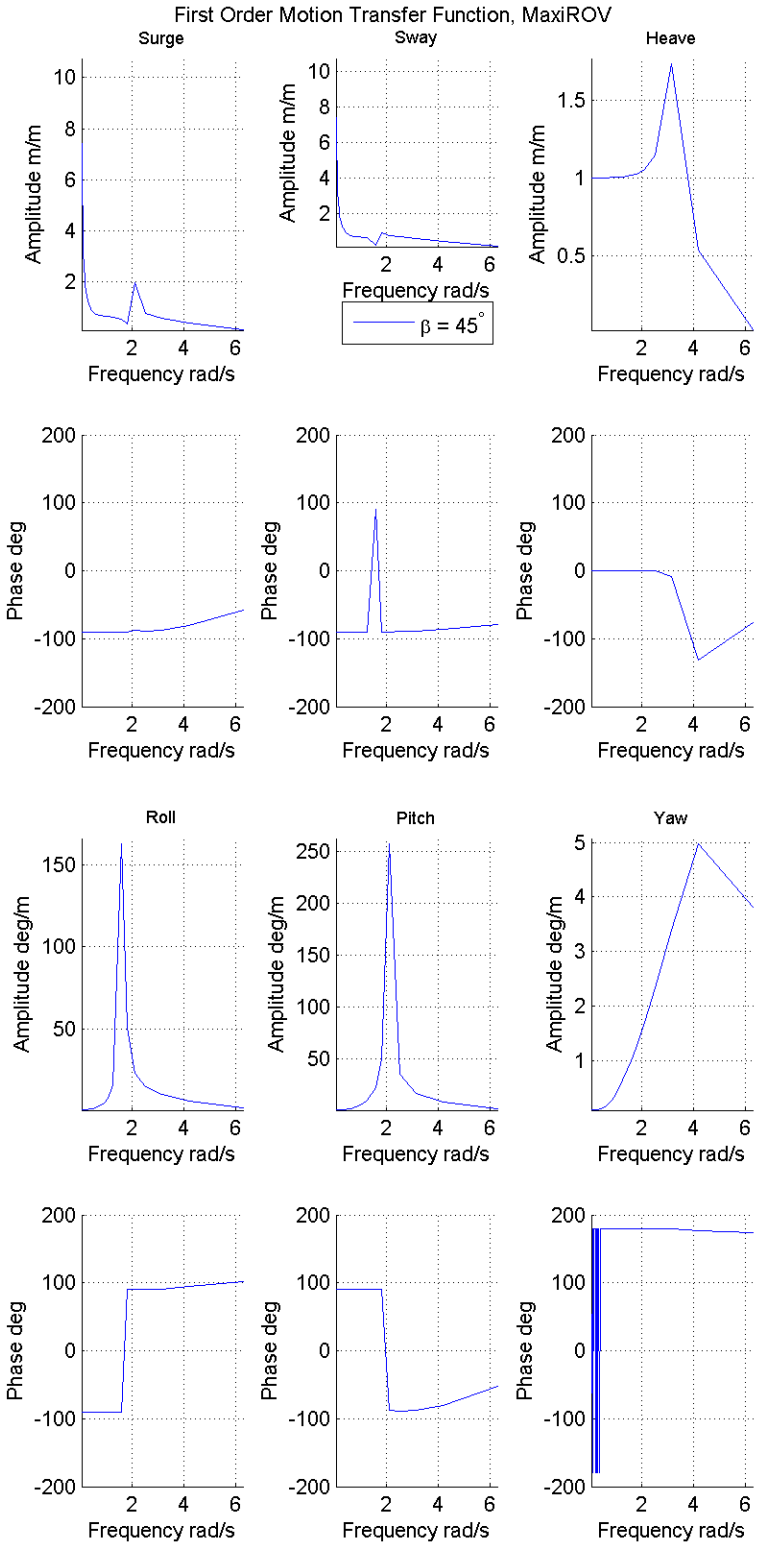

Figure 4.10: The first order motion transfer function for 45 °, MaxiROV.

4.5.4 90 °, Beam Sea

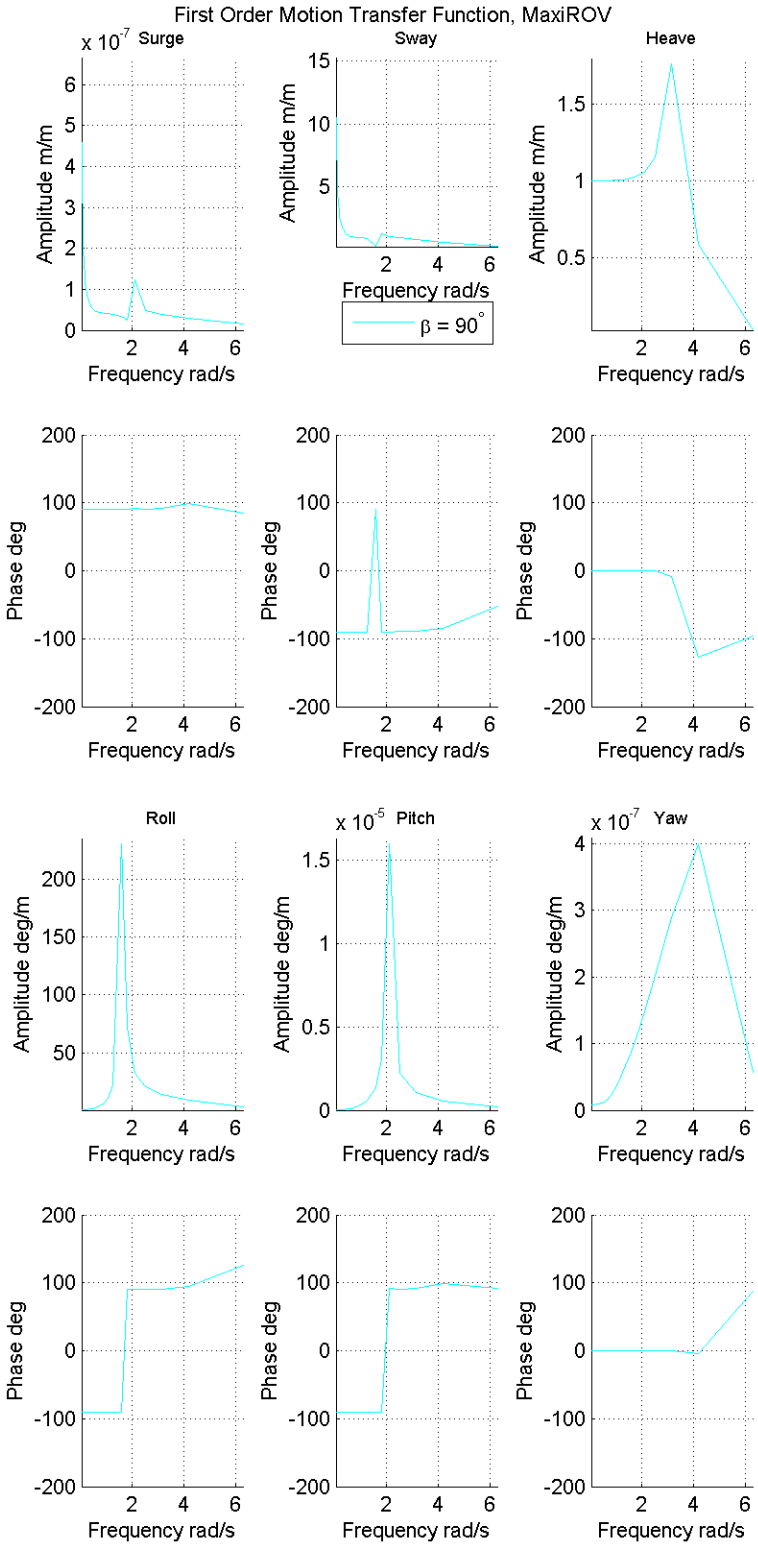

Figure 4.11: The first order motion transfer function for 90 °, MaxiROV.

4.5.5 135 °

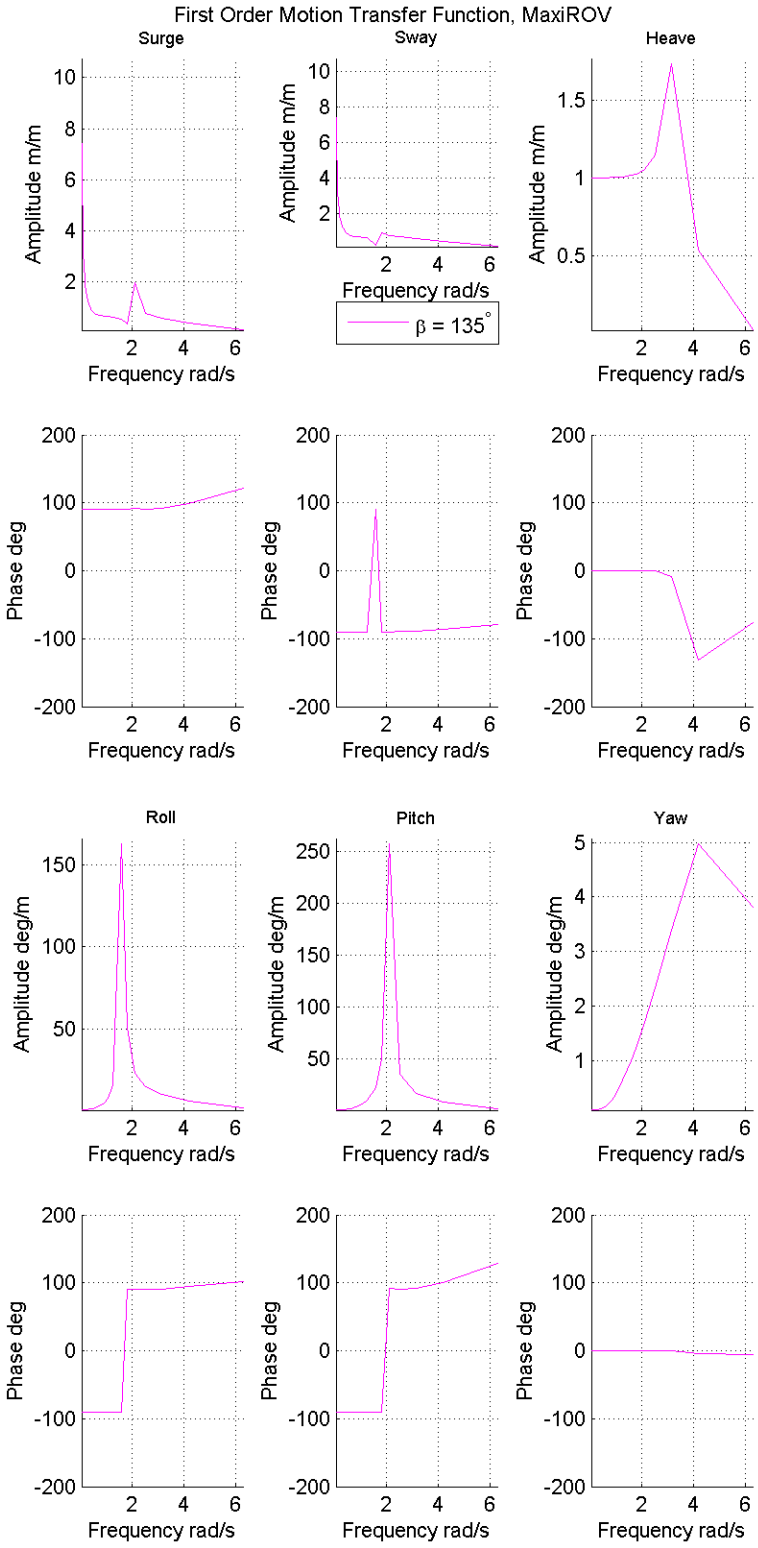

Figure 4.12: The first order motion transfer function for 135 °, MaxiROV.

4.5.6 180 °

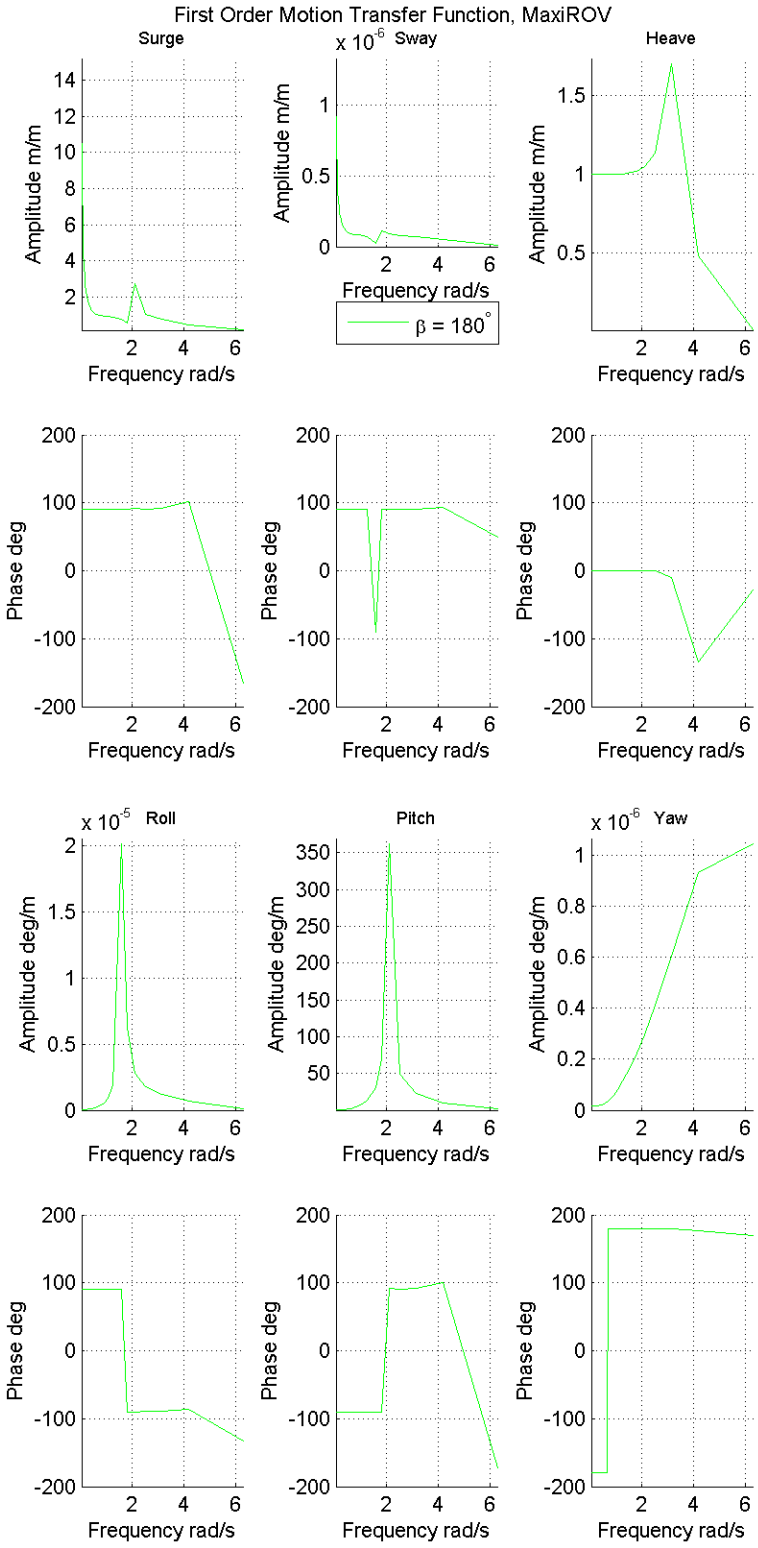

Figure 4.13: The first order motion transfer function for 180 °, MaxiROV.

Chapter 5

Simulation in Sima

The frequency domain results are imported to Sima, where they are pre-processed and placed in a SIMO-task. First, the pre-prosessor takes the frequency dependent added mass and potential damping and calculates the retardation functions for each ROV in all coupled and uncoupled DOFs, thus the fluid memory effects can be added to the time domain model. The retardation functions can be found in section 5.6. Alterations explained in section 5.1 are next performed on the results and the ROVs are moved to the correct depths.

Next, the design of thrusters and their configuration (from section 3.2) are added to the models. Simulation cases are then defined in condition sets, which are are given by the Jonswap wave spectra with a unidirectional spreading code and main direction of zero degrees (head sea), as described in Chapter 2. The sea states are determined from the eight simulation cases in table 1.3. Two environments are created within the SIMO-tasks; Rataren Environment (Case 1-7) and Calm Sea (Case 8). The next step involves defining and tuning control systems for the ROVs, as explained in section 5.3. The simulation length is set to 2000 seconds with a time step of 0.100 seconds. After simulations are finished, they will be post-processed and presented in MATLAB (R2013b).

5.1 Alterations to Wadam Results

SIMO takes the frequency domain results and transforms them in to time domain results. The frequency domain model is simplified by assuming linear theory, and the equations of motions are optimally described in the seakeeping frame {s}. By comparison of the model in eq. (2.57) to the nonlinear model in eq. (2.61) it is evident that the linearisation has resulted in neglected dynamics. For example, it is common for potential theory programs to assume that viscous forces can be neglected. In Wadam this has been addressed by adding Morison and Strip theory. As the ROV is not slender, it was decided that a Morison model should not be applied. A quadratic damping term was added in SIMO instead with results from model scaling of full scale model tests of Minerva. See below.

5.1.1 Quadratic Damping

For some cases it is possible to neglect viscous forces on a vessel or structure because they are very small compared to the other forces. This is the case when the vehicle is slender, or large-body. The three ROVs are neither slender nor large-bodied, and as the viscous forces are not calculated in Wadam by default, this needed to be addressed. Morrison theory is used to find the viscous contributions in the equations of motions. This contribution will act as a quadratic damping force (Faltinsen, 1993);

$$F_D = \frac{1}{2}\rho C_D A|u_r|u_r \tag{5.1}$$

where C_D is the drag coefficient, A is the projected area and u_r is the relative velocity in the current direction. Based on model tests done on Minerva and the theses of Kirkeby (2010) and Berg (2012) the drag coefficients will be assumed in the same manner. This assumption is based on the geometrical similarities between ROV Minerva and the proposed ROV designs. Model tests were performed by Ludvigsen and Ødegaard (2004) on Minerva, and results gave $C_{d,1} = 0.87$, $C_{d,2} = 0.99$. Full scale tests performed by Kirkeby (2010) gave $C_{d,3} = 1.05$. The entire nonlinear damping matrix for Minerva is:

$$\boldsymbol{D}_{NL} = \text{diag}(292|u_r|, 584|v_r|, 635|w_r|, 84|\phi_r|, 148|\theta_r|, 100|\psi_r|) \tag{5.2}$$

Using the same coefficients, the nonlinear damping matrix in DOFs 1-3 for MaxiROV becomes:

$$\boldsymbol{D}_{NL}(1:3, 1:3) = \text{diag}(345|u_r|, 611|v_r|, 678|w_r|) \tag{5.3}$$

For MidiROV and MiniROVthe terms are, respectively:

$$\boldsymbol{D}_{NL}(1:3, 1:3) = \text{diag}(181|u_r|, 318|v_r|, 350|w_r|) \tag{5.4}$$

$$\boldsymbol{D}_{NL}(1:3, 1:3) = \text{diag}(99|u_r|, 180|v_r|, 215|w_r|) \tag{5.5}$$

The remaining coefficients for the rotational DOFs can be found using the methodology of model-scaling, comparing Minerva and the three ROVs, as performed and explained in section 3.2.1. Taking the results for Minerva from Kirkeby (2010) and finding the largest scale factor based on the dimensions of Minerva and MaxiROV ($\lambda = 1.0976$), the coefficients were determined to be:

$$\boldsymbol{D}_{NL} = \text{diag}(111|\phi_r|, 196|\theta_r|, 132|\psi_r|) \tag{5.6}$$

The damping will be added as quadratic damping in the Kinetics folder describing the ROVs in SIMO.

5.1.2 Restoring

As linear theory is assumed and analysis in Wadam are performed by presuming surface vessels, this gives the wrong restoring terms, see eq. (2.30). The special case of restoring forces for submerged vessels is not taken into account in the software. The restoring should be calculated as in eq. (2.28). So, the restoring matrix $\boldsymbol{C}$ computed is correct only when the ROVs are floating around their equilibrium point in the surface. Normally, the

ROVs will not be operating in the surface; it will follow the net all the way down to the bottom ring chain.

MaxiROV will be simulated without altering the restoring terms, to show how the ROV acts when placing the ROV at 10 meters depth in Wadam. The quadratic damping terms will still be added to slow down the ROV as it rises. This is necessary for Simo to perform the simulation without errors. The simulation is performed for four arbitrary cases, see the wave elevation in fig. 5.1 and the heave position of the ROV in fig. 5.2. As predicted, the hydrostatic stiffness in heave results in too large total heave force on MaxiROV (the result is exactly equal to $C_{33}\eta_3 = \rho g A_{wp} 10m = 126650N$), see fig. 5.3.

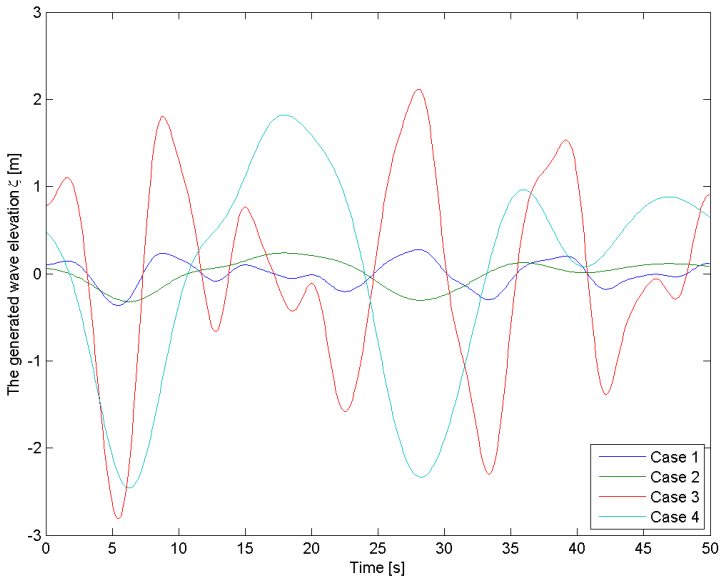

Figure 5.1: Wave elevation, four examples.

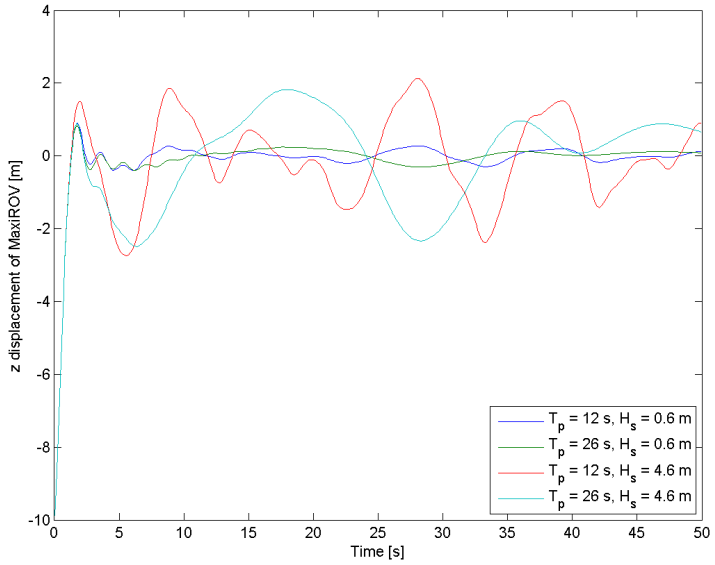

Figure 5.2: The z position of MaxiROV.

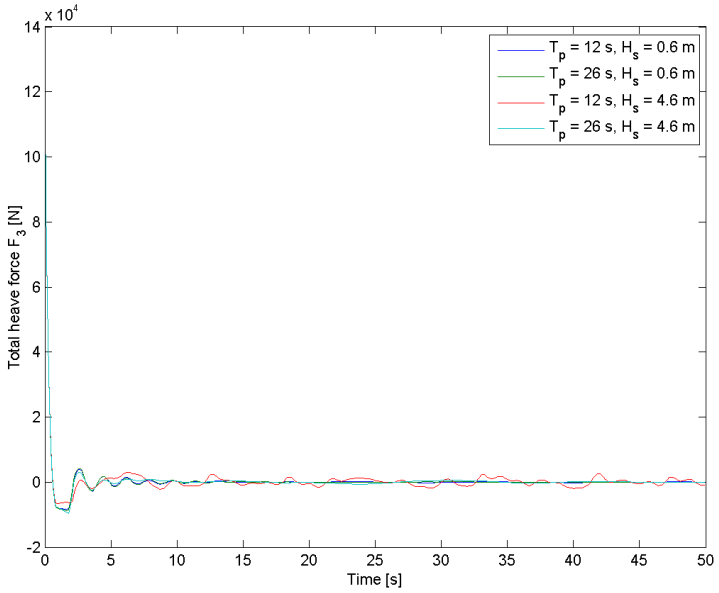

Figure 5.3: The total heave force.

As the control system in SIMO can only control horizontal DOF (surge, sway, yaw), the restoring terms $C_{33,ROV}$ are increased and the reference point for the restoring matrices are set to equal the depth of which the ROVs are situated at. This will force the ROVs to not move in the heave direction, but results for the other DOFs will still be usable. The new restoring matrices are as follows:

MaxiROV

$$\boldsymbol{C}_{alt} = \begin{bmatrix} 0 & 0 & 0 & 0 & 0 & 0 \\ 0 & 0 & 0 & 0 & 0 & 0 \\ 0 & 0 & 400000 & 0 & 0 & 0 \\ 0 & 0 & 0 & 1853 & 0 & 0 \\ 0 & 0 & 0 & 0 & 3066 & 0 \\ 0 & 0 & 0 & 0 & 0 & 0 \end{bmatrix} \tag{5.7}$$

MidiROV

$$\boldsymbol{C}_{alt} = \begin{bmatrix} 0 & 0 & 0 & 0 & 0 & 0 \\ 0 & 0 & 0 & 0 & 0 & 0 \\ 0 & 0 & 100000 & 0 & 0 & 0 \\ 0 & 0 & 0 & 466 & 0 & 0 \\ 0 & 0 & 0 & 0 & 780 & 0 \\ 0 & 0 & 0 & 0 & 0 & 0 \end{bmatrix} \tag{5.8}$$

MiniROV

$$\boldsymbol{C}_{alt} = \begin{bmatrix} 0 & 0 & 0 & 0 & 0 & 0 \\ 0 & 0 & 0 & 0 & 0 & 0 \\ 0 & 0 & 10000 & 0 & 0 & 0 \\ 0 & 0 & 0 & 109 & 0 & 0 \\ 0 & 0 & 0 & 0 & 240 & 0 \\ 0 & 0 & 0 & 0 & 0 & 0 \end{bmatrix} \tag{5.9}$$

5.2 Simulation Environment

The Rataren environment is specified in SIMO using a three parameter Jonswap spectra. The three parameters are H_s, T_p and γ. H_s is taken as the largest value in the H_s class, while T_p is taken as the middle value within the T_p class. The peakedness factor γ is determined from eqs. (2.42) and (2.43), see table 5.1.

Case	H_s [m]	T_p [s]	γ [-]
1	0.5	24.5	1.0
2	0.5	9.5	1.0
3	1.0	10.5	5.0
4	1.0	3.5	1.0
5	1.5	12.5	1.0
6	2.0	17.5	1.0
7	2.5	7.5	1.0

Table 5.1: Simulation environment in SIMO.

5.3 ROV Control System for Active Wave Compensation

Motions of a vehicle influenced by fluid, can, when assuming steady state conditions, be divided in to (Faltinsen, 1993):

- Wave frequency motion/high frequency motion (HF)
- Low frequency motion (LF) and
- Mean drift motion

The WF motion is mainly linearly excited, but does also include a nonlinear component. Nonlinear effects will cause LF motions and mean drift motions. These motions are usually the interest of control strategies for vessels in the ocean, as they are slowly varying and hence more easily controlled. To make sure that the HF motions are not compensated for, it is common to use a *wave filter*.

Wave filtering will protect the thrusters from additional wear and tear, and will cause less fuel consumption. In addition, a vessel might not even have enough power or thrust capacity to overcome these loads. A wave filter is certainly necessary for a ship, or for operations outside the wave zone, where first order wave loads are small compared to for instance current. The focus of this thesis, however, is on ROVs in the wave zone. In this area, the first order wave loads will be the dominating forces, and thus, a wave filter will not be suitable for the application of wave compensation. It is however, of interest to remove measurement noise and to compute the velocity, which is possible in an observer.

5.4 Design of Control System

This section will describe the structure and tuning of a controller and an observer. The main objective of this feasibility study is to find out if an ROV can operate through automatic control in the wave zone. Different controllers have been evaluated at an early stage of this work. SIMO does not have an interface for development of internal control systems, but it is possible to develop external controllers and connect it to models in SIMO. Due to simplicity, a control system structure already developed in SIMO has been chosen for this feasibility study. The system includes a proportional, integral and derivative (PID) controller, and a Kalman filter, as developed by Balchen et al. (1980).

This control structure is intuitive and the behaviour of the system is easily changed. Some alterations to the Kalman filter must be done, as it does filter the HF motions. The procedure is explained in section 5.4.3. Only the horizontal motions are controlled, surge (1), sway (2) and yaw (6). The ROV is assumed stable in roll (4) and pitch (5), as explained in section 3.1. Results from time domain simulations will also illustrate this, see section 5.6.2. It is not preferable to neglect the heave motion; however, when dealing with software that assumes surface vessels, it seems to be an advantage. This is because of the wrongly computed restoring matrix and the linearity assumption. Henceforth, the heave DOF has been fixed and the heave motions registered are constantly equal to the depth of which the ROVs are operating.

5.4.1 Design of DP Controller

The objective of a dynamic positioning (DP) system is, following the definition of Det Norske Veritas (DNV) (2011), to use the vehicles thrusters to maintain a fixed location or a predetermined trajectory. The maintenance tasks of an ROV operating on a fish farm, is within this scope. This can be illustrated by envisioning the ROV pursuing a path generated to follow the contours of the net, while cleaning the net or, making sure there are no tears or other damages in the net. As mentioned, the DP system in SIMO will be used. The inputs and outputs to the DP systems are:

In:

Position measurement

Wind measurement

Thrust measurement

Out:

Desired thrust from the thrusters

5.4.2 DP Control Structure

The controller used by SIMO (DNV Software, 2014a) for DP operations in surge, sway and yaw is a PID controller (Proportional, integral and derivative). The control law is:

$$F_{T0} = K_D\dot{\epsilon}(t) + K_p\epsilon(t) + K_I\int_0^t \epsilon(\tau)d\tau \tag{5.10}$$

$$\epsilon(t) = x_0 - x(t) \tag{5.11}$$

$$\dot{\epsilon}(t) = \dot{x}_0(t) - \dot{x}(t) \tag{5.12}$$

where $x(t)$ is the filtered position, $x_0(t)$ is the desired position and $\epsilon(t)$ is the position error. F_{T0} is the desired control force from thrusters and K_D, K_P and K_I are the derivative, proportional and integral feedback gains.

5.4.3 Tuning of DP Controller

The controller is tuned as explained in (Fossen, 2011, Chapter 12.2.3), where added mass and desired natural periods are taken as a starting point for tuning:

$$K_p = m\omega_n^2 \tag{5.13}$$

$$K_d = 2\zeta\omega_n m \tag{5.14}$$

$$K_i = \frac{\omega_n}{10}K_p \tag{5.15}$$

Taking desired natural period T_n as 100 s and a damping ratio ζ of 0.7, the gains for surge, sway and yaw for the three ROVs is:

$$K_{p,Maxi} = \text{diag}\{108.3, 135.0, 22.9\}$$
$$K_{d,Maxi} = \text{diag}\{75.8, 94.5, 16.0\}$$
$$K_{i,Maxi} = \text{diag}\{0.68, 0.85, 0.14\}$$

$$K_{p,Midi} = \text{diag}\{35.3, 43.0, 3.9\}$$
$$K_{d,Midi} = \text{diag}\{24.7, 30.1, 2.7\}$$
$$K_{i,Midi} = \text{diag}\{0.22, 0.27, 0.02\}$$

$$K_{p,Mini} = \text{diag}\{8.0, 9.4, 0.6\}$$
$$K_{d,Mini} = \text{diag}\{5.6, 6.6, 0.4\}$$
$$K_{i,Mini} = \text{diag}\{0.05, 0.06, 0.004\}$$

These gains does not yield optimal performance, and new gains will be decided from trial and error. The new coefficients for MaxiROV are:

$$K_{p,Maxi} = \text{diag}\{29.6, 34.3, 98.7\}$$

$$K_{d,Maxi} = \text{diag}\{659.7, 765.3, 628.3\}$$

$$K_{i,Maxi} = \text{diag}\{0.19, 0.22, 0.62\}$$

For MidiROV they are:

$$K_{p,Midi} = \text{diag}\{9.9, 11.1, 1.2\}$$

$$K_{d,Midi} = \text{diag}\{220.0, 246.3, 26.4\}$$

$$K_{i,Midi} = \text{diag}\{0.062, 0.070, 0.008\}$$

And for MiniROV the gains are:

$$K_{p,Mini} = \text{diag}\{2.5, 2.9, 0.2\}$$

$$K_{d,Mini} = \text{diag}\{56.3, 65.1, 3.5\}$$

$$K_{i,Mini} = \text{diag}\{0.016, 0.018, 0.001\}$$

5.4.4 Results from Tuning

The controllers were tuned during simulation of the ROVs in calm sea, i.e. Case 8. The simulation is performed over 2000 seconds, or 33.3 minutes, to be sure that the controllers are not unstable. Desired positions are set to 2 meters, 4 meters and 15 degrees for surge, sway and yaw. In the following figures, the behaviour of MaxiROV when changing the gains are displayed (figs. 5.4 to 5.6). MidiROV and MiniROV will be tuned in the same manner and the results are very similar to the following figures. The plots are shorted down to 200 seconds for better readability. The gains are changed by a factor of 10^k, where k is -1 and 1 for the proportional and derivative part and k is -2 and 2 for the integral part:

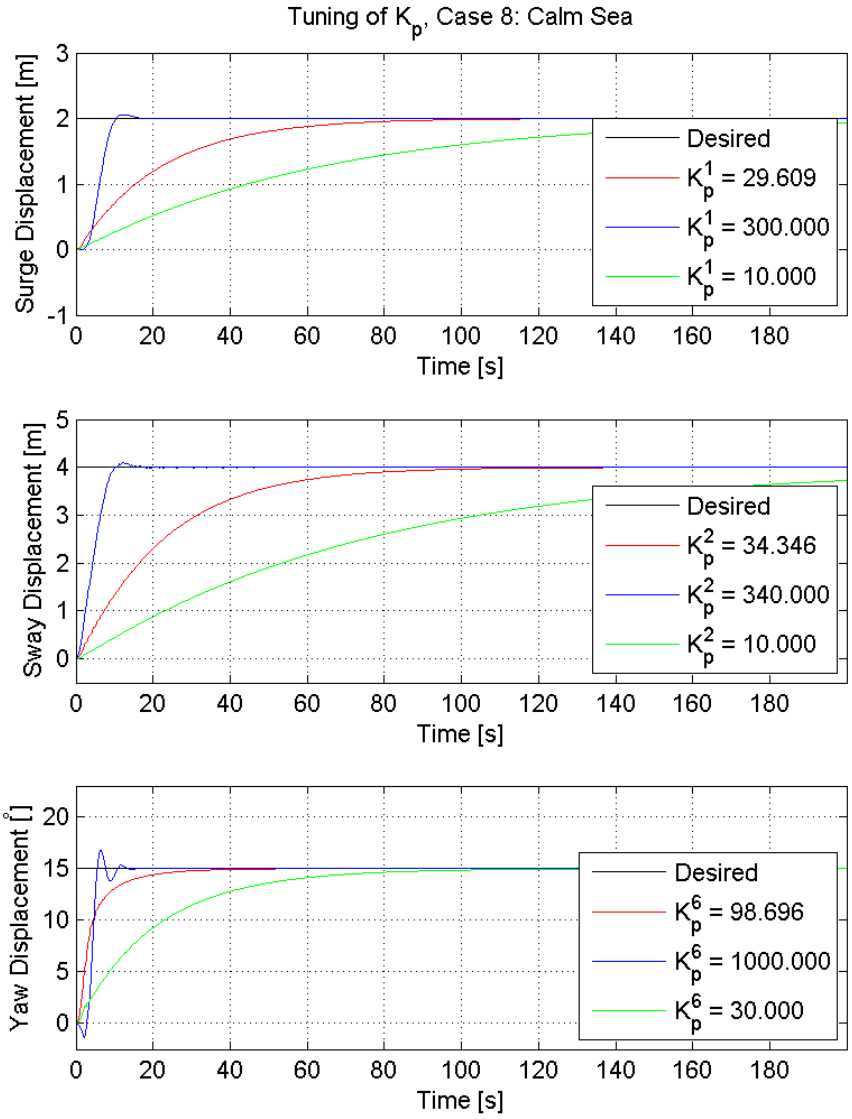

Figure 5.4: Surge, sway and yaw performance of MaxiROV for different K_p.

K_p decreased by a factor of 10^{-1} made the system unstable, so the decreased gains are decreased to 30% instead. The red lines are the performance of MaxiROV with the chosen proportional gains. In all the DOFs, the red lines give a fast enough controller, and no overshoot. When no waves are present, the ROV is expected to move smoothly towards

its desired position. If increasing the proportional gains, the system acts really fast, making the ROV go slightly passed its desired position. Considering that the ROVs will be operating at exposed locations, it will most likely be an advantage that the ROV moves relatively slow. In this way the system will hopefully not push the ROV past its desired position, as large wave loads are also interacting with the vehicle. Still, the maintenance tasks must be performed within an acceptable time limit, and the ROV can not use several minutes to obtain one (of many) desired position. Thus, the smaller proportional gains (green lines) are rejected, as more than three minutes passes before the ROV acquires its position. Next are the derivative gains:

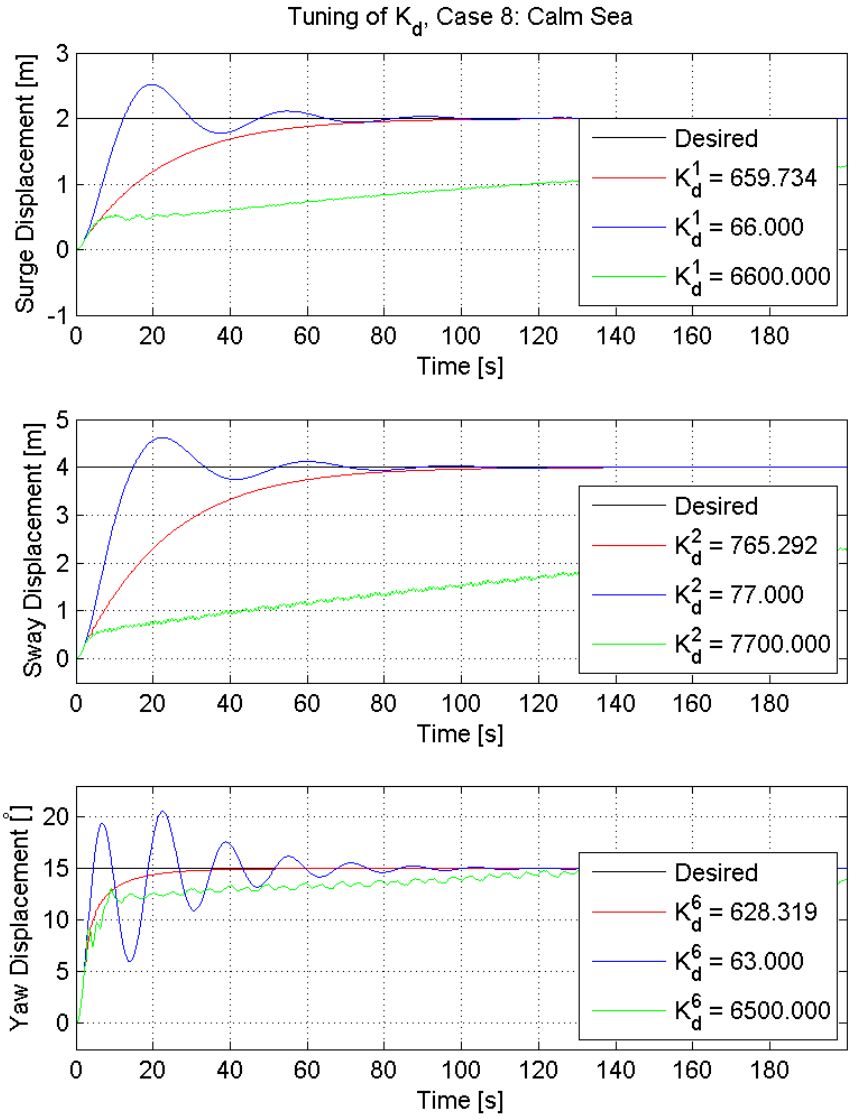

Figure 5.5: Surge, sway and yaw performance of MaxiROV for different K_d.

Again, it is expected that the ROV moves smoothly with no overshoot in calm water. The red lines represent the preferred behaviour. Increasing the gain (green lines) makes the system more slow and yields small local variations which are unwanted. Decreasing the gains (blue lines) increases the overshoot a great deal and yields a longer transient behaviour in yaw. The behaviour of the ROV is not sensitive to small change in the integral gains and is for this reason decreased and increased by 10^{-2} and 10^{2} instead:

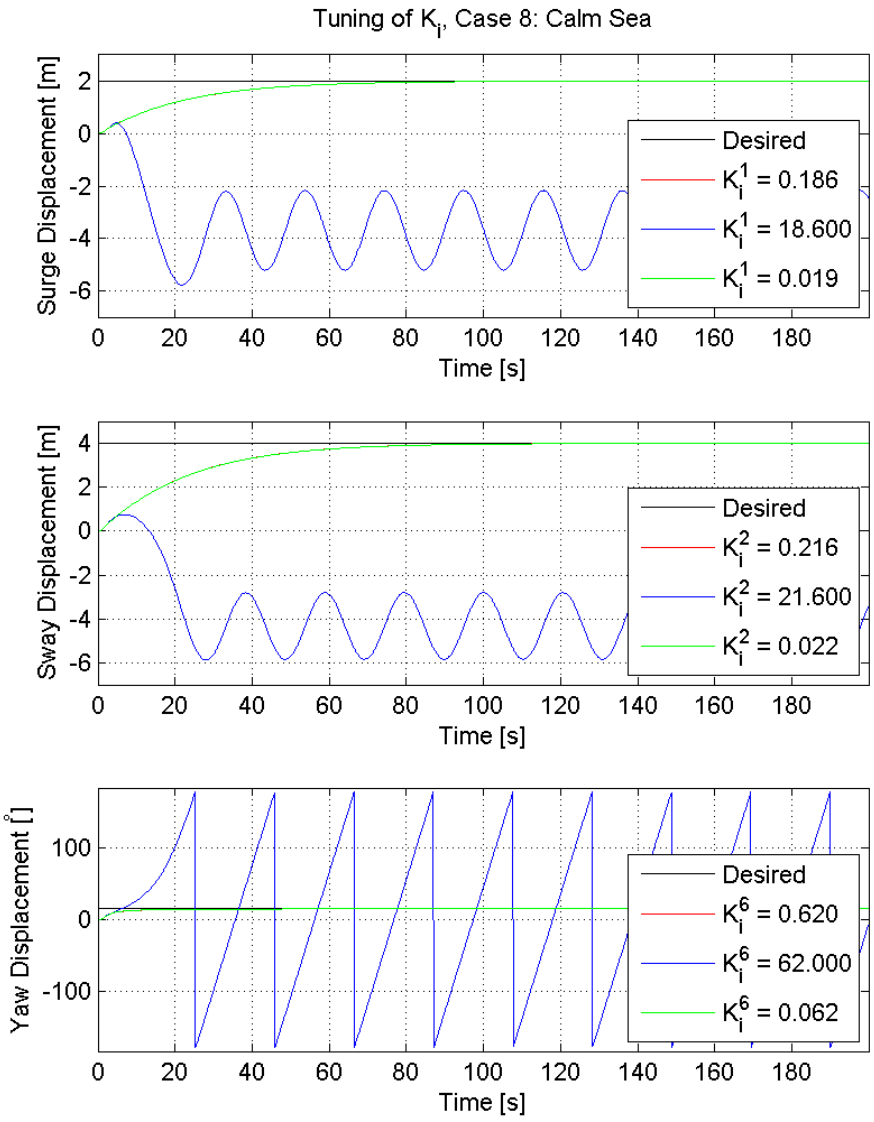

Figure 5.6: Surge, sway and yaw performance of MaxiROV for different K_i.

When amplifying the integral term (blue lines), the ROVs performance is not acceptable. The ROVs is spinning and the mean position in surge and sway is more than 6 meters off. An attenuation of the term resulted in very similar behaviour as the original gains, the green lines almost completely covers the red lines.

5.5 Design of Observer

As mentioned, the observer is a Kalman filter developed by Balchen et al. (1980). The observer will be able to perform optimal estimation of vessel motions and environmental loads from waves. It includes a feedback from the motions where the HF motion is removed, as common in wave filters. It also includes a feedforward from the wind force estimates. The design is originally an extended Kalman filter, simplified to decrease heavy computational loads by a series of approximations. The surge-, sway- and yaw-motions of the vessel is assumed decoupled in the measurements, so that if a prediction error in

one of the measurements does not induce an update of the position and velocity of the other measurements. The motions are still coupled in the prediction model.

Design of Kalman Filter

The Kalman filter consists of a low pass (LP) filter and a wave filter (WF). The LP decreases measurement noise and differentiate the measurements, which gives an estimate of the velocity. The WF is a band-stop filter. It lets most frequencies pass through, and attenuates frequencies in a specific "band" around a given frequency.

Slowly varying forces caused by second order wave forces and current can be estimated either by estimating the global current velocity or local bias forces. Inputs and outputs to the Kalman filter are:

Constants in:

$\boldsymbol{\eta}_{ref} = [x_{ref}, y_{ref}, \psi_{ref}]^\top$ - Position reference.

$\boldsymbol{\eta}_{loc} = [x_{loc}, y_{loc}]^\top$ - Point of vehicle to be positioned.

$\boldsymbol{C}_d = [C_{d,x}, C_{d,y}, C_{d,\psi}]^\top$ - Quadratic drag coefficients.

v_{typ} - Typical velocity, used for linearising quadratic damping, default: $v_{typ} = 0.25$ m/s.

$\boldsymbol{M} = \text{diag}(M_{11}, M_{22}, M_{66})$ - Mass and added mass.

$\boldsymbol{R}_{3\times 2}$ - Kalman filter gain matrix.

$\boldsymbol{G}_{3\times 2}$ - Linear controller matrix.

Variables in:

$\boldsymbol{F}_m = [F_{m,x}, F_{m,y}, F_{m,\psi}]^\top$ - Measured forces.

$\boldsymbol{\eta}_m = [x_m, y_m, \psi_m]^\top$ - Measured position of body origin.

Out:

$\boldsymbol{F}_T = [F_{T,x}, F_{T,y}, F_{T,\psi}]^\top (= \boldsymbol{tau})$ - Thrust demand

The state variables of the filter include:

$\boldsymbol{\eta}_{LF} = [x_{LF}, y_{LF}, \psi_{LF}]^\top$ - LF position

$\dot{\boldsymbol{\eta}}_{LF} = [\dot{x}_{LF}, \dot{y}_{LF}, \dot{\psi}_{LF}]^\top$ - LF velocity.

$\boldsymbol{F}_B = [F_{B,x}, F_{B,y}, F_{B,\psi}]^\top / \boldsymbol{v}_c = [v_{c,x}, v_{c,y}]^\top$ - Local bias force/current velocity.

$\boldsymbol{\eta}_{HF} = [x_{HF}, y_{HF}, \psi_{HF}]^\top$ - HF position.

$\dot{\boldsymbol{\eta}}_{HF} = [\dot{x}_{HF}, \dot{y}_{HF}, \dot{\psi}_{HF}]^\top$ - HF velocity.

$\boldsymbol{\omega} = [\omega_x, \omega_y, \omega_\psi]^\top$ - Oscillation frequency.

Additional variables in the filter:

$\boldsymbol{\delta} = [\delta x, \delta y, \delta\psi]^\top$ - Positioning error.

$\boldsymbol{\epsilon} = [\epsilon_x, \epsilon_y, \epsilon_\psi]^\top$ - The innovations.

The innovations represent the difference between the position measurement from the vehicle and the estimated measurements in the filter. These variables are multiplied by the Kalman filter gains and used to update the state variables. The equations within the routines in the filter are further described in the SIMO theory manual (DNV Software, 2014a). The initial gains are determined from the input constants:

$$\begin{aligned} G(1,1) &= -\frac{2\pi}{T_x}M_{11} \qquad G(1,2) = -2\xi_x\sqrt{G(1,1)M_{11}} \\ G(2,1) &= -\frac{2\pi}{T_y}M_{22} \qquad G(2,2) = -2\xi_y\sqrt{G(2,1)M_{22}} \\ G(3,1) &= -\frac{2\pi}{T_\psi}M_{66} \qquad G(3,2) = -2\xi_\psi\sqrt{G(3,1)M_{66}} \end{aligned}$$

where T_x, T_y and T_ψ are the chosen natural period and ξ_x, ξ_y and ξ_ψ are the damping factors, which typically is 0.7. Through trial and error these parameters will be chosen, investigating the error in position of the vehicles. The resulting parameters are for all three ROVs:

$$\begin{aligned} T_x = 100s, \quad T_y = 100s, \quad T_\psi = 100s \\ \xi_x = 0.1, \quad \xi_y = 0.1, \quad \xi_\psi = 0.1 \end{aligned}$$

The initial Kalman filer gain matrix is:

$$\begin{aligned} R(1,1) &= 2\xi_x\omega_{c,x} \qquad R(1,2) = \omega_{c,x}^2 \\ R(2,1) &= 2\xi_y\omega_{c,y} \qquad R(2,2) = \omega_{c,y}^2 \\ R(3,1) &= 2\xi_\psi\omega_{c,\psi} \qquad R(3,2) = \omega_{c,\psi}^2 \end{aligned}$$

where the cut off frequency ω_c is set below the peak frequency in each ROVs first order wave force transfer function for DOFs 1, 2 and 6.

$$\begin{aligned} MaxiROV &: T_{c,x} = 1.2s, \qquad T_{c,z} = 1.2s, \qquad T_{c,\psi} = 0.8s \\ MidiROV &: T_{c,x} = 1.2s, \qquad T_{c,z} = 1.2s, \qquad T_{c,\psi} = 0.8s \\ MiniROV &: T_{c,x} = 1.2s, \qquad T_{c,z} = 0.8s, \qquad T_{c,\psi} = 0.8s \end{aligned}$$

Different starting periods for wave frequency estimation will be tested ranging from 0.1 s to the average peak periods to 1800 s. For very low values the ROV behaviour was unstable. When increasing the value the vehicles became stable, but due to inadequate results in yaw, the starting period was set to 1800 s for all ROVs.

5.6 Results

5.6.1 Retardation Functions

As stated by Fossen (2011) and Ogilvie (1964) the retardation functions should converge to zero as $t \to \infty$. Equation (2.59) implies that when $\omega = \infty$, $\boldsymbol{B}_{total}(\omega) - \boldsymbol{B}_{total}(\infty)$ is exactly zero. So, the retardation functions should die out. Some programs uses eq. (2.24) to calculate the functions instead. When using numerical integration this will produce small oscillations as $t \to 0$. Also, the asymptotic values of $\boldsymbol{K}(t)$ when $t \to 0$ should never be zero. Figure 5.7 is consistent with these properties of $\boldsymbol{K}(t)$. A time step of 0.100 s is used to compute the functions. **Comment:** The figure does not properly show the

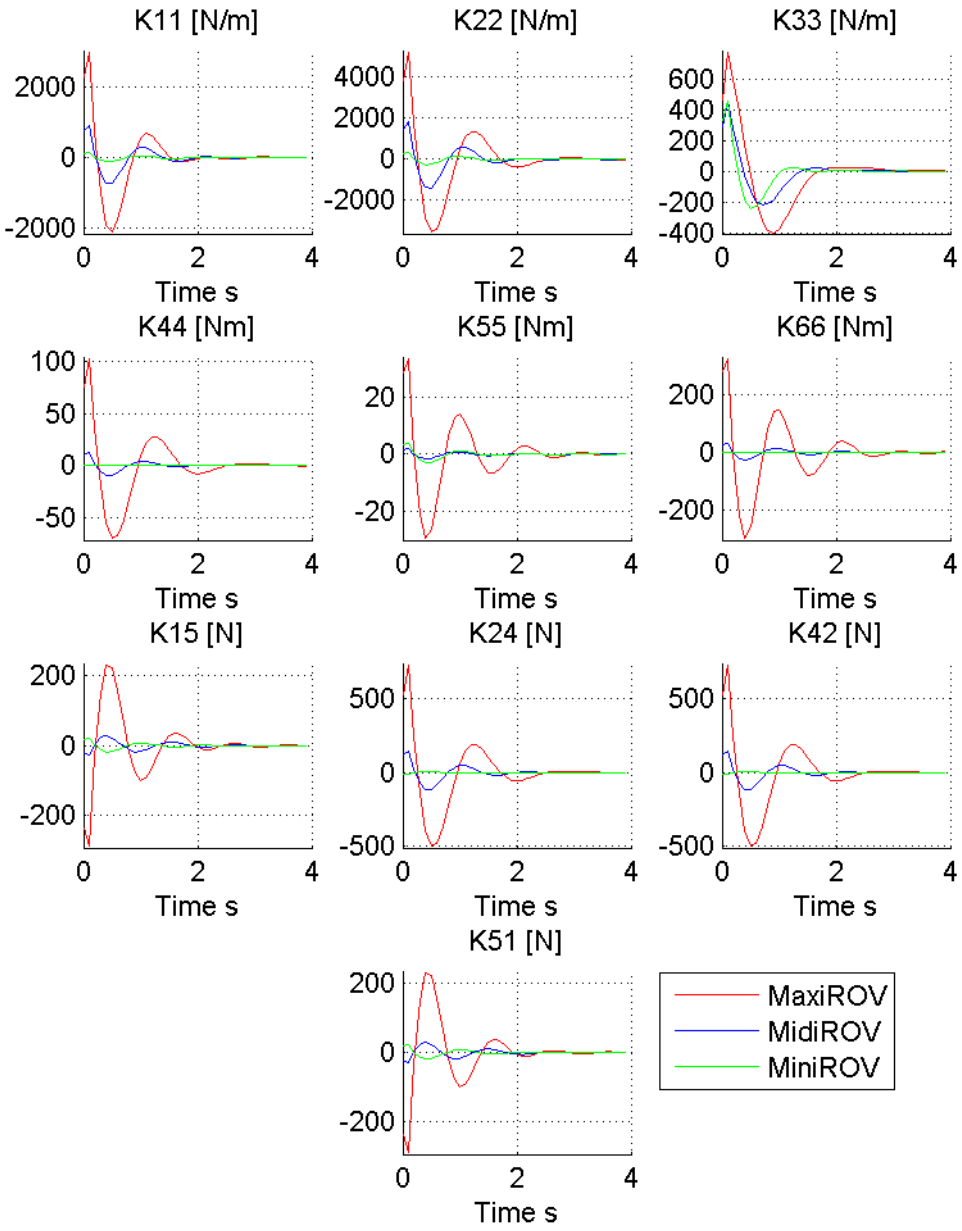

Figure 5.7: The retardation functions $\boldsymbol{K}(t)$ for MaxiROV, MidiROV and MiniROV.

retardation functions for MiniROV, as the smallest ones $K_{44}(t)$ and $K_{66}(t)$ have maximum values of 0.27 Nm (at $t = 0.1s$) and 1.67 Nm (at $t = 0.1s$). Their starting values are $K_{44}(0) = 0.214$ Nm and $K_{66}(0) = 1.433$ Nm.

5.6.2 Stability in Pitch and Roll

The stability in roll and pitch are investigated in this section. As the results for depth 20 meters are very similar to the results at 10 meters depth, the results of the largest depth are not shown here. In any case, as the wave loads decay exponentially with the depth, they ROVs should display better results. Only Cases 1, 2, 4, 5, 7 and 8 are discussed here, as these results are representable also for Cases 3 and 6. In general the amplitude of the displacement angle in pitch is expected to be larger than in roll, as the ROVs are operating in mostly head sea, and a desired angle smaller than 45°.

Case 1

All the ROVs display stability in roll and pitch for this sea state. The simulation duration is 2000 seconds. For better readability a smaller section of the time series is shown here. This is the case with the highest occurrence.

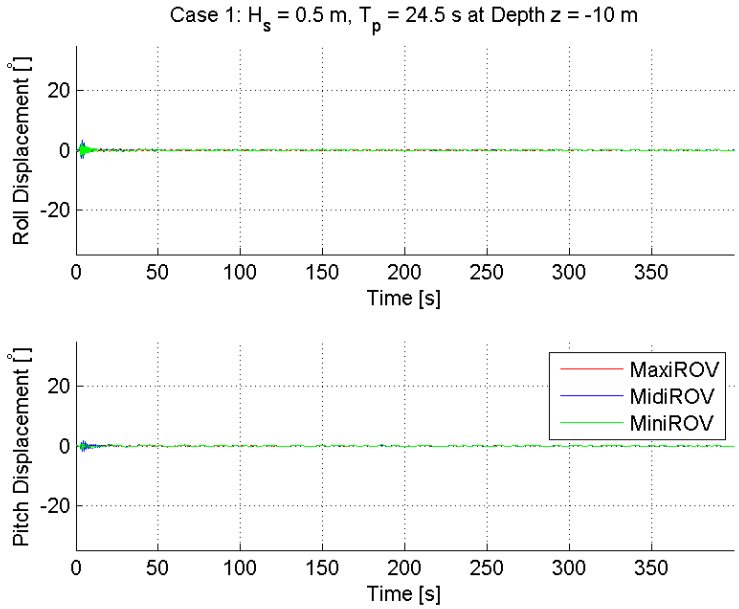

Figure 5.8: Roll and pitch of ROVs, Case 1 at depth 10 m.

Case 2

Both MidiROV and MiniROV display desired behaviour in Case 2. Their displacements are small, and stable. MaxiROV however has a higher displacement, especially in pitch. This perturbation is on the limit of what is acceptable. In roll the perturbations are justifiably small.

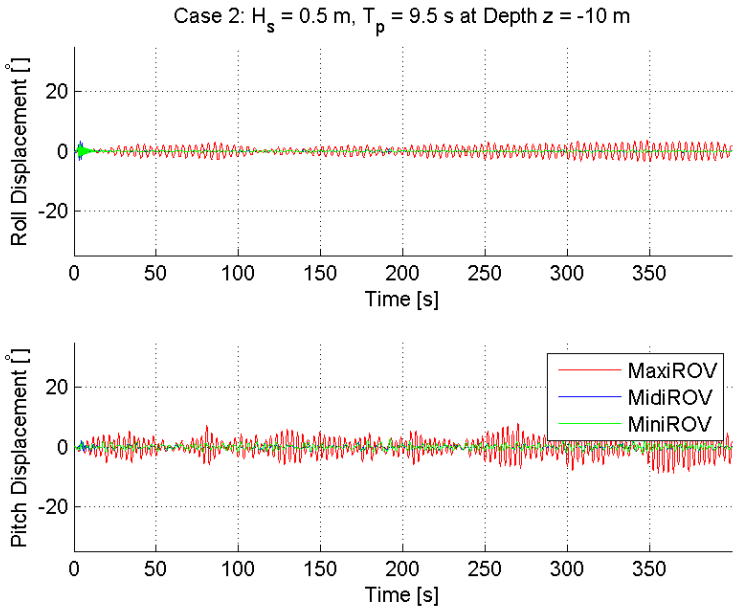

Figure 5.9: Roll and pitch of ROVs, Case 2 at depth 10 m.

Case 4

Case 4 is a rougher sea state, which still results in adequate results for MidiROV and MiniROV in roll. The ROVs are exceeding 10° and more in pitch and MaxiROV's transverse righting arm does not seem to be satisfactory large.

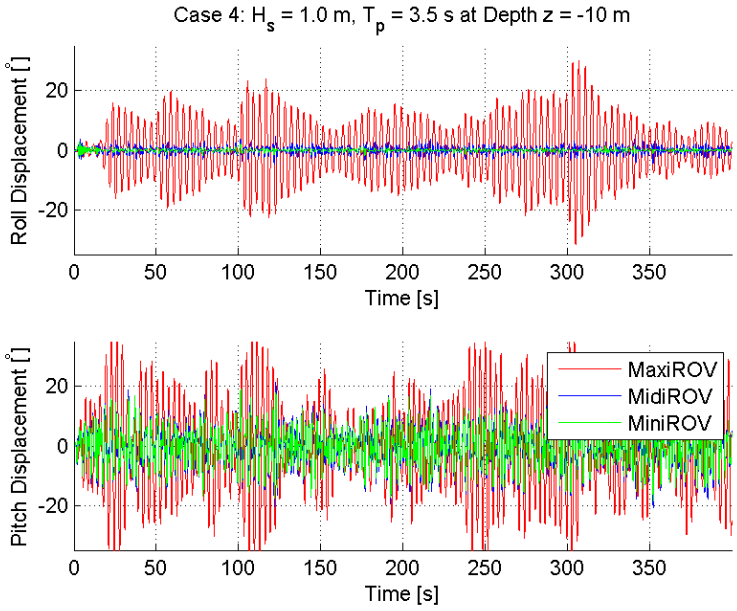

Figure 5.10: Roll and pitch of ROVs, Case 4 at depth 10 m.

Case 5

Stability in pitch and roll is achieved for both MidiROV and MiniROV. MaxiROV's resulting pitch and roll displacement are not satisfactory in this case.

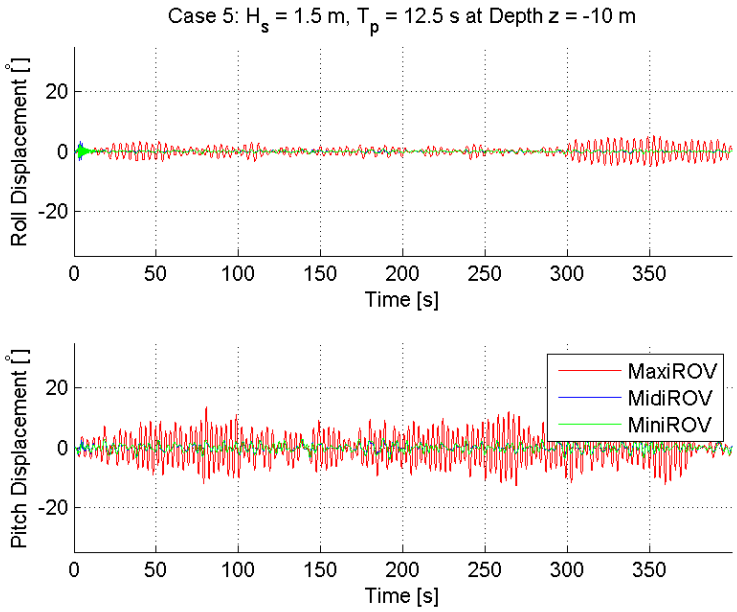

Figure 5.11: Roll and pitch of ROVs, Case 5 at depth 10 m.

Case 7

In Case 7 the significant wave height is quite large (2.5 m) and the period is a fairly common one at the aquacultural site. Again the values for MaxiROV are severe and will

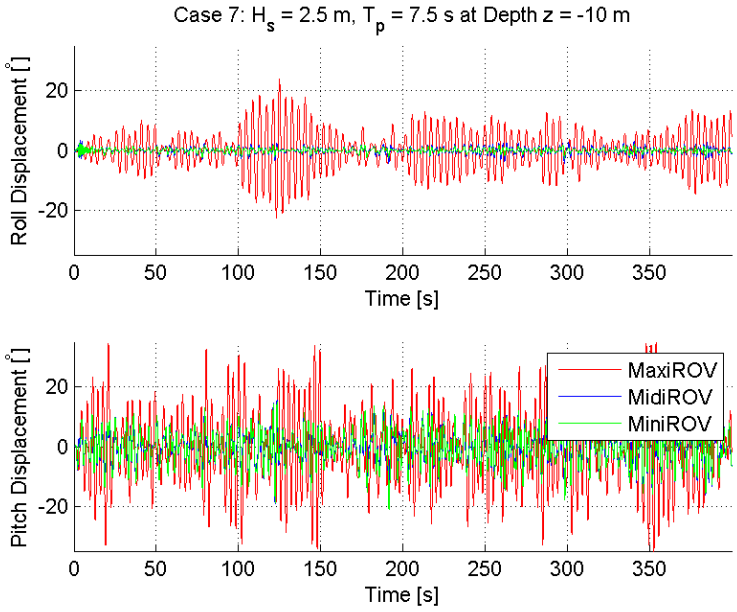

Figure 5.12: Roll and pitch of ROVs, Case 7 at depth 10 m.

result in unacceptable working conditions. The roll angles of MidiROV and MiniROV are acceptable; however, the pitch angles are close to 10°.

Case 8

In calm sea all three ROVs show exemplary behaviour as both pitch and roll angles are close to zero. The largest angle observed in Case 8 among the ROVs is 3.5 °, which only occurs within the transient period.

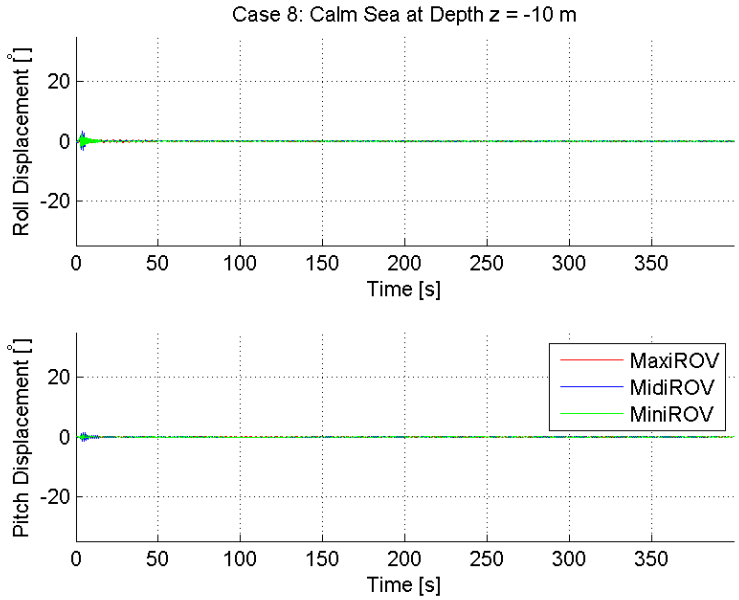

Figure 5.13: Roll and pitch of ROVs, Case 8 at depth 10 m.

5.6.3 ROV Position Performance at Depth 10 m

The time series for surge, sway and yaw displacement for all three ROVs are presented here. The results for depths 10 and 20 meters are very similar, and for this reason the results at 20 meters depth is placed in Appendix D. The total simulation length is again 2000 seconds, but due to readability, a smaller set of results are presented here.

When evaluating the ROVs performance, it is important to be aware of the tasks at hand. For this thesis those tasks are identified as visual inspection of the netpen as well as washing of the netpen. The desired position has been set to $x = 2$ m, $y = 4$ m and ψ =15°. The performance is accepted if the ROVs can maintain the desired position without larger deviations than 0.5 m in position and about $\pm$ 5 degrees in heading. In addition to time series of the ROVs positions, the generated wave elevation is given in figs. 5.14, 5.17, 5.20, 5.23, 5.26, 5.29 and 5.32.

Case 1

As the desired yaw angle is set to 15 degrees, the angle from the ROVs starting position towards the desired position is $\arctan(4/2) = 63.4°$, and so the desired heading angle is

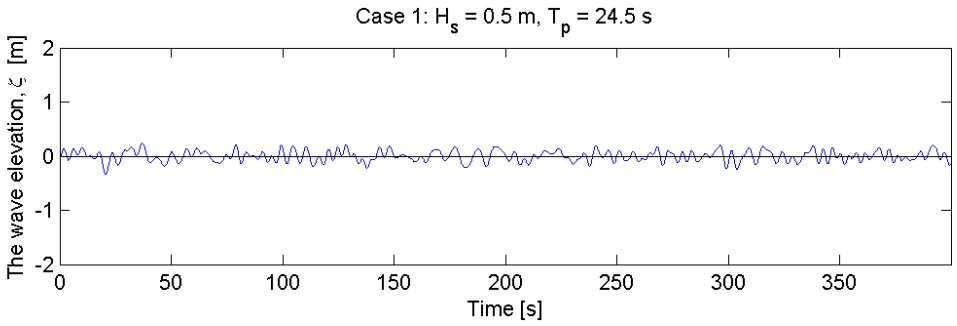

Figure 5.14: The generated wave elevation for Case 1.

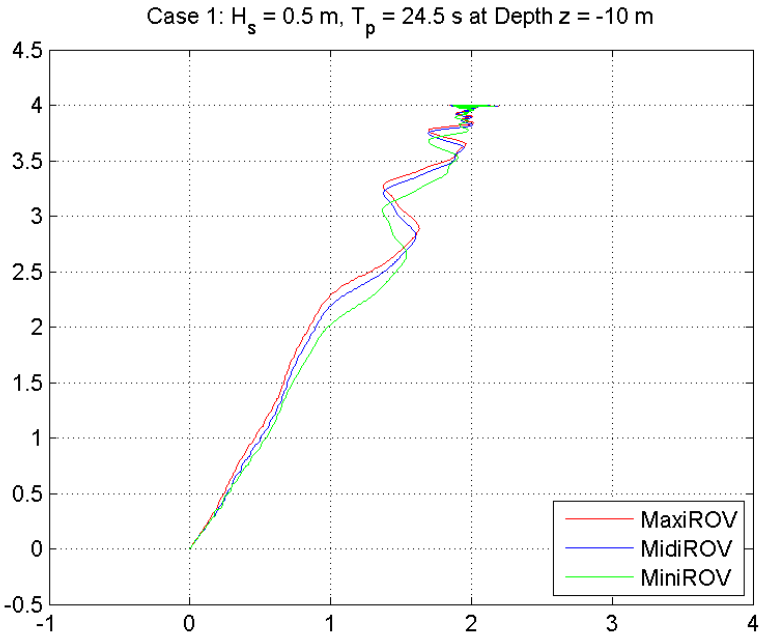

Figure 5.15: XY position of ROVs, Case 1 at depth 10 m.

not optimal. This is easily seen in the xy plot, fig. 5.15, as the ROVs cradle from side to side as they move towards the desired position. The desired position is reached after about 90 seconds, with sway performance better than the surge performance due to head sea. The performance in Case 1 is highly acceptable.

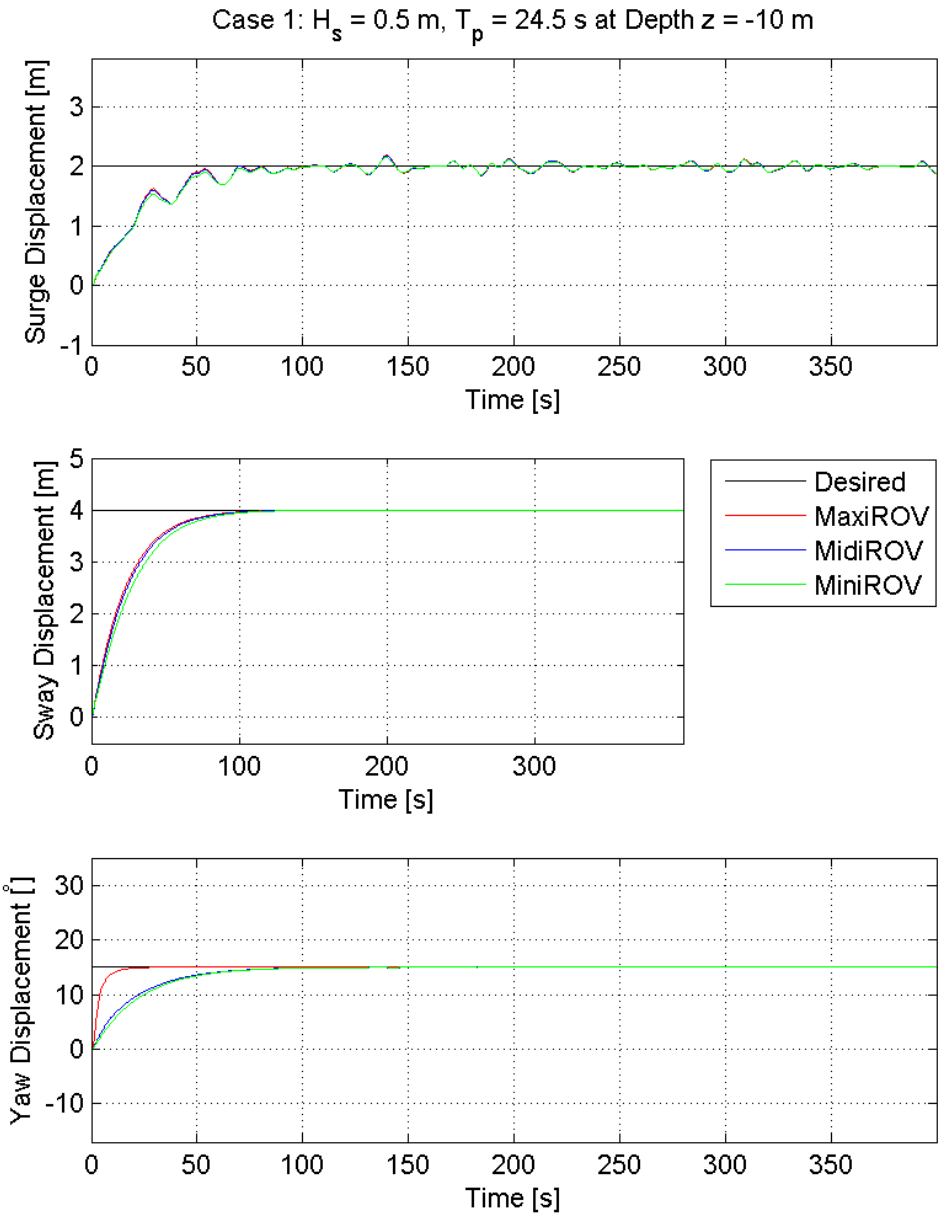

Figure 5.16: Position of ROVs, Case 1 at depth 10 m.

Case 2

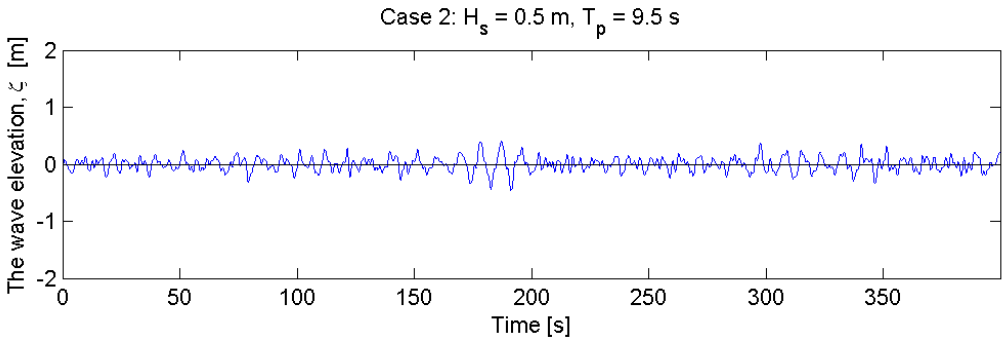

Figure 5.17: The generated wave elevation for Case 2.

Case 2 has large occurrence at Rataren. The positions varies around the desired position, but within the acceptance criteria. The ROVs again cradle towards the desired position, which is obtained after about 100 seconds. The sway displacements are smooth and the ROVs are constantly in the correct y-position. The ROVs are struggling a bit more to stand still, but the deviations are still acceptable.

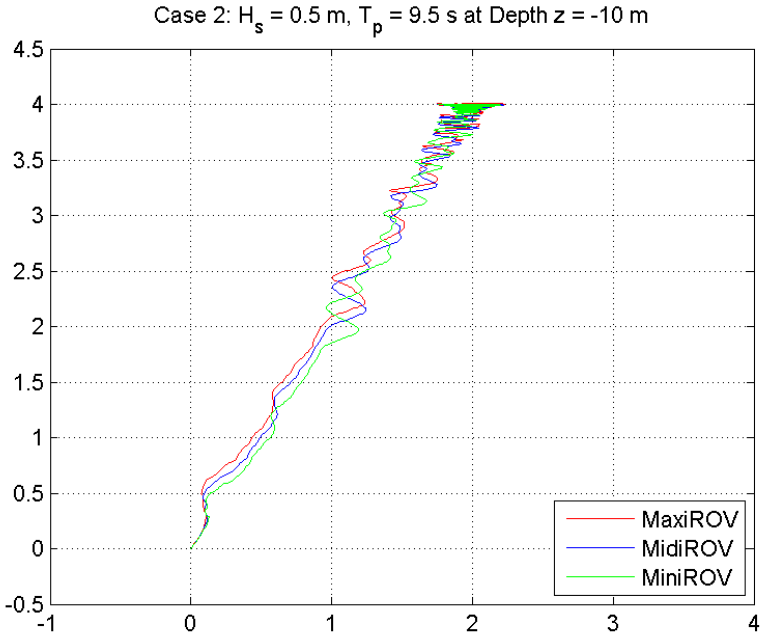

Figure 5.18: XY position of ROVs, Case 2 at depth 10 m.

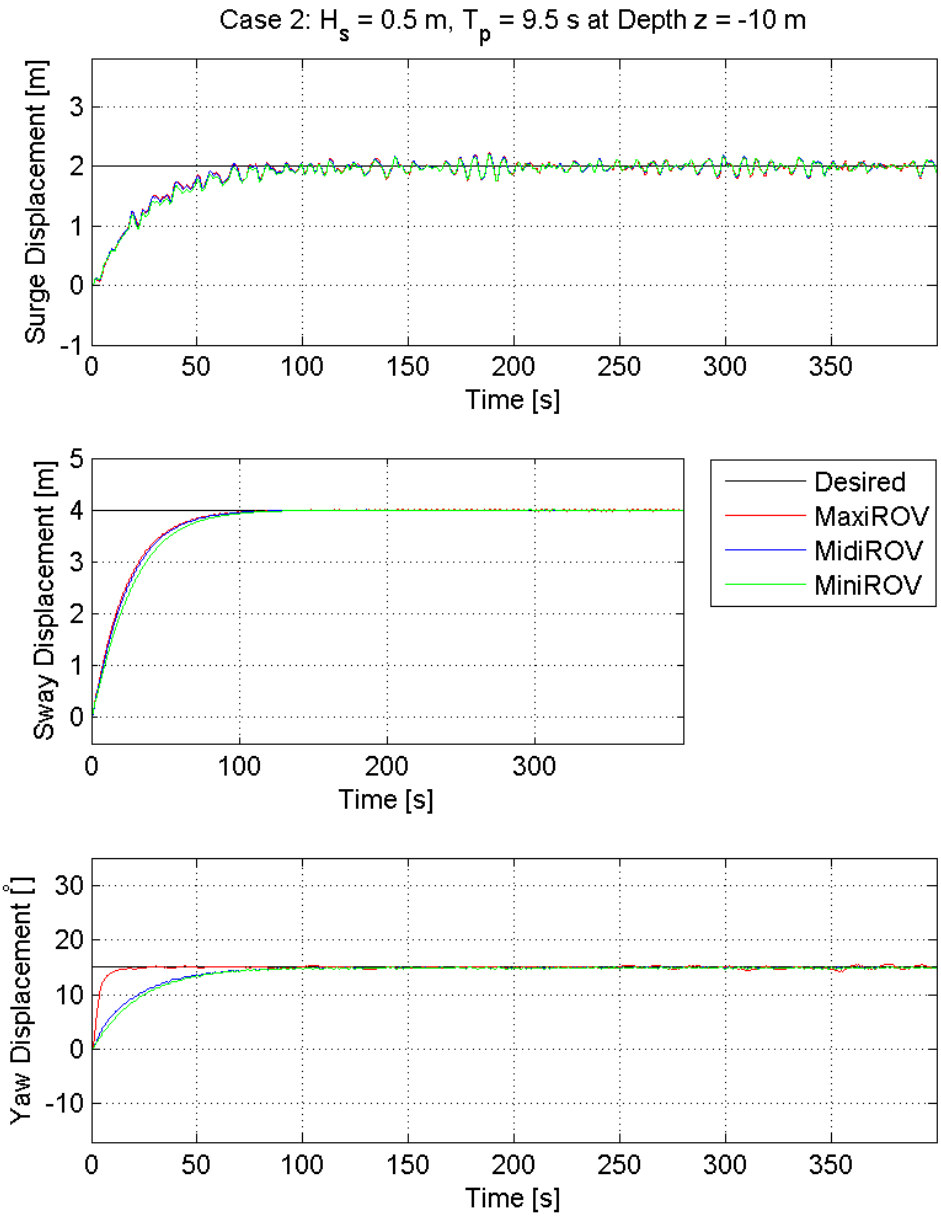

Figure 5.19: Position of ROVs, Case 2 at depth 10 m.

Case 3

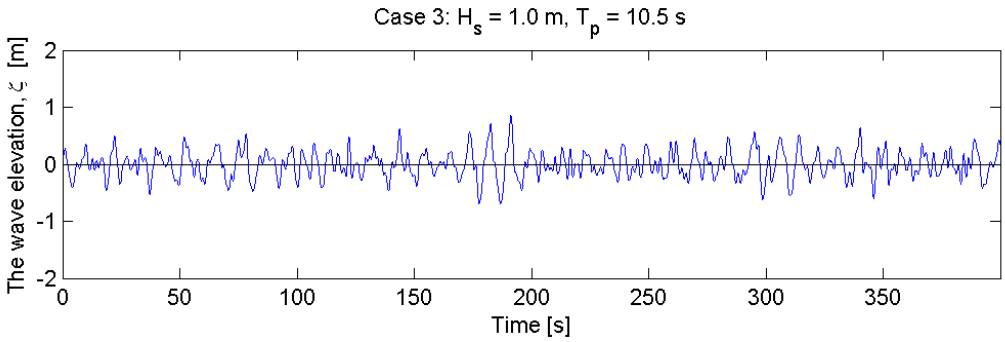

Figure 5.20: The generated wave elevation for Case 3.

In Case 3 the sea state and generated wave elevation in fig. 5.20 is fairly similar to Case 2. As so are the results. The only difference is the magnitude of the deviations in x-position. This is due to the 0.5 m increase in H_s. The results are still within the acceptable limits of operation.

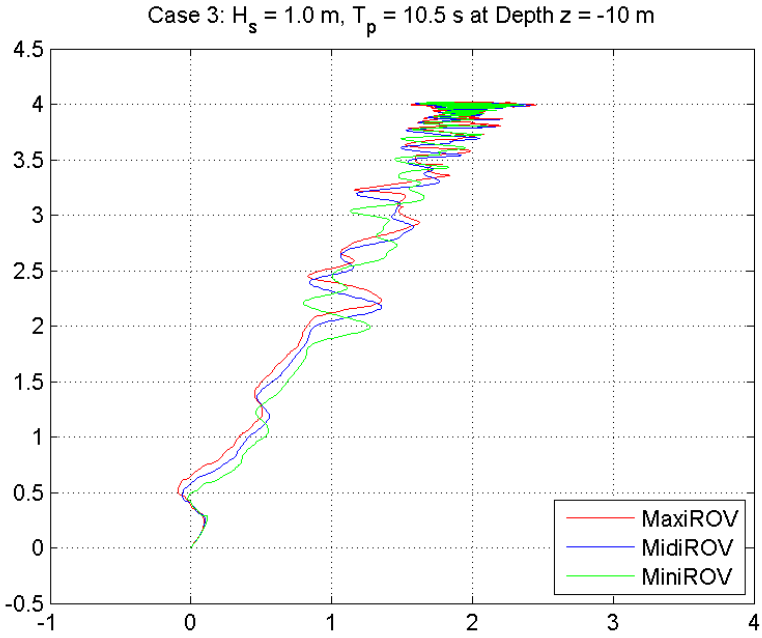

Figure 5.21: XY position of ROVs, Case 3 at depth 10 m.

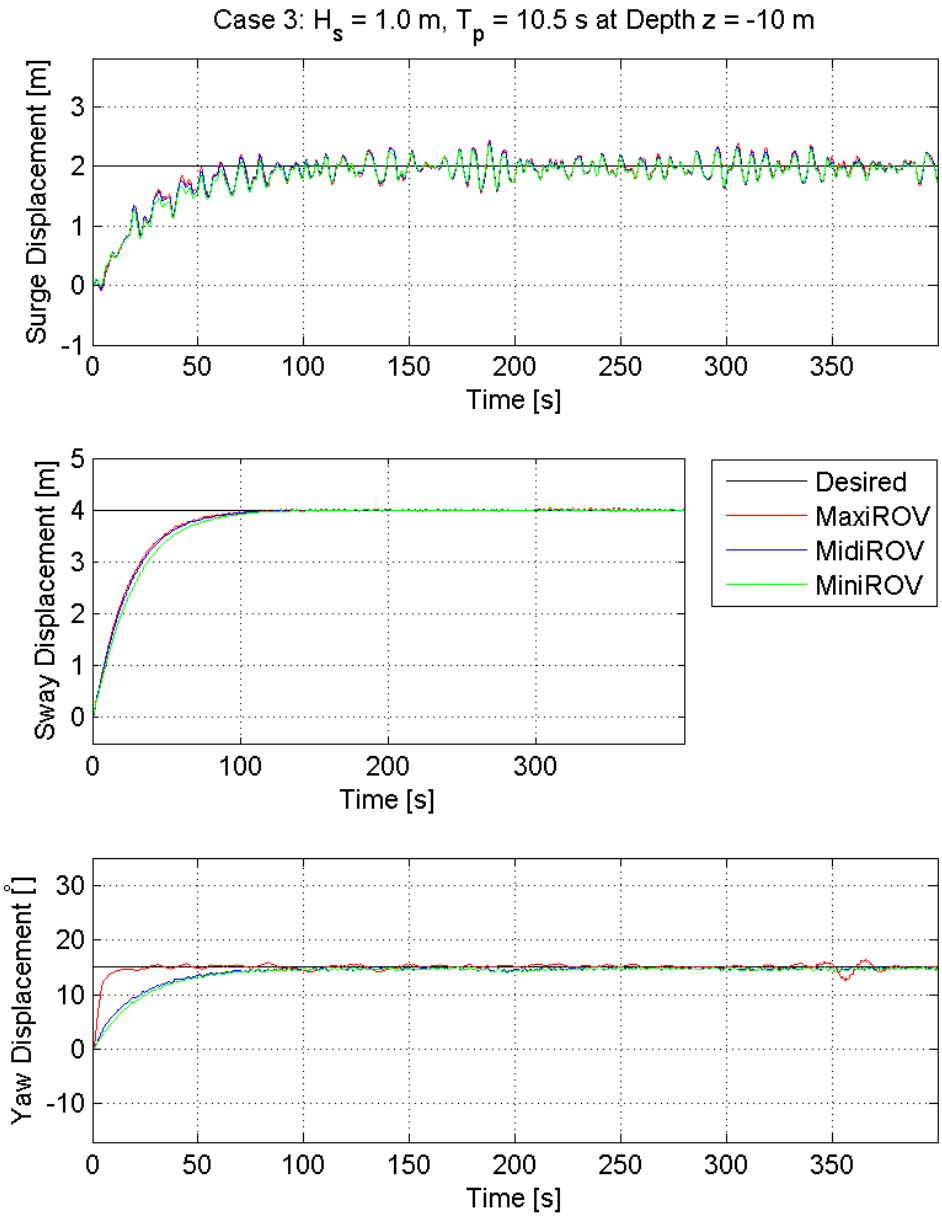

Figure 5.22: Position of ROVs, Case 3 at depth 10 m.

Case 4

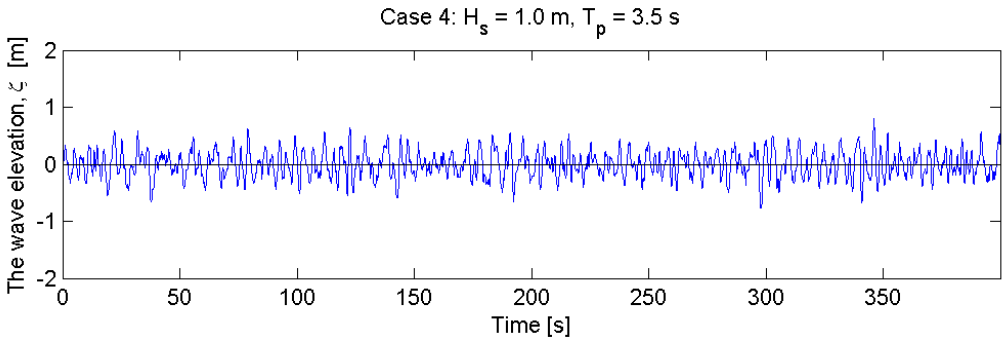

Figure 5.23: The generated wave elevation for Case 4.

As seen when pitch and roll displacement were presented for this case, the ROVs are heavily influenced by the wave loads. The deviations in xy-position are only barely crossing the limit, but the heading angle is unfortunately quite large. The ROVs should not operate in this sea state.

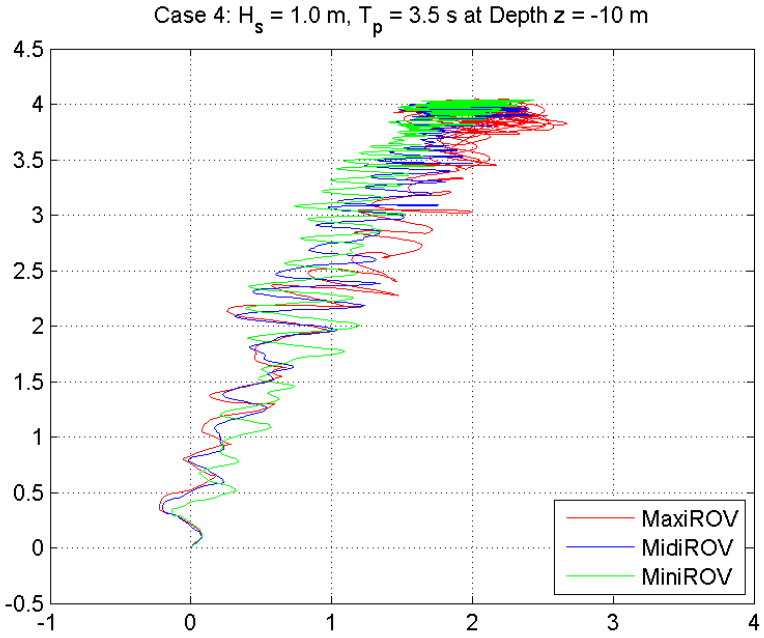

Figure 5.24: XY position of ROVs, Case 4 at depth 10 m.

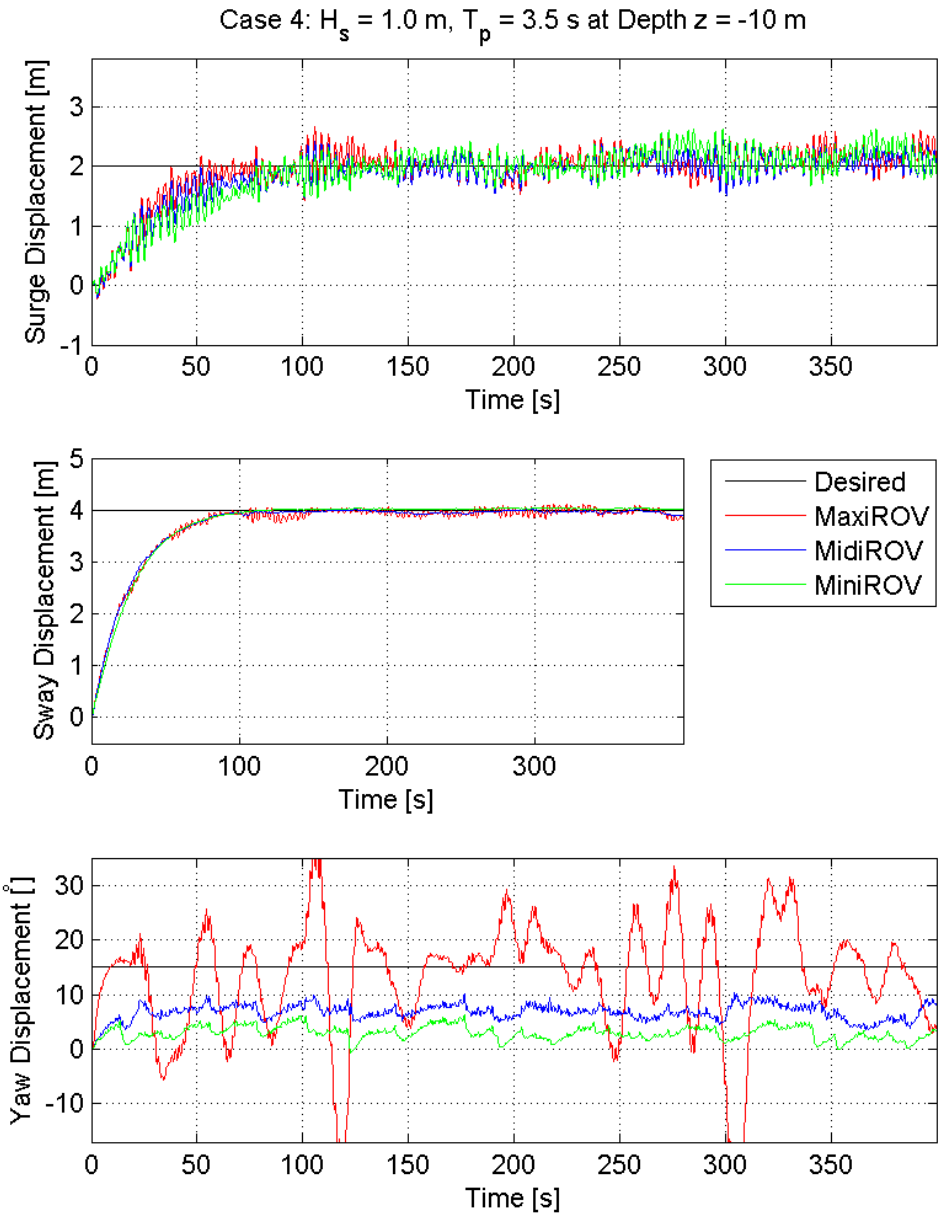

Figure 5.25: Position of ROVs, Case 4 at depth 10 m.

Case 5

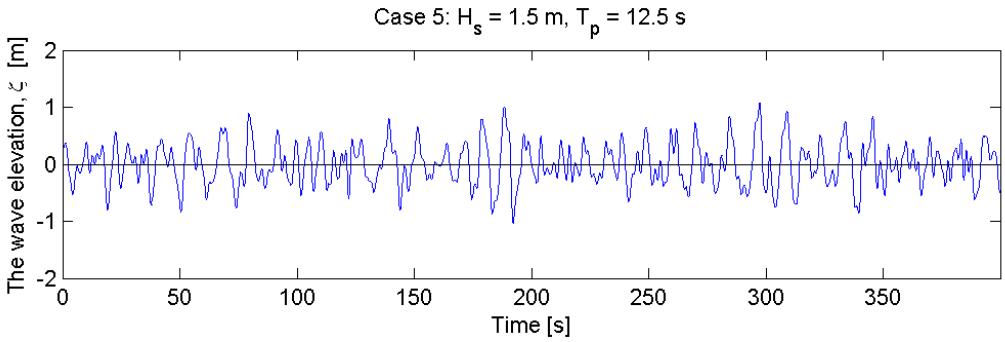

Figure 5.26: The generated wave elevation for Case 5.

In Case 5 H_s is increased to 1.5 m. The performance in yaw and sway are quite satisfactory. However, the displacement in surge is close to the limiting criteria. For such large H_s an evaluation should be performed at the site as continuing operations may provide bad maintenance and even damage to the net.

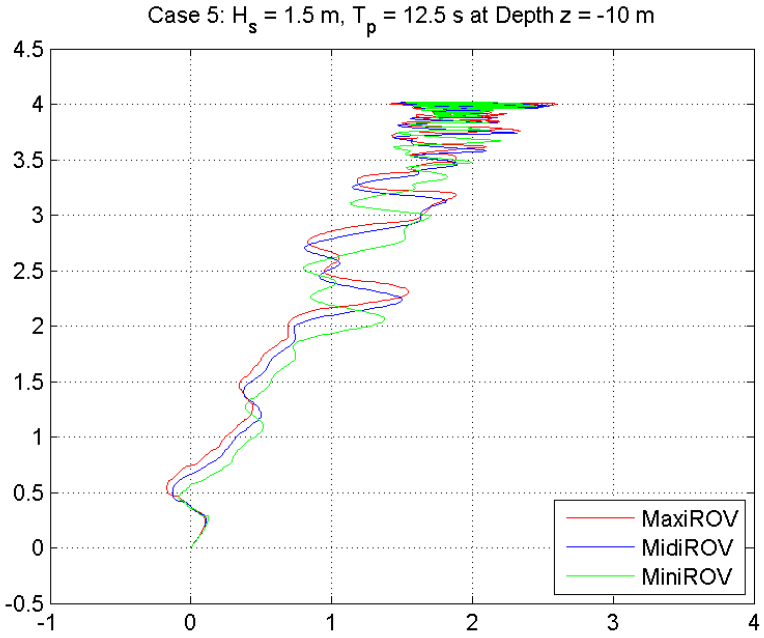

Figure 5.27: XY position of ROVs, Case 5 at depth 10 m.

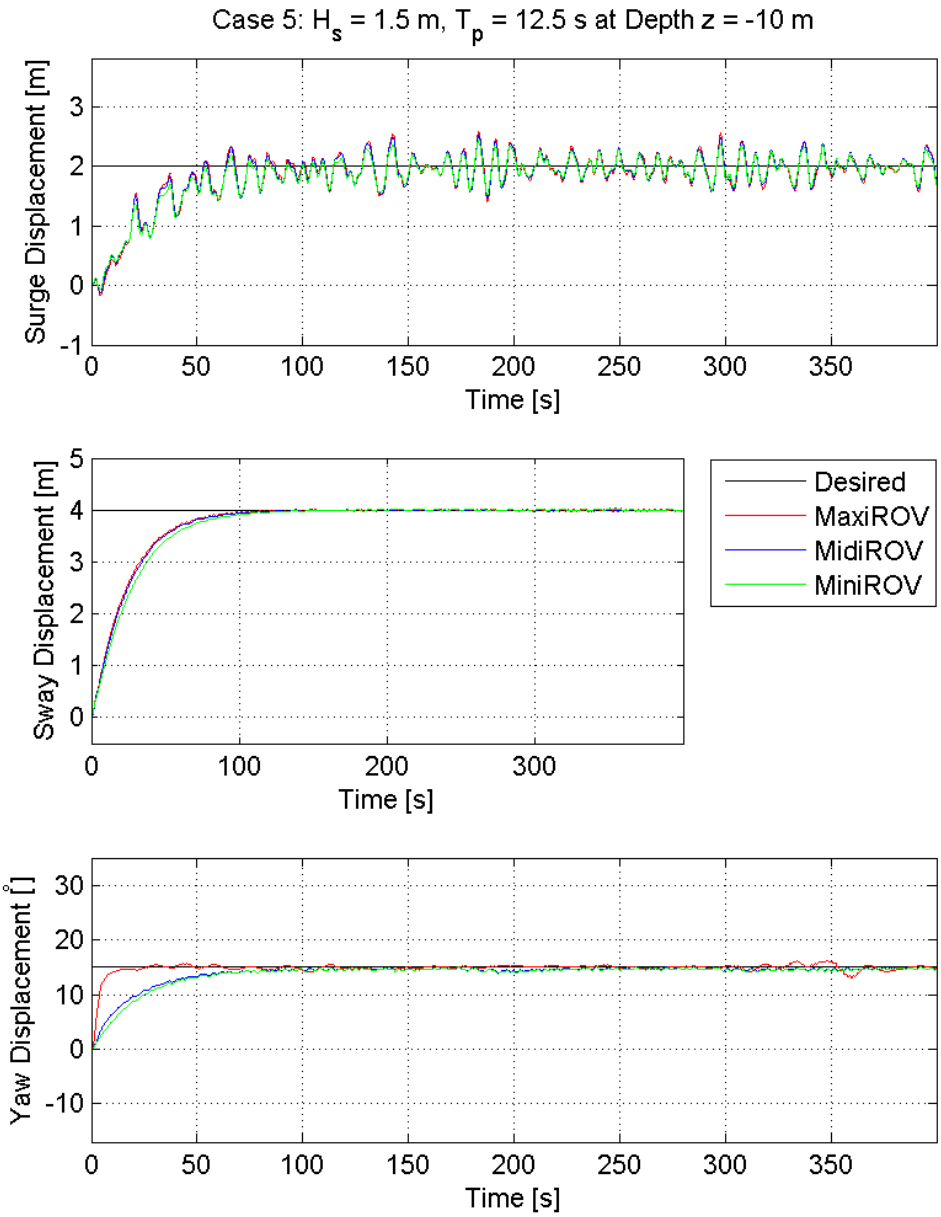

Figure 5.28: Position of ROVs, Case 5 at depth 10 m.

Case 6

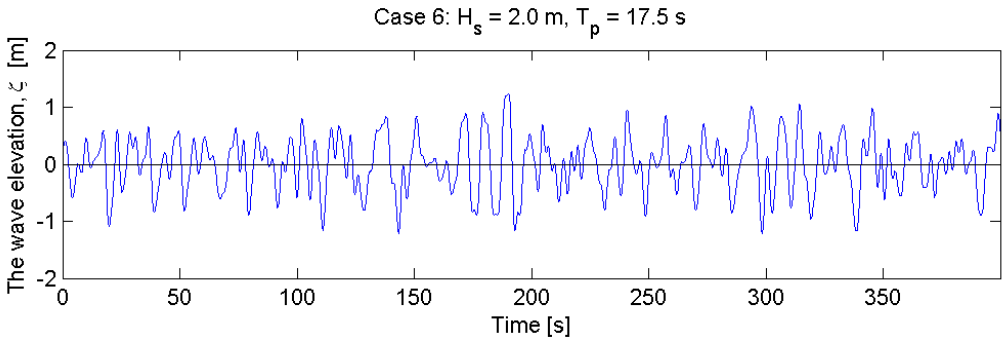

Figure 5.29: The generated wave elevation for Case 6.

Case 6 shows similar results as Case 5, however the surge deviations are even larger. The ROV mostly stays within the acceptable criteria, but has off jumps which pass the acceptable limit.

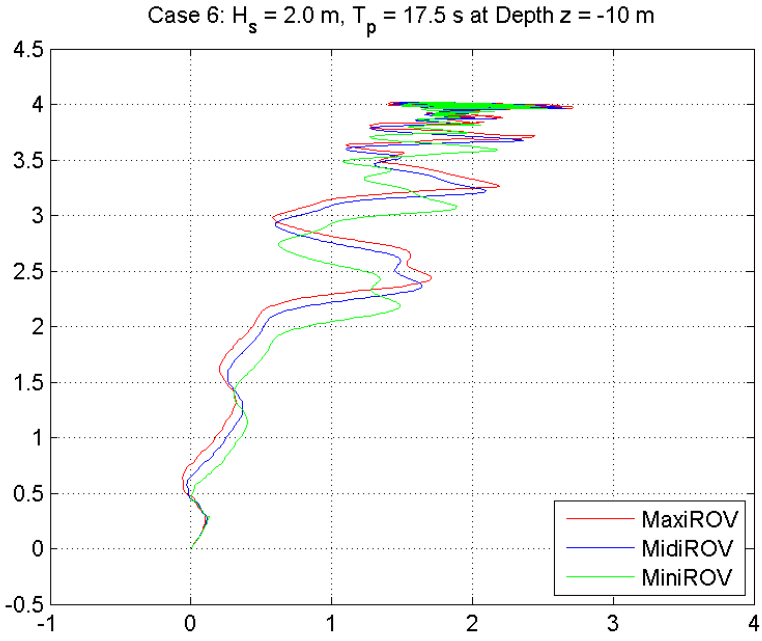

Figure 5.30: XY position of ROVs, Case 6 at depth 10 m.

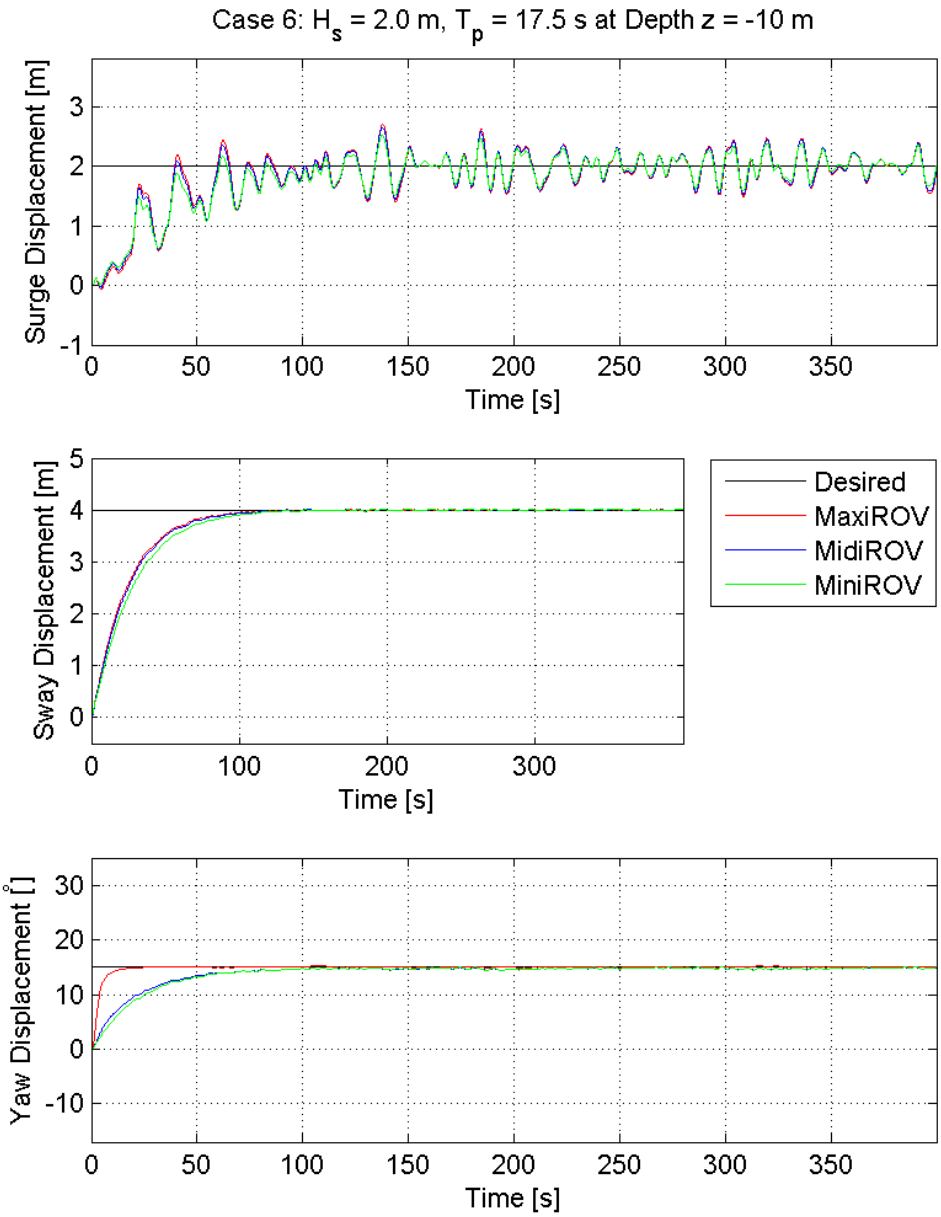

Figure 5.31: Position of ROVs, Case 6 at depth 10 m.

Case 7

Now H_s is 2.5 m and the results are certainly not satisfactory. The ROVs should not operate in this sea state.

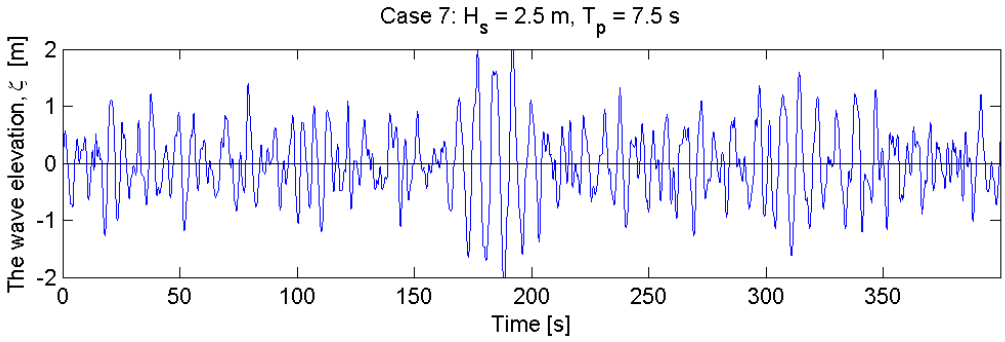

Figure 5.32: The generated wave elevation for Case 7.

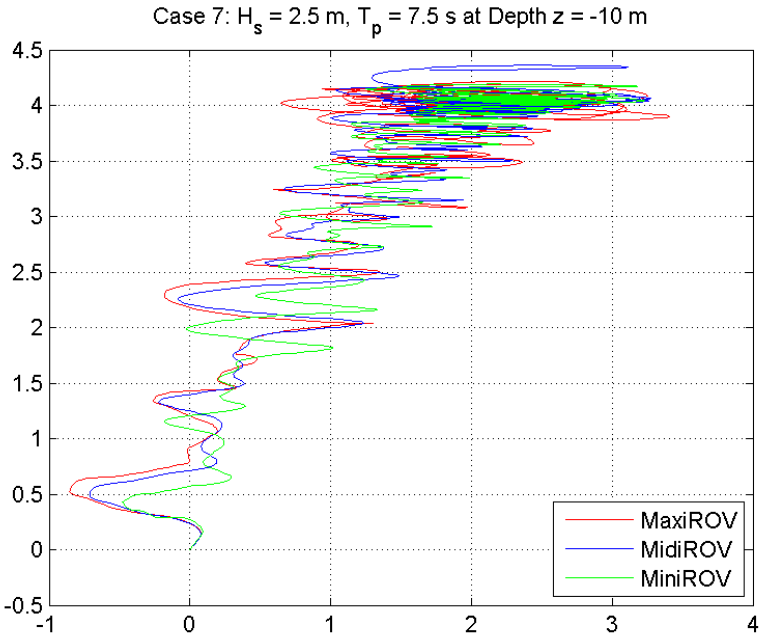

Figure 5.33: XY position of ROVs, Case 7 at depth 10 m.

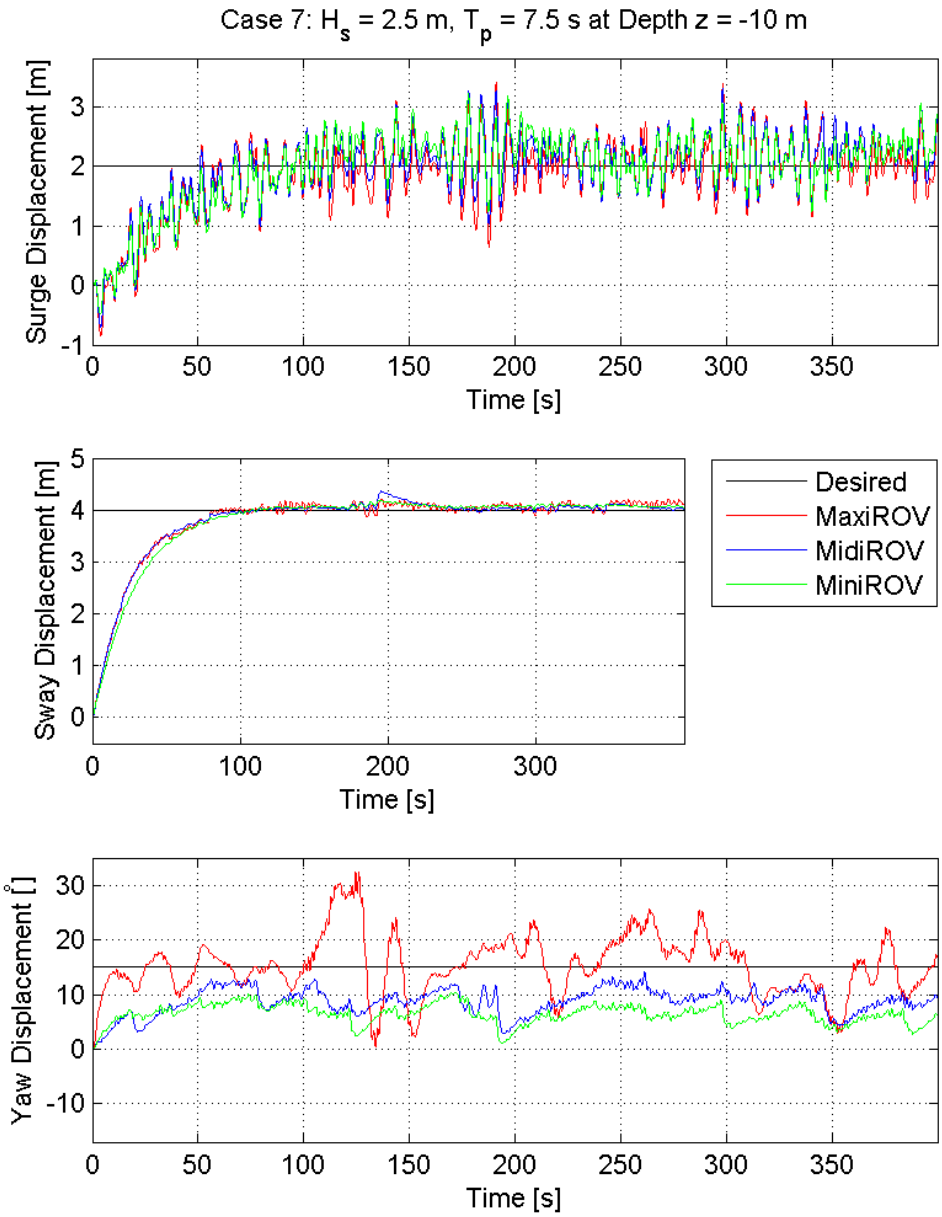

Figure 5.34: Position of ROVs, Case 7 at depth 10 m.

Case 8

There are no generated waves, as Case 8 is calm sea. At calm sea, the ROVs again display exemplary behaviour.

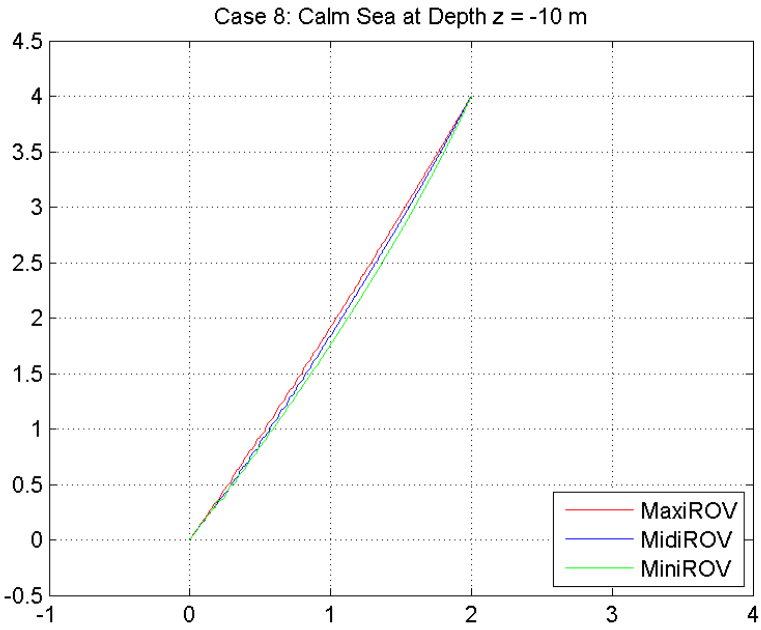

Figure 5.35: XY position of ROVs, Case 8 at depth 10 m.

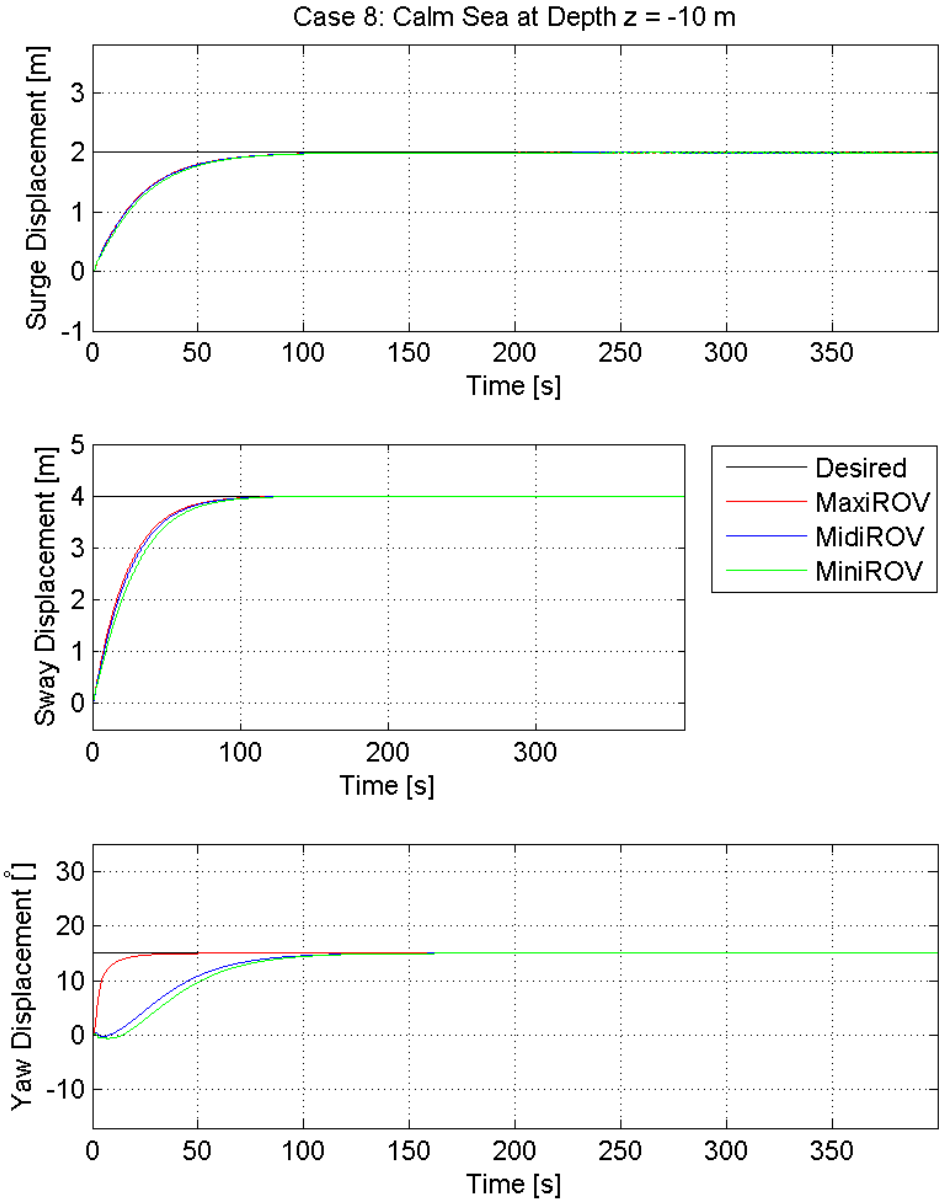

Figure 5.36: Position of ROVs, Case 8 at depth 10 m.

5.6.4 Total Force

During the simulation, the total force exerted by the thruster system is logged. The maximum absolute values (or the $\mathcal{L}_\infty$ norms) are found and given in table 5.2. The values are taken as the maximums after a short period of transient effects have stopped, about 20 seconds in to the simulation time. In the table all thrust values that have exceeded the determined maximum thrust capacity of table 3.4 are highlighted with a color. Red is used for severe exceedance, while orange represents less severe cases.

Depth $[m]$	ROV	DOF/Case	1	2	3	4	5	6	7
-10	Maxi	Surge $[N]$	64	242	388	632	388	321	632
		Sway $[N]$	59	85	136	483	141	138	394
	Midi	Surge $[N]$	20	69	112	240	121	99	240
		Sway $[N]$	7	22	35	54	38	34	77
	Mini	Surge $[N]$	5	16	24	117	27	21	80
		Sway $[N]$	2	5	8	10	9	7	14
-20	Maxi	Surge $[N]$	64	242	388	632	388	321	632
		Sway $[N]$	59	85	136	483	141	138	394
	Midi	Surge $[N]$	20	69	112	240	121	99	240
		Sway $[N]$	7	22	35	54	38	34	77
	Mini	Surge $[N]$	5	16	24	117	27	21	80
		Sway $[N]$	2	5	8	10	9	7	14

Table 5.2: Maximum thrust given in sway and surge for each ROV for each simulation case.

The thrust capacity of MaxiROV in sway is 258 N, and the thrust capacity of MidiROV in surge is 238 N. The thrust allocation has been chosen from the surge limits, so this explains the exceedance in sway. The red numbers are 225 N over the limit. This occurs only for the sea state in Case 4, which has shown to be one of the most severe cases. The orange numbers are only exceeded by 2 N, and are probably caused by rounding errors in the input data for the control systems in SIMO. These numbers will still be deemed as valid limits. The maximum numbers are equal for depths 10 and 20 meters.

Chapter 6

Discussion

6.1 Frequency Domain Results

The analysis in Wadam showed that it is possible to use potential theory programs, such as Wadam, to evaluate submerged vehicles. This was possible through some alterations, though. The results have been compared to existing results for frequency dependent added mass, potential damping, first order excitation wave load transfer function and first order motion transfer function. The comparison did verify all the results found in the analysis, except the surge wave load and motion TF, which it partly rejected. The literature studied did not offer data for all DOFs, therefore some results could not be verified though this approach. Nevertheless, through validation of most of the results, it may be possible to accept the remaining results, as they are connected to each other.

The surge motion TF has a truly large amplitude for $\omega = 0$. In surge, when the period increases and $\omega \to 0$ the waves become longer and longer. The waves will act more or less as current, at least in amplitudes. A vehicle that is experiencing these waves, will, as when affected by current, be dragged along with the waves. However, this only explains an increase in the first order transfer function of motion in surge, not such a large increase.

The approach chosen for performing the analyses in Wadam was highly depending on SIMO as the ROVs had to be translated to their correct depth here. In the analyses performed with the ROVs at the correct depth, the performance of the vehicles in the time domain were unphysical and thereby rejected.

6.2 Time Domain Results

The time domain results reveal that the ROVs in most cases are able to satisfactorily counteract the first order wave loads in the sea states that were investigated. For Case 4 and 7 the results were deemed unacceptable when considering the tasks investigated; namely, cleaning and visual inspections of a netpen.

The ROVs were investigated at depths 10 and 20 meters. As waves exponentially decay with the depth (e^{-kz}) the results of the ROVs at 20 meters depth was expected to be even more satisfactory than at 10 meters depth. The results were in fact almost exactly

equal, suggesting that the method used to place the ROVs at the correct depths in SIMO had no effect. This may happen if SIMO does not consider such a decay in the waves, as the vessels and structures usually evaluated in this program are floating and large have displacements are not expected. If this is the case, it proposes that the loads calculated might have been *over estimated*, thereby opening the possibility that the operational window might be even more extended.

The heave DOF has not been evaluated due to the wrongly calculated restoring terms from Wadam. From the time simulations, it is clear that the ROVs are capable of counteracting the first order wave loads in surge for most of the sea states simulated. The capacity of for example MaxiROV in heave is 514 N, and from the transfer function of the first order wave loads in heave the maximum load is more than 12000 N, twice the size of the maximum in surge. For all ROVs, the maximum value match the value of C_{33} found in Wadam. These results are quite dependent on the restoring terms, and can not be trusted, thus it is difficult to estimate if the ROVs can counteract the wave loads also in heave. If these loads are estimated to have the same magnitude as in surge, the thrust capacity implies that the ROVs should be able to hoover at a certain depth with fairly good precision.

Only one generated wave elevation is investigated within each case/sea state. To raise the confidence level in the results, more wave seeds in SIMO can be used to generate sets of wave elevations that can occur within the given sea states. This will lead to the option of studying statistics of the results, which is valuable information.

6.2.1 Stability in Roll and Pitch

The results from MidiROV were similar to the results of MiniROV, which suggests that they might be more equal in geometry compared to MaxiROV. This may be explained by the ROVs projected area (i.e. $B \times L$), suggesting that the distribution of weight inside the boxes, and their dimensions should be investigated further. MaxiROV did in most cases not provide enough stability in pitch and roll, however it did not capsize. Still, the working conditions for the ROV might be difficult. As cleaning the net does not require a very high accuracy these tasks might still be possible to perform. However, visual inspections with a camera that moves $2 \times l_{camera} \times \cos(\angle)$ from side to side and even estimated to be as often as once every 3.3 seconds in Case 2, may be impossible.

6.3 Sources of Errors and Criticism of Assumptions

6.3.1 Assumptions and Proposed Design

Identifying all hydrostatic and hydrodynamic terms that affect vehicles in the sea can be challenging. Potential theory has been used in analysis of the ROVs. Several software offer computational fluid dynamics (CFD) instead . Potential theory assumes inviscid and irrotational fluid. In CFD programs the boundary layer will be taken into account, providing more accurate results for drag forces/friction. However, and even though the quadratic drag forces in this thesis have been estimated, they have been estimated using

full scale test data. These forces must be evaluated in the correct perspective. By comparison of the ROV behaviour, it is very likely that they do influence the results in the expected manner.

Control System

The Kalman filter parameters are set to values that are not really close to the recommended values. This is due to multiple factors. Only first order loads are present, and so, when choosing common values, second order motions of the ROVs were induced by the filter. This is highly unwanted behaviour and in some cases this lead to a *drift off*. The other reason is that the first order motions, the HF motions, are usually filtered out, which was not wanted in this study. Perhaps it would be beneficial to tune the controller and filter for each sea state. Doing this introduces a control system which uses online tuning. In real life applications this require a sea state estimator. Sea state estimators are currently being developed, by amongst others Brodtkorb (2014), but is not part of the industry standard yet.

Geometry of Proposed Design

Existing underwater vehicles are either torpedo shaped (AUVs) or "box"-shaped with a top buoyancy part, a metal frame, external equipment and areas of large flow through (ROVs). The proposed design was simplified to a closed box of so called equivalent height. This geometry is not very feasible as it is neither hydrodynamically advantageous nor it makes space for all necessary equipment. The design was chosen to simplify the study and due to this simplification, some degree of accuracy has been lost. However, when possible the ROV geometry, thruster configuration and coefficients has been inspired by existing designs, and thereby some of this accuracy has been maintained.

Thrust Capacity

If one assumes that using model scaling for the three ROV designs will not give correct results, this method probably has provided too low capacities. Which only provides additional safety factors for the resulting operation window. When comparing the capacities of MidiROV and MiniROV to similar ROVs, the capacities are of lower values. Either way it is possible to provide the ROVs with larger thrusters, as power limitations are only restricted by the mother ship's or the auxiliary power source's capacity.

In SIMO, the thrusters have been limited to ensure that the capacity of each ROV *in surge* could not be exceeded. If the sway capacity was considered, this would limit the thrusters additionally. Thus, the thrust configuration should be considered differently, to ensure that both limits in surge and sway are not exceed. However, from the resulting total thrust in surge and sway, these limits were only exceeded in the extreme Case 4.

In this thesis maintenance of the fish net has been of concern. While the capacity has been proven adequate for positioning of the ROV in the wave zone, loads induced by maintenance work has not been considered. When the ROV is flushing the net, the thrusters must also be able to withstand the loads that arise from the flow coming out

of the washing device, which often uses jet flows. These loads are interacting with the sea water, as well as the net. The size of these loads are not in the scope of this thesis, but should be considered when developing a DP system for the ROV. The loads could be counteracted if the forces was modelled and used in a feed forward term in the control system. When considering visual inspections, no additional loads are expected.

Environment

As mentioned in section 2.3.1, the Jonswap spectra is a good model for wind generated sea if H_s and T_p lie within a certain area. This area is defined as when T_p lies within the limits of eqs. (2.42) and (2.43), that is: $3.6\sqrt{H_s} \geq T_p \leq 5.0\sqrt{H_s}$. The sea states given in Cases 1-7 does generally fall outside this area (except for cases 4 and 7 which lies on the outer edge of the interval). Therefore, other wave spectra models should perhaps be investigated to model the sea states present on Rataren fish farm more accurately. For instance, Torsethaugen has developed a simplified two peaked spectra which include both swell waves and wind generated sea.

Chapter 7

Conclusions and Further Work

7.1 Conclusions

In this thesis modelling, analysis and simulation of three ROVs of sizes 600 kg, 200 kg and 50 kg have been performed to assess if automatic control of ROVs performing maintenance tasks on exposed aquacultural sites is possible. The vehicles have been evaluated in sea states that are likely to occur and sea states that happen more rarely at Rataren fish farm. The results illustrate that an operational window can be set for the ROVs. A limiting significant wave height H_s of 2.0 m and a peak period T_p no less than 5 s should be operated in. However, H_s and T_p must be evaluated simultaneously. As Case 4 and Case 7 illustrate, small significant wave heights or larger peak periods can also cause wave loads that are impossible to operate in.

7.2 Further Work

The discussion presents some ideas for further work. This includes looking at more accurate, and thus more complicated, forms of wave and fluid theory, like CFD. More sea states should be simulated, also using non-unidirectional spreading codes.

Different controllers should be tested to determine if the ROVs performance will be improved by for instance a model based controller using the technique of Model-predictive-control (MPC) or perhaps Backstepping. For the controller it may be necessary to derive wave disturbance information through an observer. If so, it could be designed to estimate the wave velocities and ROV relative velocities by using position and attitude measurement.

The launch and recovery of ROVs are critical parts of operations of an ROV. Launch and recovery systems (LARS) for the ROV designs proposed in this thesis should be further evaluated and may impose more harsh restrictions on the window of operations concluded here.

Other concepts for investigating the fisheries instead of an ROV could be evaluated. For instance a net with a sort of flexible track along it, to attach a vehicle that can simply go along the track and do the maintenance on the go. Such a device does however restrain the

work environment of the maintenance vehicle. However, such a device could be small and fairly simple, thereby more cost efficient than an ROV. If such a device is designed there are other aspects that need to be considered as well. For instance it must be determined if it should be able to clean the netpen and fix simple damages temporary or not.

Bibliography

ACE Project. Rataren - flyfoto, Project: Fôringskontroll, November 2014. Retrived November 11, 2014. http://aceaqua.no/prosjekter/foringskontroll/.

AquaCulture Engineering. Seawatch Rataren May 1, to December 1, 2013. Provided October 8, 2014. Courtesy of Finn Victor Willumsen, CEO of ACE.

J.G. Balchen, N.A. Jenssen, and S. Sælid. A Dynamic Positioning System Based on Kalman Filtering and Optimal Control. In *Proc. of the 19th IEEE Conf. on Decision and Control*, volume 1, pages 135–163. New York, US, 1980.

Viktor Berg. Development and Commissioning of a DP system for ROV SF 30k. 2012.

Astrid Helene Brodtkorb. Dynamic Positioning in Extreme Sea States: Improving Operability Using Hybrid Design Methods. 2014.

Robert D. Christ and Robert L. Wernli Sr. *The ROV manual: a user guide for observation class remotely operated vehicles*. Butterworth-Heinemann, 2011.

W. E. Cummins. The Impulse Response Function and Ship Motions. Technical report, David Taylor Model Basin. Hydrodynamics Laboratory, USA, 1962.

Det Norske Veritas (DNV). Rules for Classification of SHIPS. Part 6, Ch. 7. Newbuildings, Special Equipment and Systems. Technical report, Norway, July 2011. ADDITIONAL CLASS. Dynamic Positioning Systems.

DNV GL. Sesam, 2014. http://www.dnv.com/services/software/products/sesam/.

DNV Software. *SESAM User Manual - SIMO - Theory Manual*, August 2014a.

DNV Software. *SESAM User Manual - Wadam - Wave analysis by Diffraction and Morison Theory*, 12. edition, April 2014b.

DNV Software. *SESAM User Manual - GeniE*, June 2014c.

Fredrik Dukan and Asgeir J. Sørensen. Altitude estimation and control of ROV by use of DVL. In *MCMC, 2012 IFAC-Italy*, pages 1–12. IFAC, 2012.

Fredrik Dukan and Asgeir J. Sørensen. Sea floor geometry approximation and altitude control of ROVs. 2013.

Odd M. Faltinsen. *Sea loads on ships and offshore structures*, volume 1. Cambridge University Press, 1993.

FORUM Energy Technology. FORUM's Sub-Atlantic brand - Observation ROVs, Everything Remotely Possible. Technical report, June 2013. Retrived November 11,

2014. http://www.f-e-t.com/our_products_technologies/subsea-solutions/rovs-observation/.

Thor I Fossen. *Nonlinear modeling and control of underwater vehicles*. PhD thesis, Norwegian Institute of Technology, 1991.

Thor I Fossen. *Handbook of marine craft hydrodynamics and motion control*. John Wiley & Sons, 2011.

Hilde Hagen. Small Size ROV in the Wave Zone - Modelling and Analysis in Wadam - Simulation in SIMO. Part of TMR4515 Advanced model-based design and testing of marine control systems at The Norwegian University of Science and Technology, November 2014a.

Hilde Hagen. Small Size ROV Operating in the Wave Zone - Control Strategies for Wave Compensation. Part of TMR4555 Underwater robotics in safe and autonomous subsea operations at The Norwegian University of Science and Technology, November 2014b.

HydroD. SESAM, V4.7-01 .

IMT Software Wiki. Software in use at IMT department- Example Models, November 2011. Retrived September 30, 2014. http://www.ivt.ntnu.no/imt/software/sesam:models.

National Instruments. NI LabView, 2014. URL http://norway.ni.com/labview. Retrieved April 8th 2014.

Marianne Kirkeby. Comparison of controllers for dynamic positioning and tracking of ROV Minerva, 2010.

Masanori Kyo, E Hiyazaki, Satoshi Tsukioka, Hiroshi Ochi, Yasutaka Amitani, Toshio Tsuchiya, Taro Aoki, and Shinichi Takagawa. The sea trial of "kaiko", the full ocean depth research rov. In *OCEANS'95. MTS/IEEE. Challenges of Our Changing Global Environment. Conference Proceedings.*, volume 3, pages 1991–1996. IEEE, 1995.

Martin Ludvigsen and Øyvind T. Ødegaard. "Fullskala thrust-test av Minerva". Fullscale thrust test of ROV Minerva, performed in main towing tank at MARINTEK, Trondheim, November 2004.

MATLAB. The MathWorks, Inc., R2013b. http://www.mathworks.com/.

MatWeb. DIAB Divinycell® HCP 100 and H 35 Sandwich Core Material, 2014. Material property data. Retrieved November 11, 2014 from http://www.matweb.com/.

MET. Ekstremvêrrapport - Hendig: Hilde, 16.-17.11.2013. MET info 15/2013, Meteorologisk Institutt, Bergen, December 2013. ISSN 1503-8017.

Drew Michel, Robert L Wernli, MTS ROV Committee, et al. *Operational effectiveness of unmanned underwater systems*. MTS Remotely Operated Vehicle Committee, 1999a.

Drew Michel, Robert L. Wernli, MTS ROV Committee, et al. *Operational effectiveness of unmanned underwater systems*. ROV Committee of The Marine Technology Society, 1999b.

Microsoft Excel Starter. Microsoft Corporation. http://www.microsoft.com, 2010.

Dag Myrhaug. *Marin dynamikk - Uregelmessig sjø*. Institutt for Marin teknikk, Marinteknisk senter, 2007.

NS 9415. Marine fish farms - Requirements for site survey, risk analyses, design, dimensioning, production, installation and operation. Technical report, Norwegian Standard, November 2009.

T. F. Ogilvie. Recent progress toward the understanding and prediction of ship motions. In *5th Symposium on Naval Hydrodynamics*. Bergen, Norway, 1964.

Bjørnar Pettersen. *Marin teknikk 3 - Hydrodynamikk*. Institutt for Marin teknikk, Marinteknisk senter, 2007.

J.A. Pinkster. *Low frequency second order wave exciting forces on floating structures*. PhD thesis, October 1980.

ROV Committee of The Marine Technology Society. ROVs - A brief history, 2014. Retrived September 2., 2014. `http://www.rov.org/rov_history.cfm`.

Merete G. Sandberg, Andreas Myskja Lien, Leif Magne Sunde, SINTEF Fiskeri og havbruk AS, Kristine Vedal Størkersen, NTNU samfunnsforskning ved Studio Apertura, Lars Helge Stien, Havforskningsinstituttet, Finn Victor Willumsen, and AquaCulture Engineering AS (ACE). Drift av eksponerte oppdrettslokaliteter - hvor trykker skoen? *Norsk fiskeoppdrett*, 2012.

SINTEF Fisheries and Aquaculture. "Exposed salmon farming in high currents and waves" Ongoing project (2011-2015), 2014. Retrieved November 17, 2014. `https://www.forskningsradet.no/prosjektbanken_beta/#/project/207116`.

Society of Naval Architects and Marine Engineers SNAME. Nomenclature for treating the motion of a submerged body through a fluid: report of the american towing tank conference. *Technical and Research Bulletin*, 1950.

Asgeir J. Sørensen. *Marine Cybernetics Modelling and Control Lecture Notes*. 2013.

Sverre Steen. *Motstand og propulsjon. Propell- og foilteori*. Department of Marine Technology, 2011. Lecture notes in TMR4247 - Marine Hydrodynamics.

Sub-Atlantic. Hydraulic propulsion selection manual for engineers, 2014. Retrieved November 11, 2014. `http://pdf.nauticexpo.com/pdf/sub-atlantic/hydraulic-propulsion-selection-manual-engineers/27362-6914.html`.

Eirik Svendby. Robust control of ROV/AUVs, 2007.

Technical Specifications. Technical specifications and instrumentation of ROV Minerva, 2014. Retrieved March 25th 2014 from `http://www.ntnu.edu/marine/minerva/spesifications`.

Espen Tolpinrud. Development and implementation of computer-based control system for ROV with experimental results, 2012.

Appendix Overview

Appendix A Rataren Fish Farm

A.1: Two frequency tables are provided in this appendix, the first given in numbers [-] and the second given in percent [%]. They display the results from observations of estimated significant wave height and peak period from May 1, 2013 to December 1, 2013. In table A.2, there may be some rounding errors. The original data can be found in SeawatchMai-Now2011.xls and Observations.xlsx in the appended zip-file.

A.2: Bathymetric chart of the area where Rataren fish farm is located. The deepest points in the region of both Rataren I and Rataren II is between 40 and 50 meters, at approximately 45 m.

Appendix B Design Parameters

B.1: The resulting rigid body mass of the proposed ROV designs are presented.

B.2: This section displays MaxiROV, MidiROV and MiniROVs thruster configuration matrix and the thrust allocation matrix.

Appendix C Wadam Results

C.1: The transfer function (TF) for the first order wave forces for MidiROV and MiniROV when the incident wave heading is set to 0° , 45°, 90°, 135° and 180°.

C.2: The transfer function for the body motion, also known as the response amplitude operator (RAO), for MidiROV and MiniROV when the incident wave heading is set to 0° , 45°, 90°, 135° and 180°.

Appendix D SIMO Results

C.1: The three ROVs performance at depth 20 m are placed here.

Appendix E Zip File

E.1: Models for reading into GeniE, and the resulting FEM-files.

E.2: Wadam Analysis result files. The files are sorted into three folders, one for MaxiROV, one for MidiROV and one for MiniROV. The folders include two files each of the form explained.

E.3: The simulations in SIMO is found in the SIMA task file. In addition, some of the frequency domain results have been processed in SIMO, and written to new text files.

E.4: Diverse spreadsheets. Some Calculations and observations from Rataren fish farm (SeawatchMai-Now2011.xls). The measurements have been taken every hour over the last 10 minutes, to save power, yielding 3629 observations. The data is courtesy of AquaCulture Engineering (2013). Please note that in November 2013, a storm hit the Norwegian coast (Hilde, MET (2013)) and has caused the largest H_{m0} values ranging from 2.85 m to the largest registration of 4.57 m.

E.5: Multiple files used for reading and plotting in Matlab. The files read are in HDF5 format, and are too large to append in this thesis. However, the files may be obtained from running the simulation in Appendix D.3.

Appendix A

Rataren Fish Farm

A.1 Frequency Table Rataren Fish Farm

$H_{m0} \backslash T_p$	1	2	3	4	5	6	7	8	9	10	11	12	13	14	15	16	17	18	19	20	21	22	23	24	25	*Sum*
0.5	6	0	101	60	37	28	137	258	242	351	123	70	48	12	2	1	1	6	7	14	42	62	82	85	429	2204
1	0	0	29	35	33	21	34	91	85	73	125	106	114	70	23	1	1	0	1	0	1	0	0	0	0	843
1.5	0	0	0	3	12	27	20	16	18	21	39	30	65	44	7	1	1	1	0	0	0	0	0	0	0	305
2	0	0	0	0	1	7	10	19	10	7	10	4	11	17	23	8	0	2	0	0	0	0	0	0	0	129
2.5	0	0	0	0	1	0	4	14	11	2	4	7	18	11	13	3	0	0	0	0	0	0	0	0	0	88
3	0	0	0	0	0	0	0	3	4	6	6	5	3	5	7	2	0	0	0	0	0	0	0	0	0	41
3.5	0	0	0	0	0	0	0	0	0	0	1	1	2	3	1	2	0	0	0	0	0	0	0	0	0	10
4	0	0	0	0	0	0	0	0	0	0	0	1	2	1	2	0	1	0	0	0	0	0	0	0	0	7
4.5	0	0	0	0	0	0	0	0	0	0	0	0	0	0	1	0	0	0	0	0	0	0	0	0	0	1
5	0	0	0	0	0	0	0	0	0	0	0	0	0	1	0	0	0	0	0	0	0	0	0	0	0	1
Sum	6	0	130	98	84	83	205	401	370	460	308	224	263	164	79	18	4	9	8	14	43	62	82	85	429	**3629**

Table A.1: Frequency distribution showing the number of each sea state occurrence, given by H_{m0} [m] and T_p [s] from Rataren, 2013

$H_{m0}\backslash T_p$	1	2	3	4	5	6	7	8	9	10	11	12	13	14	15	16	17	18	19	20	21	22	23	24	25	*Sum*
0.5	0.2	0	2.8	1.7	1	0.8	3.8	7.1	6.7	9.7	3.4	1.9	1.3	0.3	0.1	0	0	0.2	0.2	0.4	1.2	1.7	2.3	2.3	11.8	60.7
1	0	0	0.8	1	0.9	0.6	0.9	2.5	2.3	2	3.4	2.9	3.1	1.9	0.6	0	0	0	0	0	0	0	0	0	0	23.2
1.5	0	0	0	0.1	0.3	0.7	0.6	0.4	0.5	0.6	1.1	0.8	1.8	1.2	0.2	0	0	0	0	0	0	0	0	0	0	8.4
2	0	0	0	0	0	0.2	0.3	0.5	0.3	0.2	0.3	0.1	0.3	0.5	0.6	0.2	0	0.1	0	0	0	0	0	0	0	3.6
2.5	0	0	0	0	0	0	0.1	0.4	0.3	0.1	0.1	0.2	0.5	0.3	0.4	0.1	0	0	0	0	0	0	0	0	0	2.4
3	0	0	0	0	0	0	0	0.1	0.1	0.2	0.2	0.1	0.1	0.1	0.1	0.1	0	0	0	0	0	0	0	0	0	1.1
3.5	0	0	0	0	0	0	0	0	0	0	0	0	0.1	0.1	0	0.1	0	0	0	0	0	0	0	0	0	0.3
4	0	0	0	0	0	0	0	0	0	0	0	0	0.1	0	0.1	0	0	0	0	0	0	0	0	0	0	0.2
4.5	0	0	0	0	0	0	0	0	0	0	0	0	0	0	0	0	0	0	0	0	0	0	0	0	0	0
5	0	0	0	0	0	0	0	0	0	0	0	0	0	0	0	0	0	0	0	0	0	0	0	0	0	0
Sum	0.2	0	3.6	2.7	2.3	2.3	5.6	11	10.2	12.7	8.5	6.2	7.2	4.5	2.2	0.5	0.1	0.2	0.2	0.4	1.2	1.7	2.3	2.3	11.8	**100**

Table A.2: Probability distribution of the occurrence for each sea state from Rataren, 2013

A.2 Rataren Fish Farm

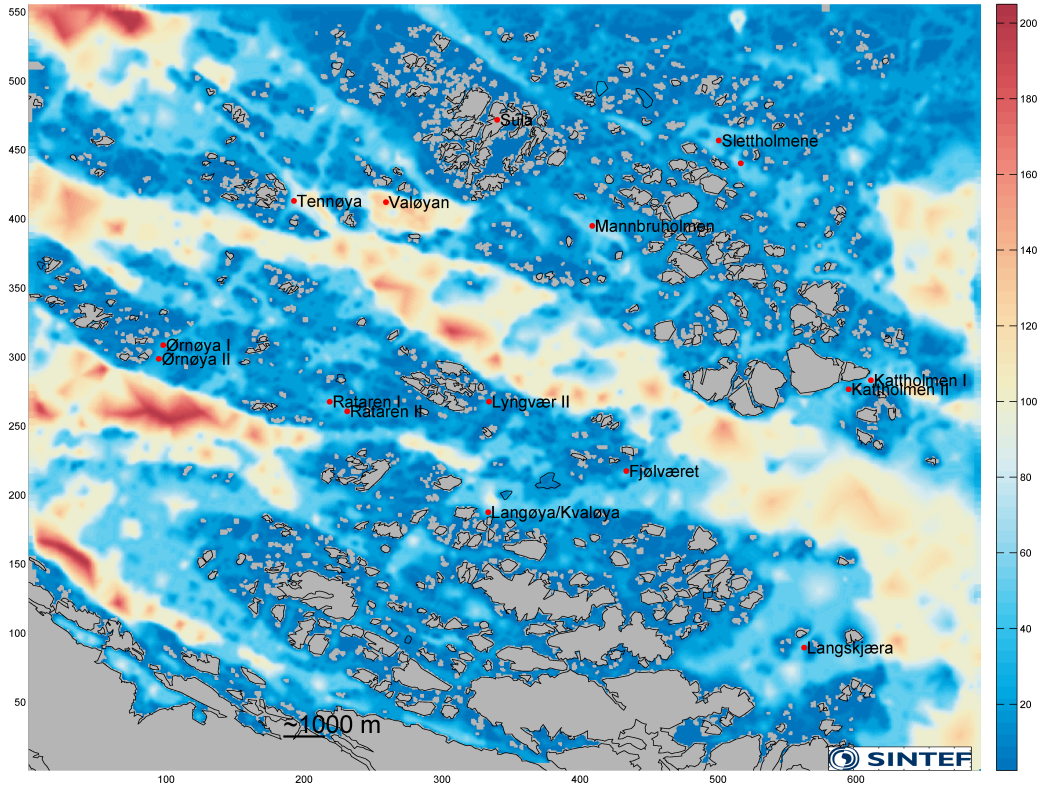

Figure A.1: Bathymetric chart of Rataren fish farm AquaCulture Engineering (2013).

Appendix B

Design Parameters

B.1 Rigid Body Mass of Proposed ROV Designs

MaxiROV

$$\boldsymbol{M}_{RB}^{CO} = \begin{bmatrix} 600.000 & 0 & 0 & 0 & -103.7589 & 0 \\ 0 & 600.000 & 0 & 103.7589 & 0 & 0 \\ 0 & 0 & 600.000 & 0 & 0 & 0 \\ 0 & 103.7589 & 0 & 118.73170 & 0 & \\ -103.7589 & 0 & 0 & 0 & 61.2317 & 0 \\ 0 & 0 & 0 & 0 & 0 & 138.5000 \end{bmatrix} \tag{B.1}$$

MidiROV

$$\boldsymbol{M}_{RB}^{CO} = \begin{bmatrix} 200.000 & 0 & 0 & 0 & -16.1317 & 0 \\ 0 & 200.000 & 0 & 16.1317 & 0 & 0 \\ 0 & 0 & 200.000 & 0 & 0 & 0 \\ 0 & 16.1317 & 0 & 18.3452 & 0 & 0 \\ -16.1317 & 0 & 0 & 0 & 8.7202 & 0 \\ 0 & 0 & 0 & 0 & 0 & 23.7083 \end{bmatrix} \tag{B.2}$$

MiniROV

$$\boldsymbol{M}_{RB}^{CO} = \begin{bmatrix} 50.000 & 0 & 0 & 0 & -2.2149 & 0 \\ 0 & 50.000 & 0 & 2.2149 & 0 & 0 \\ 0 & 0 & 50.000 & 0 & 0 & 0 \\ 0 & 2.2149 & 0 & 2.7806 & 0 & 0 \\ -2.2149 & 0 & 0 & 0 & 1.1556 & 0 \\ 0 & 0 & 0 & 0 & 0 & 3.7083 \end{bmatrix} \tag{B.3}$$

B.2 Thrust Configuration

MaxiROV

$$\boldsymbol{T}_{3\times4}(\boldsymbol{\alpha},\boldsymbol{a}) = \begin{bmatrix} -0.7660 & -0.7660 & 0.8192 & 0.8192 \\ 0.6428 & -0.6428 & 0.5736 & -0.5736 \\ -0.5875 & 0.5875 & 0.5645 & -0.5645 \end{bmatrix} \tag{B.4}$$

MidiROV

$$\boldsymbol{T}_{3\times4}(\boldsymbol{\alpha},\boldsymbol{a}) = \begin{bmatrix} -0.7660 & -0.7660 & 0.8192 & 0.8192 \\ 0.6428 & -0.6428 & 0.5736 & -0.5736 \\ -0.4214 & 0.4214 & 0.4051 & -0.4051 \end{bmatrix} \tag{B.5}$$

MiniROV

$$\boldsymbol{T}_{3\times4}(\boldsymbol{\alpha},\boldsymbol{a}) = \begin{bmatrix} -0.7660 & -0.7660 & 0.8192 & 0.8192 \\ 0.6428 & -0.6428 & 0.5736 & -0.5736 \\ -0.3321 & 0.3321 & 0.3187 & -0.3187 \end{bmatrix} \tag{B.6}$$

B.2.1 Thruster Allocation

MaxiROV

$$\boldsymbol{T}^{+}_{4\times3}(\boldsymbol{\alpha},\boldsymbol{a}) = \begin{bmatrix} -0.3045 & 0.4033 & -0.4098 \\ -0.3045 & -0.4033 & 0.4098 \\ 0.3256 & 0.4197 & 0.4593 \\ 0.3256 & -0.4197 & -0.4593 \end{bmatrix} \tag{B.7}$$

MidiROV

$$\boldsymbol{T}^{+}_{4\times3}(\boldsymbol{\alpha},\boldsymbol{a}) = \begin{bmatrix} -0.3045 & 0.4034 & -0.5711 \\ -0.3045 & -0.4034 & 0.5711 \\ 0.3256 & 0.4196 & 0.6400 \\ 0.3256 & -0.4196 & -0.6400 \end{bmatrix} \tag{B.8}$$

MiniROV

$$\boldsymbol{T}^{+}_{4\times3}(\boldsymbol{\alpha},\boldsymbol{a}) = \begin{bmatrix} -0.3045 & 0.4031 & -0.7254 \\ -0.3045 & -0.4031 & 0.7254 \\ 0.3256 & 0.4200 & 0.8130 \\ 0.3256 & -0.4200 & -0.8130 \end{bmatrix} \tag{B.9}$$

Appendix C

Wadam Results

C.1 Added Mass Infinity for MidiROV and MiniROV

MidiROV

$$\boldsymbol{A}(\infty) = \begin{bmatrix} 51.5 & 0 & 0 & 0 & -3.6 & 0 \\ 0 & 83.2 & 0 & 9.0 & 0 & 0 \\ 0 & 0 & 178.4 & 0 & 0 & 0 \\ 0 & 9.0 & 0 & 4.0 & 0 & 0 \\ -4.0 & 0 & 0 & 0 & 8.0 & 0 \\ 0 & 0 & 0 & 0 & 0 & 6.4 \end{bmatrix} \tag{C.1}$$

MiniROV

$$\boldsymbol{A}(\infty) = \begin{bmatrix} 10.4 & 0 & 0 & 0 & 0.5 & 0 \\ 0 & 16.6 & 0 & 8.5e-02 & 0 & 0 \\ 0 & 0 & 81.7 & 0 & 0 & 0 \\ 0 & 8.7e-02 & 0 & 0.7 & 0 & 0 \\ 0.5 & 0 & 0 & 0 & 2.3 & 0 \\ 0 & 0 & 0 & 0 & 0 & 0.8 \end{bmatrix} \tag{C.2}$$

C.2 First Order Wave Force Transfer Function for MidiROV and MiniROV

C.2.1 0 °

MidiROV

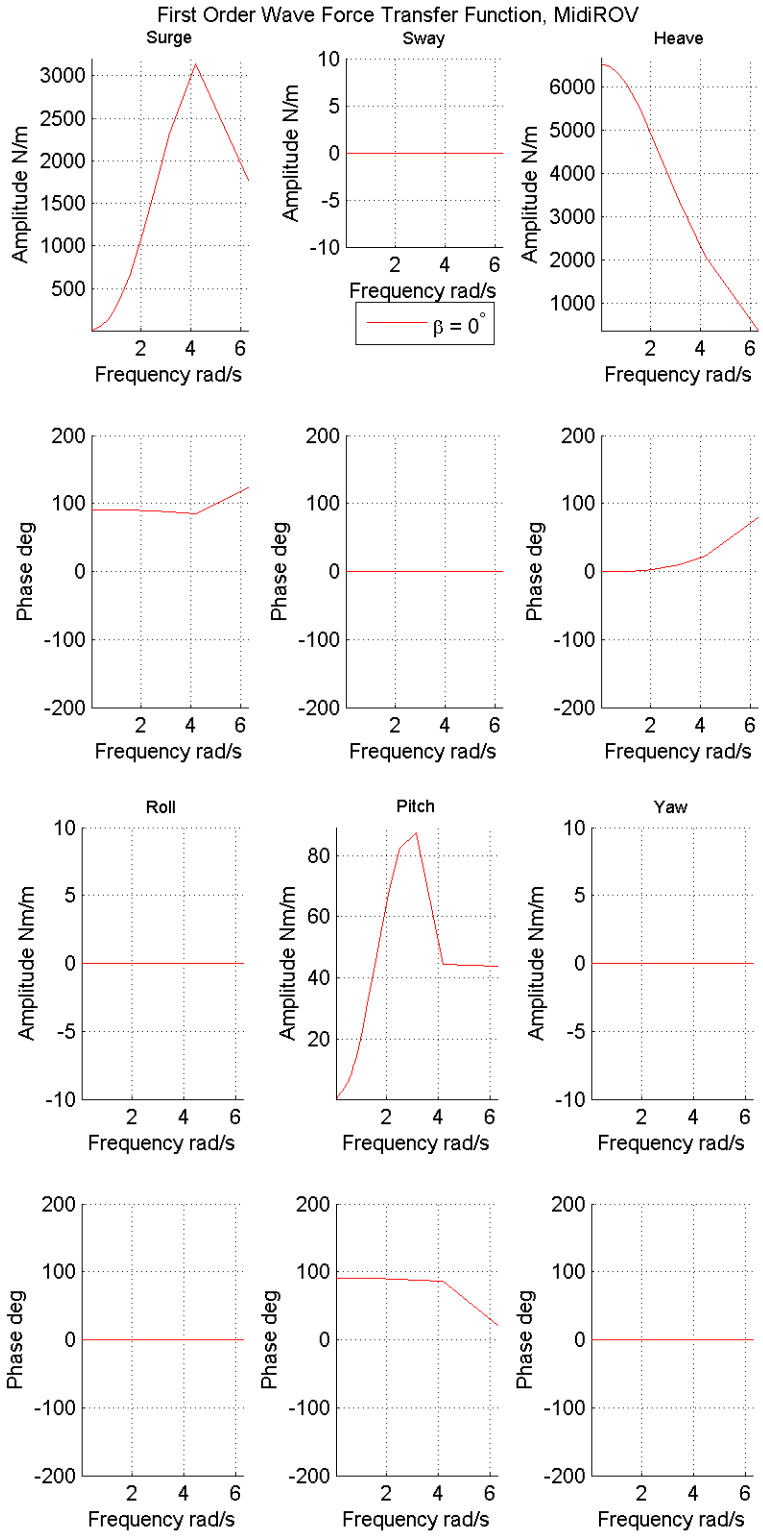

Figure C.1: The first order wave force transfer function for 0 °, MidiROV.

MiniROV

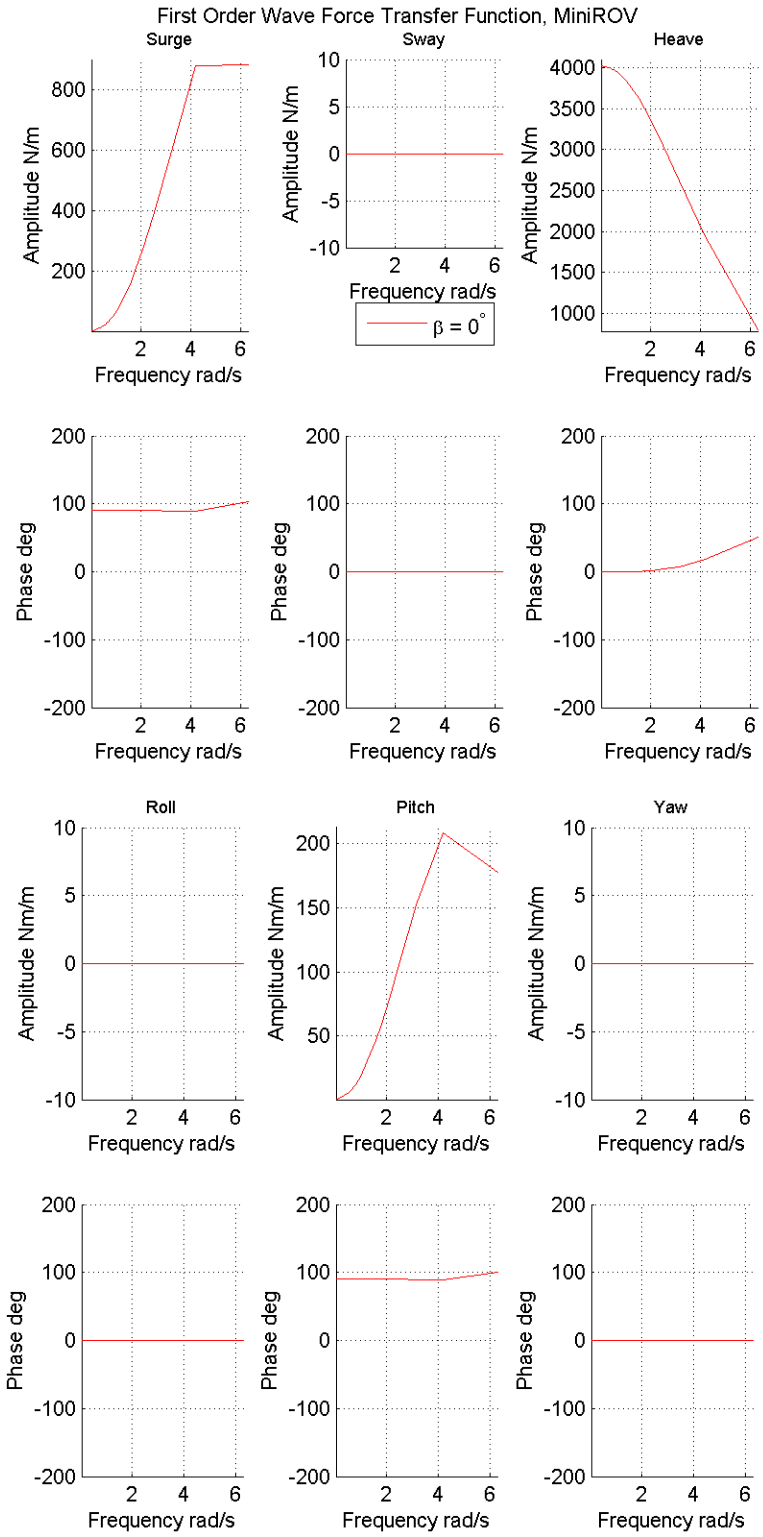

Figure C.2: The first order wave force transfer function for 0 °, MiniROV.

C.2.2 45 °

MidiROV

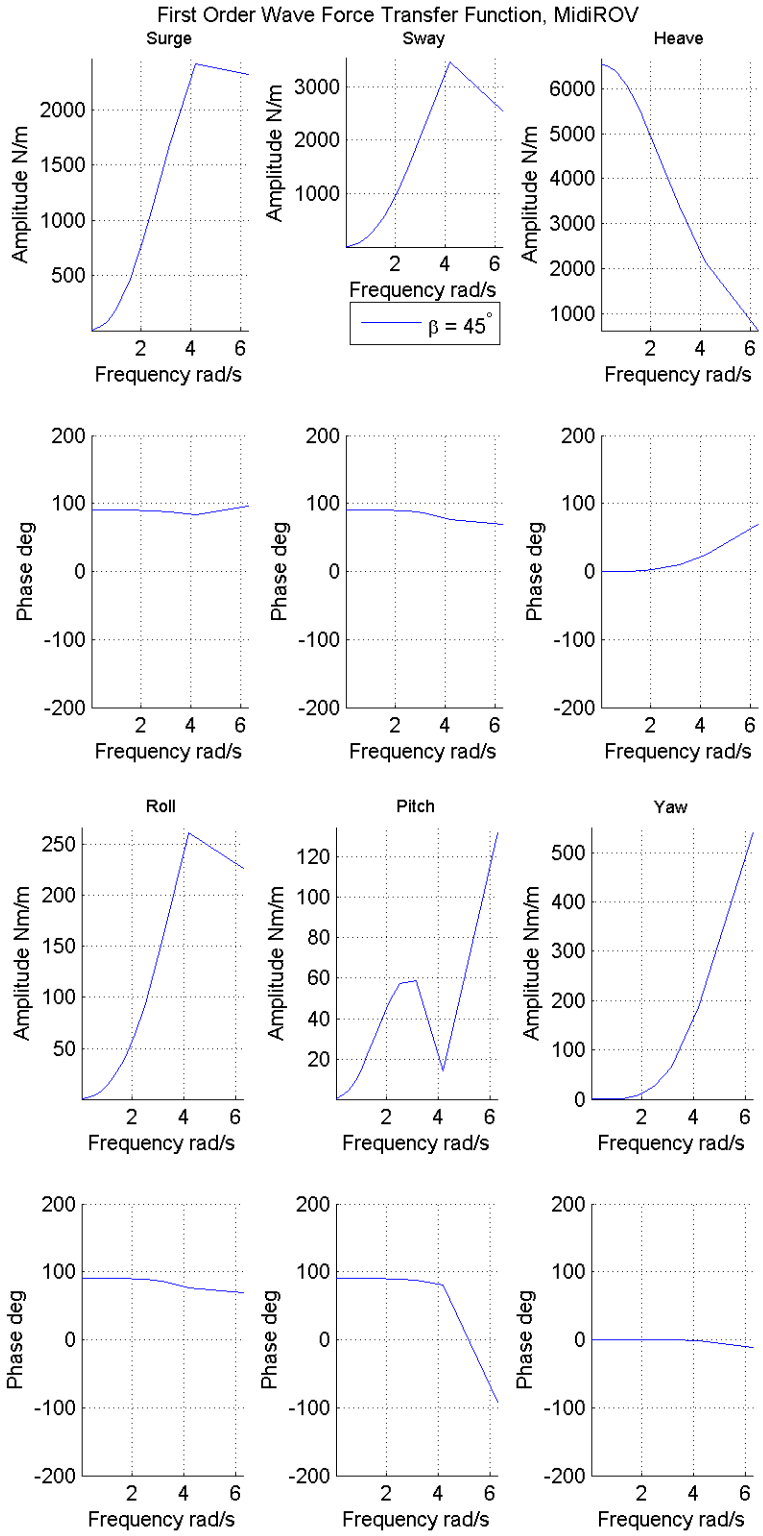

Figure C.3: The first order wave force transfer function for 45 °, MidiROV.

MiniROV

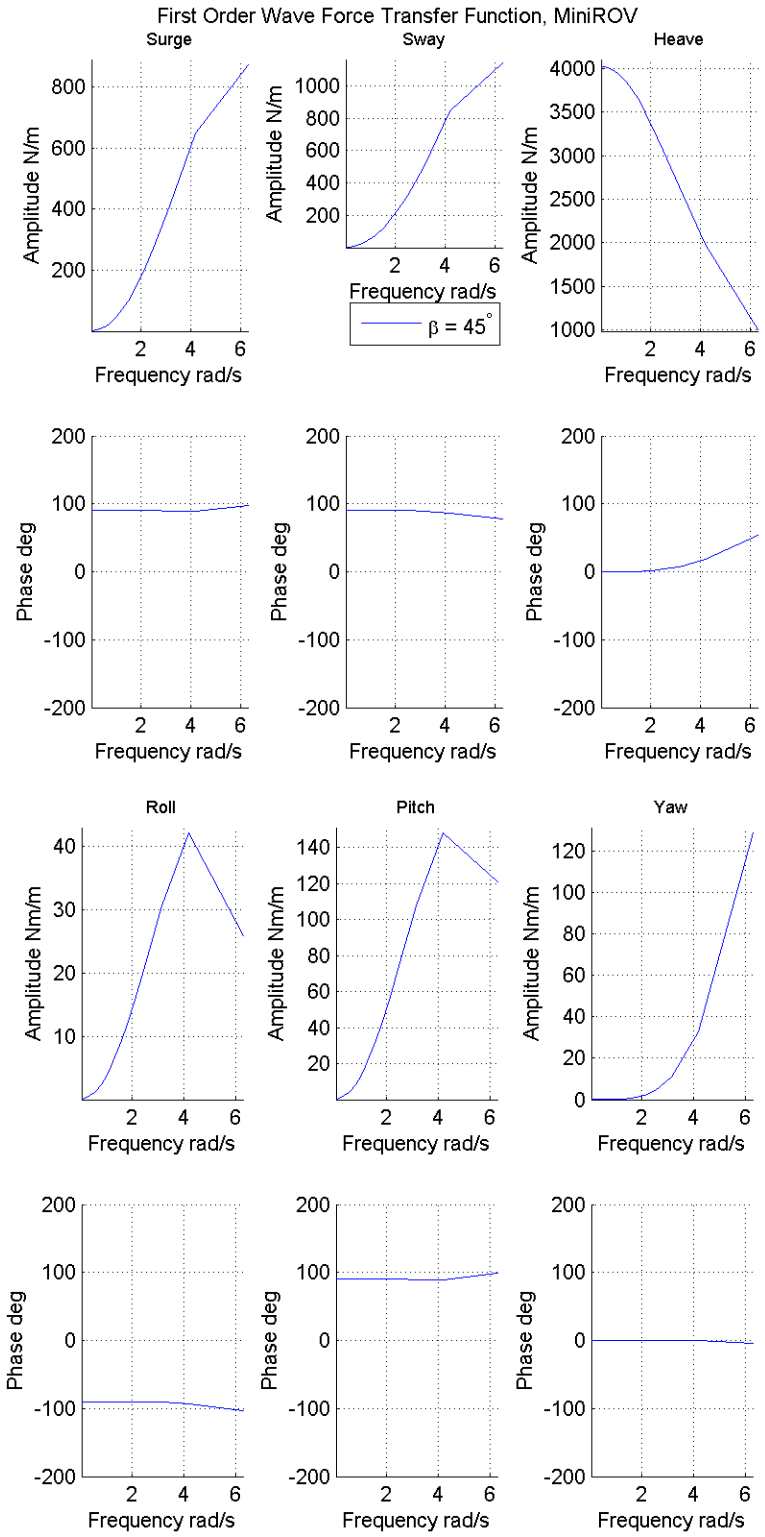

Figure C.4: The first order wave force transfer function for 45 °, MiniROV.

C.2.3 90 °

MidiROV

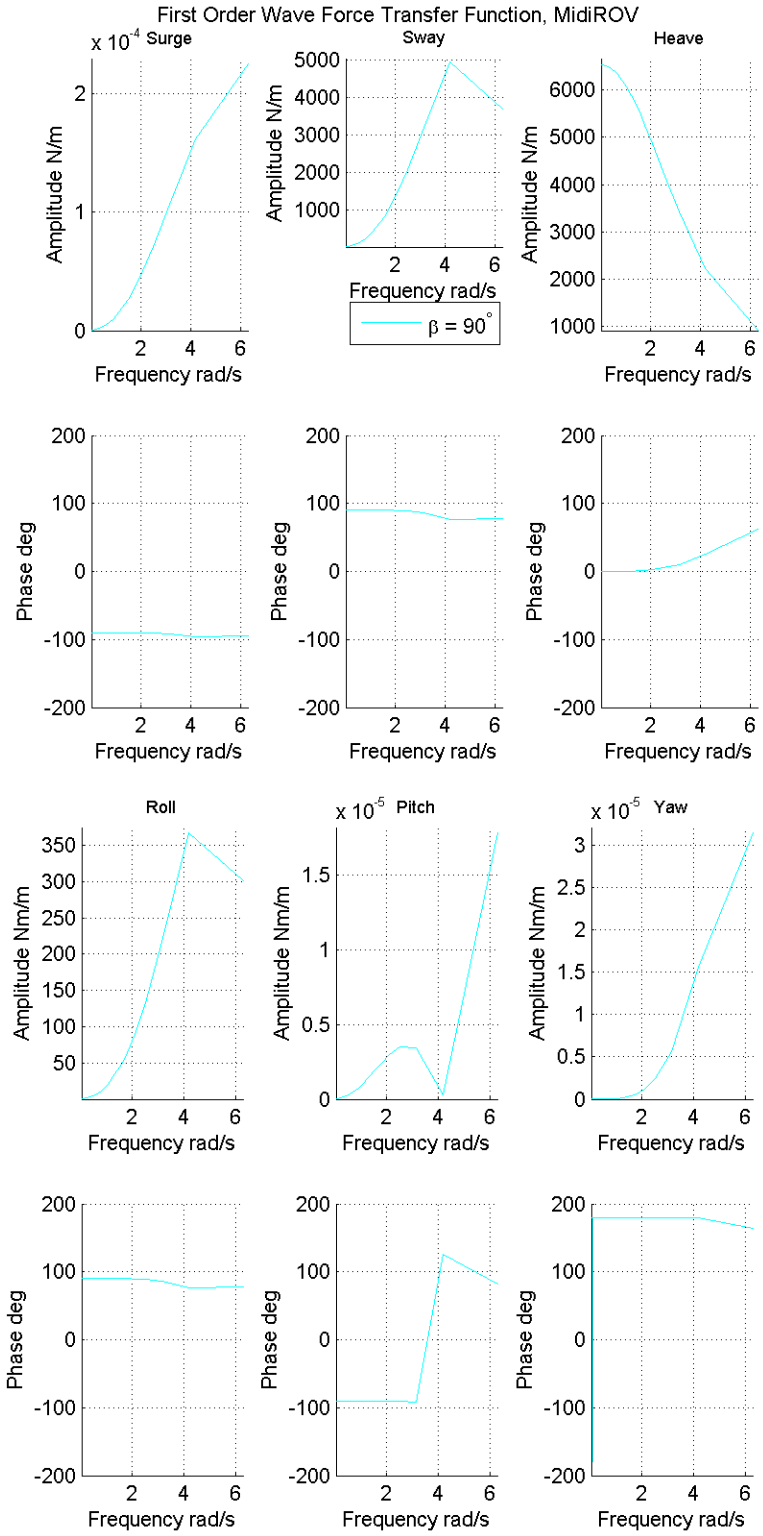

Figure C.5: The first order wave force transfer function for 90 °, MidiROV.

MiniROV

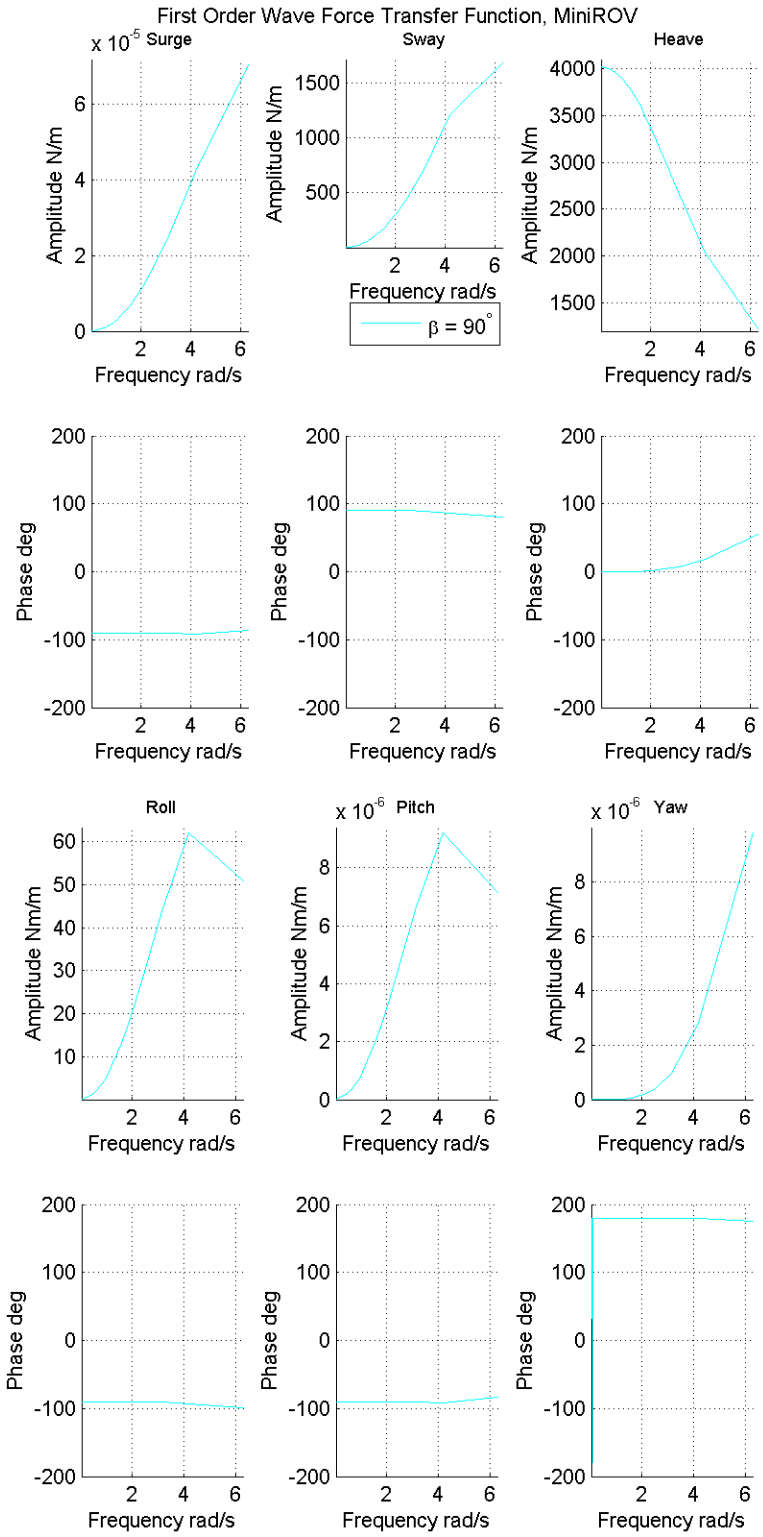

Figure C.6: The first order wave force transfer function for 90 °, MiniROV.

C.2.4 135 °

MidiROV

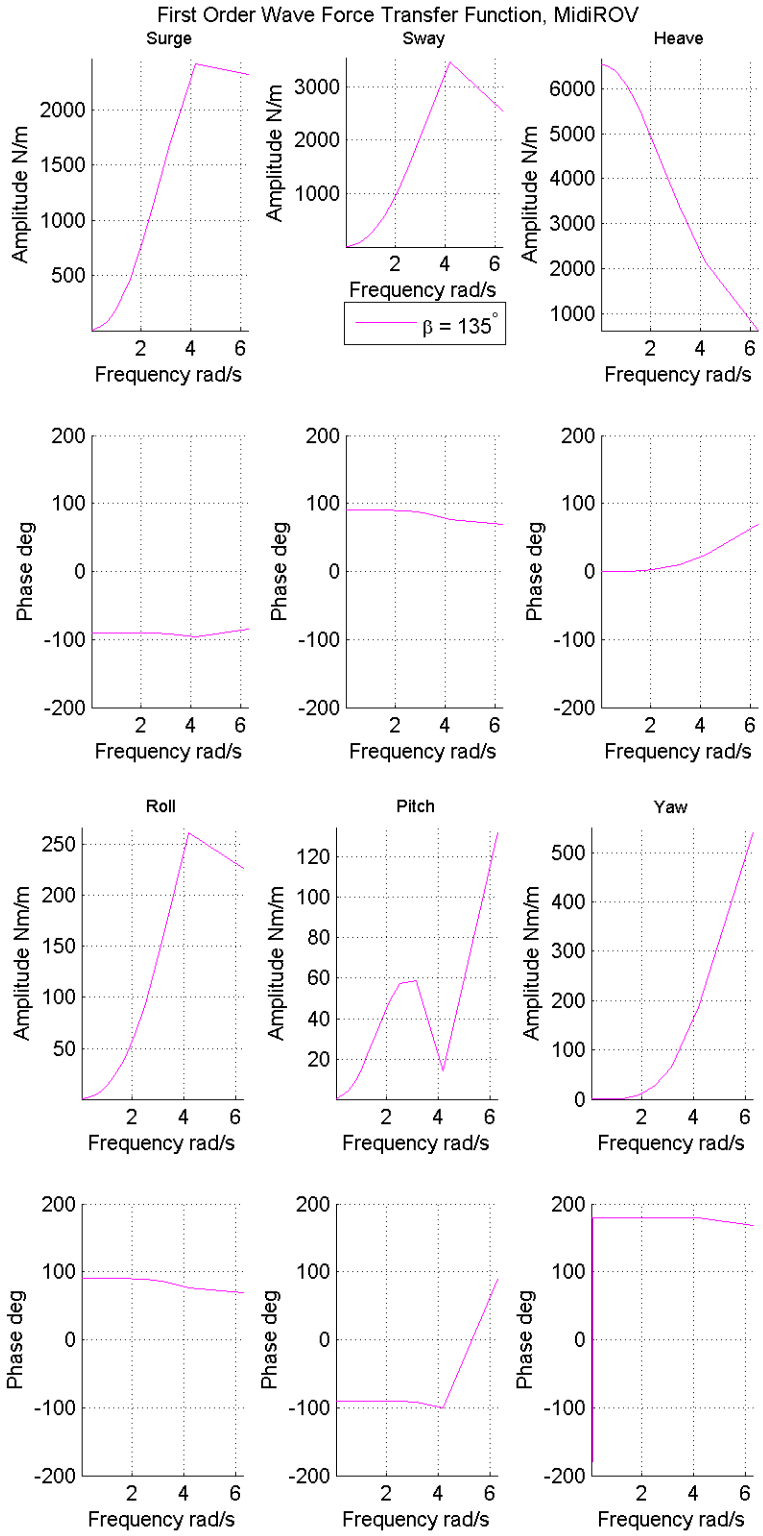

Figure C.7: The first order wave force transfer function for 135 °, MidiROV.

MiniROV

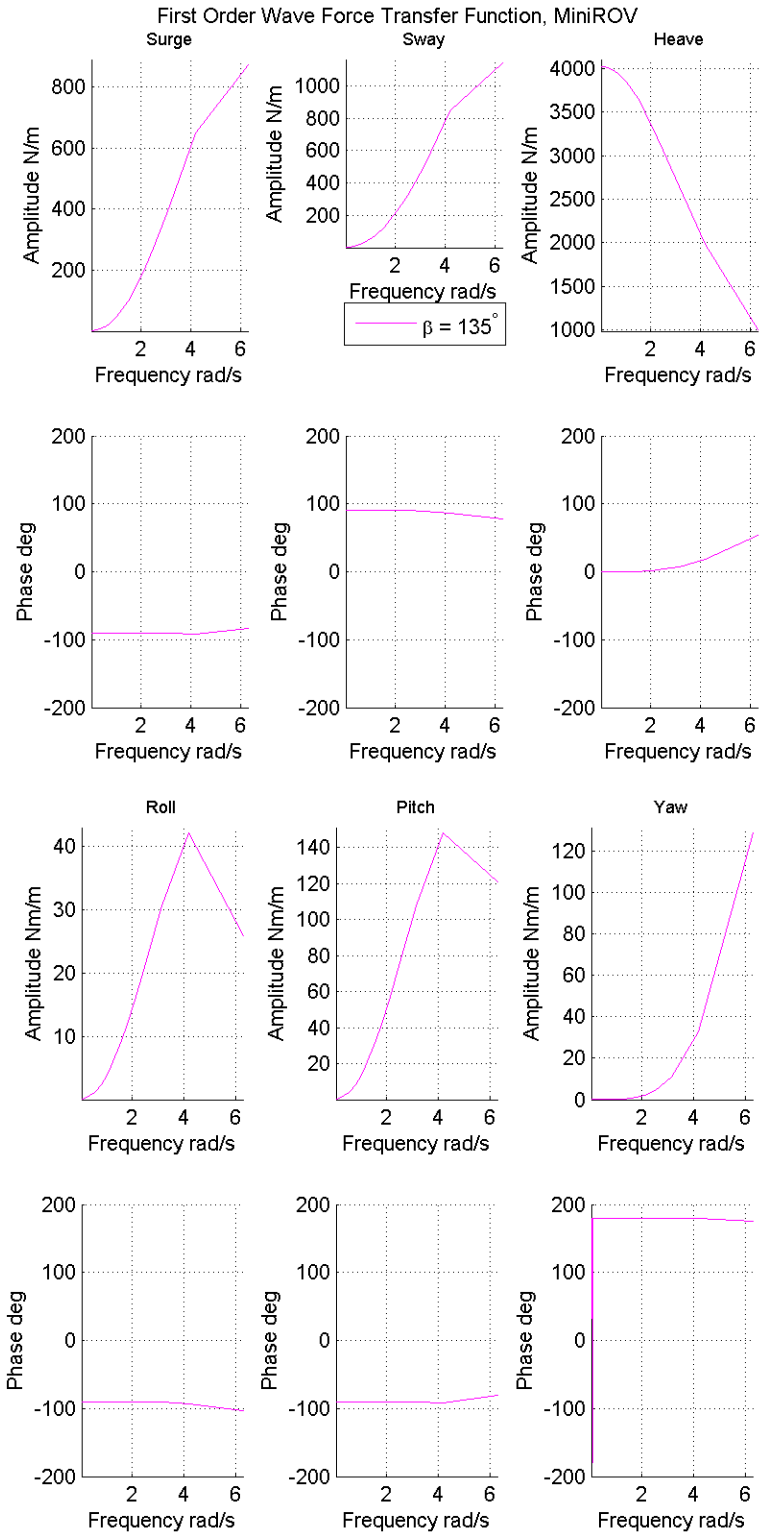

Figure C.8: The first order wave force transfer function for 135 °, MiniROV.

C.2.5 180 °

MidiROV

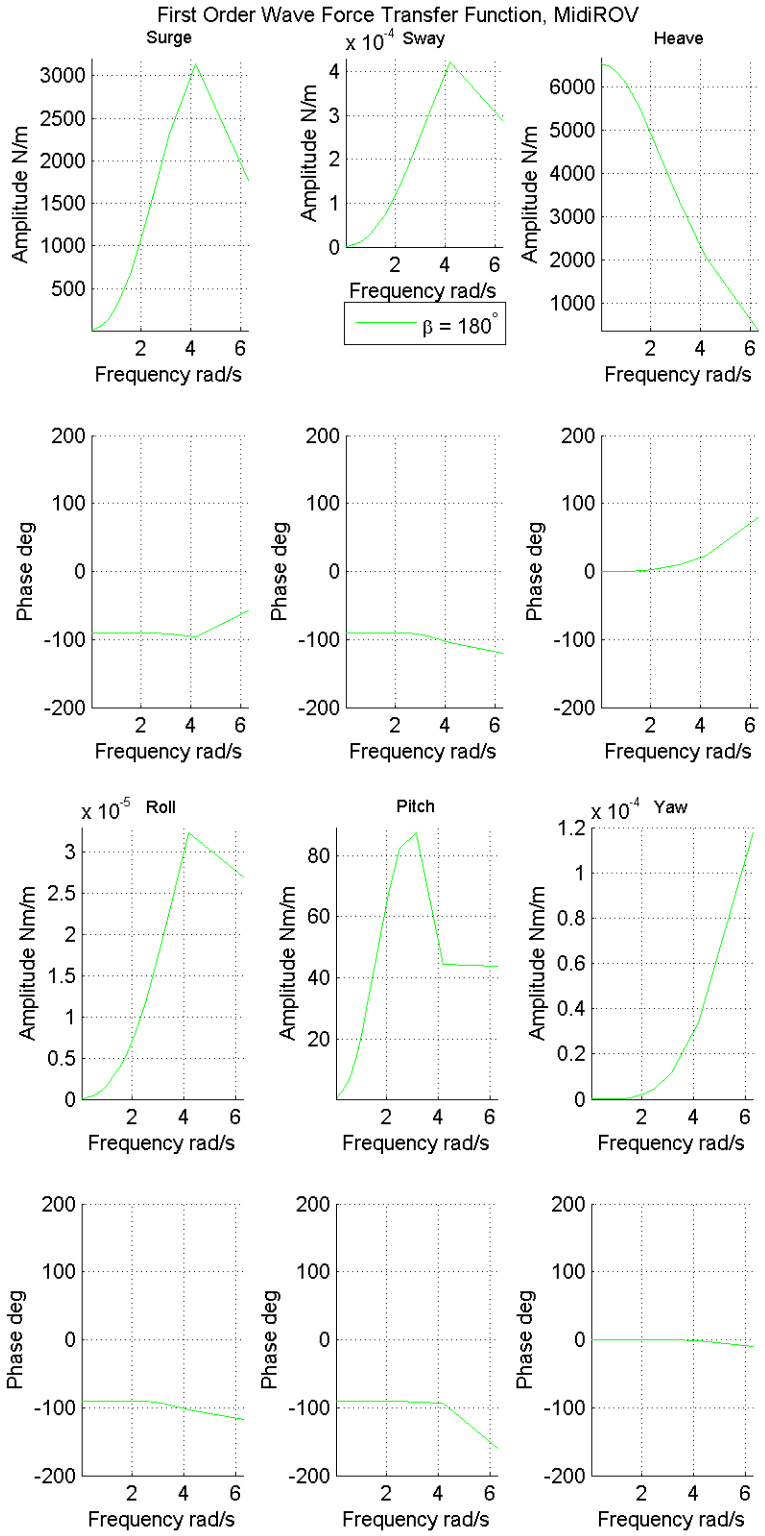

Figure C.9: The first order wave force transfer function for 180 °, MidiROV.

MiniROV

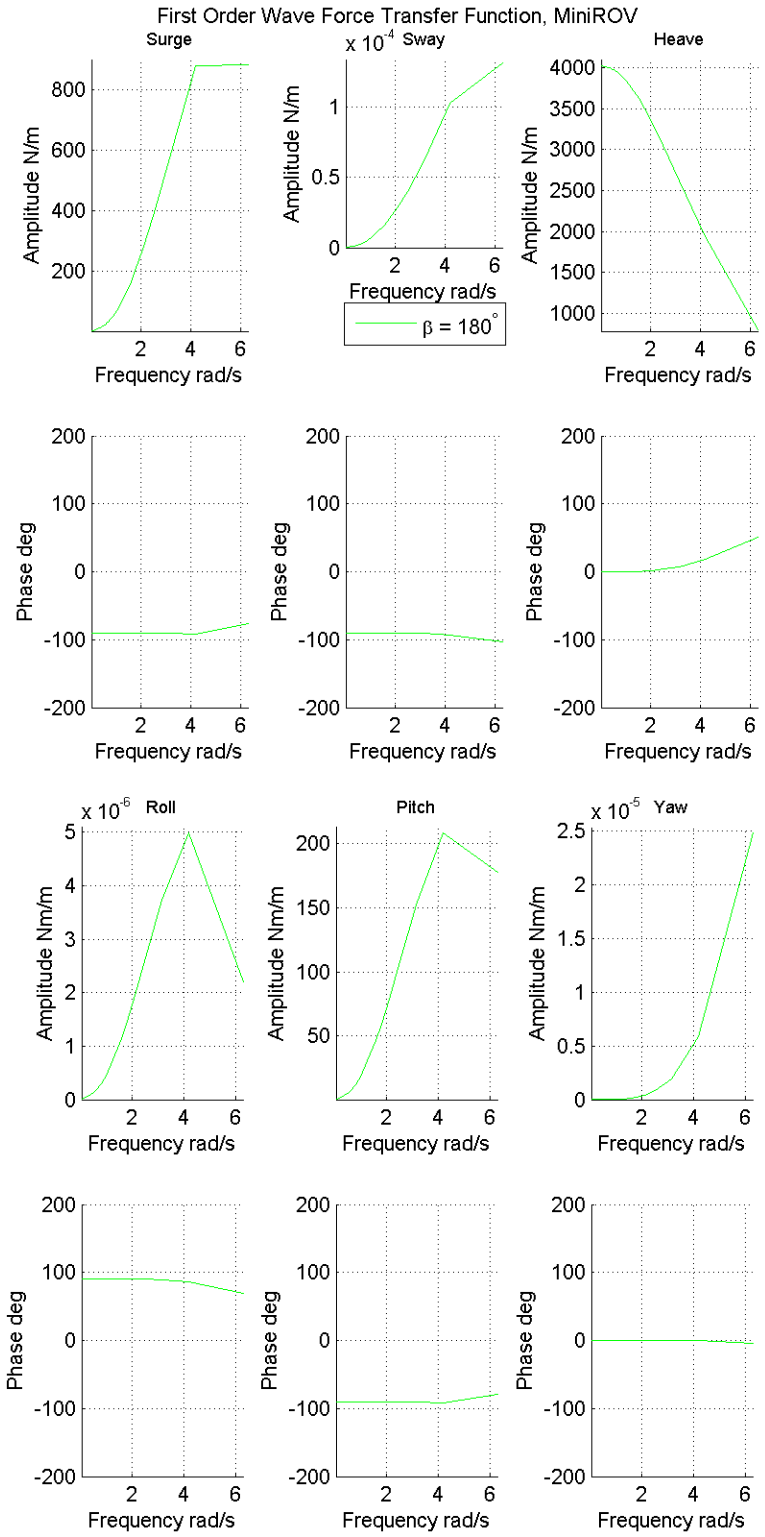

Figure C.10: The first order wave force transfer function for 180 °, MiniROV.

C.3 First Order Motion Transfer Function for MidiROV and MiniROV

C.3.1 0 °

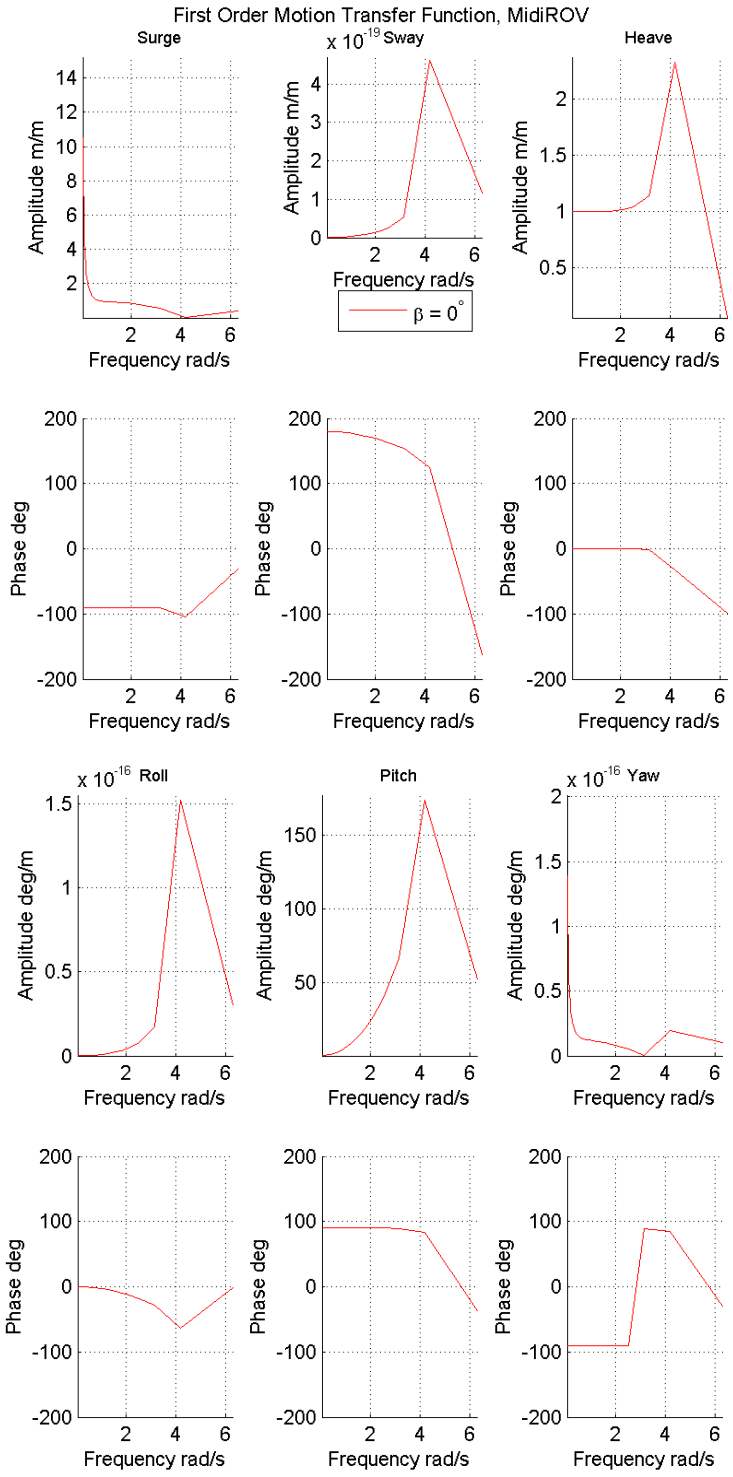

Figure C.11: The first order motion transfer function for 0 °, MidiROV.

MiniROV

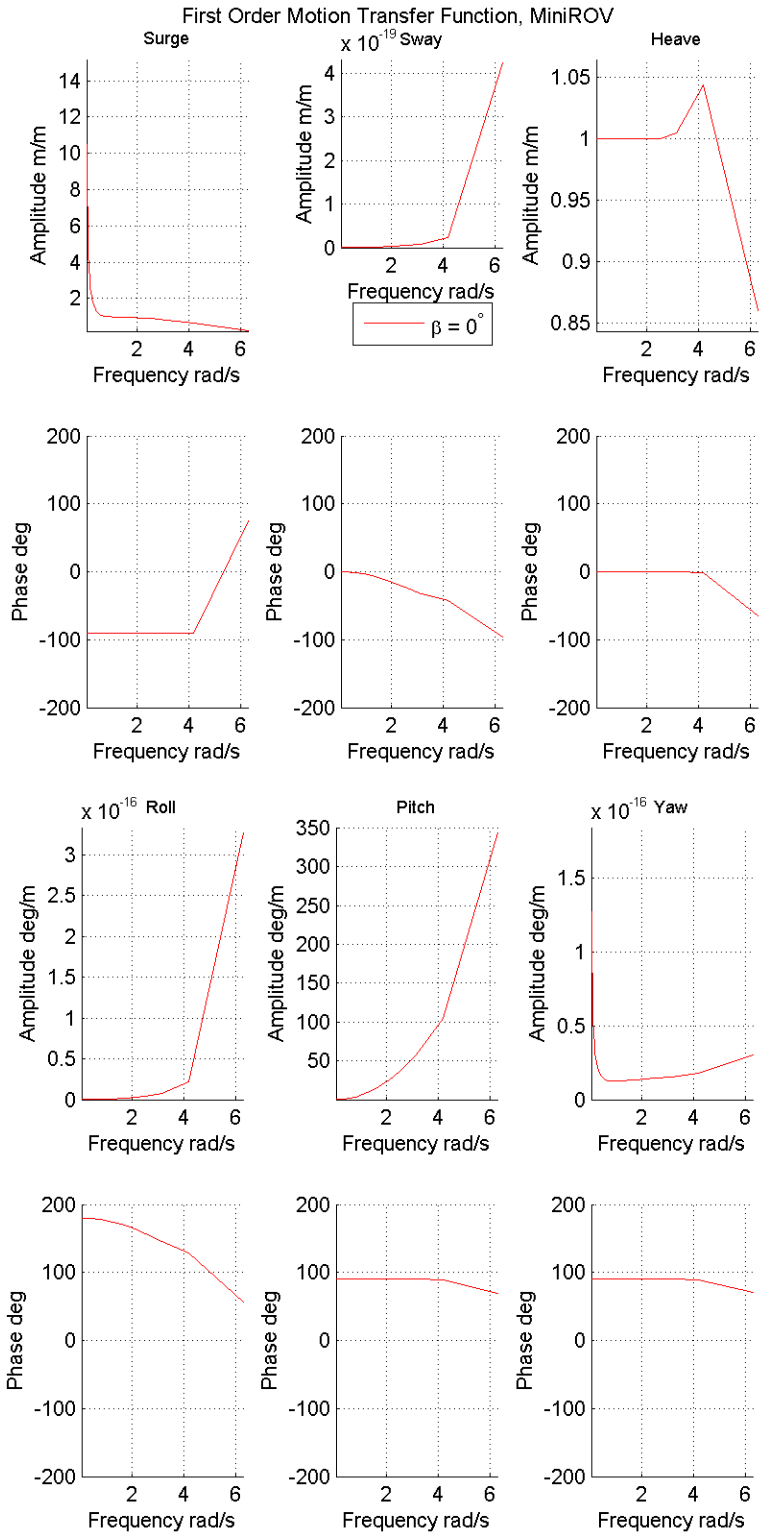

Figure C.12: The first order motion transfer function for 0 °, MiniROV.

C.3.2 45 °

MidiROV

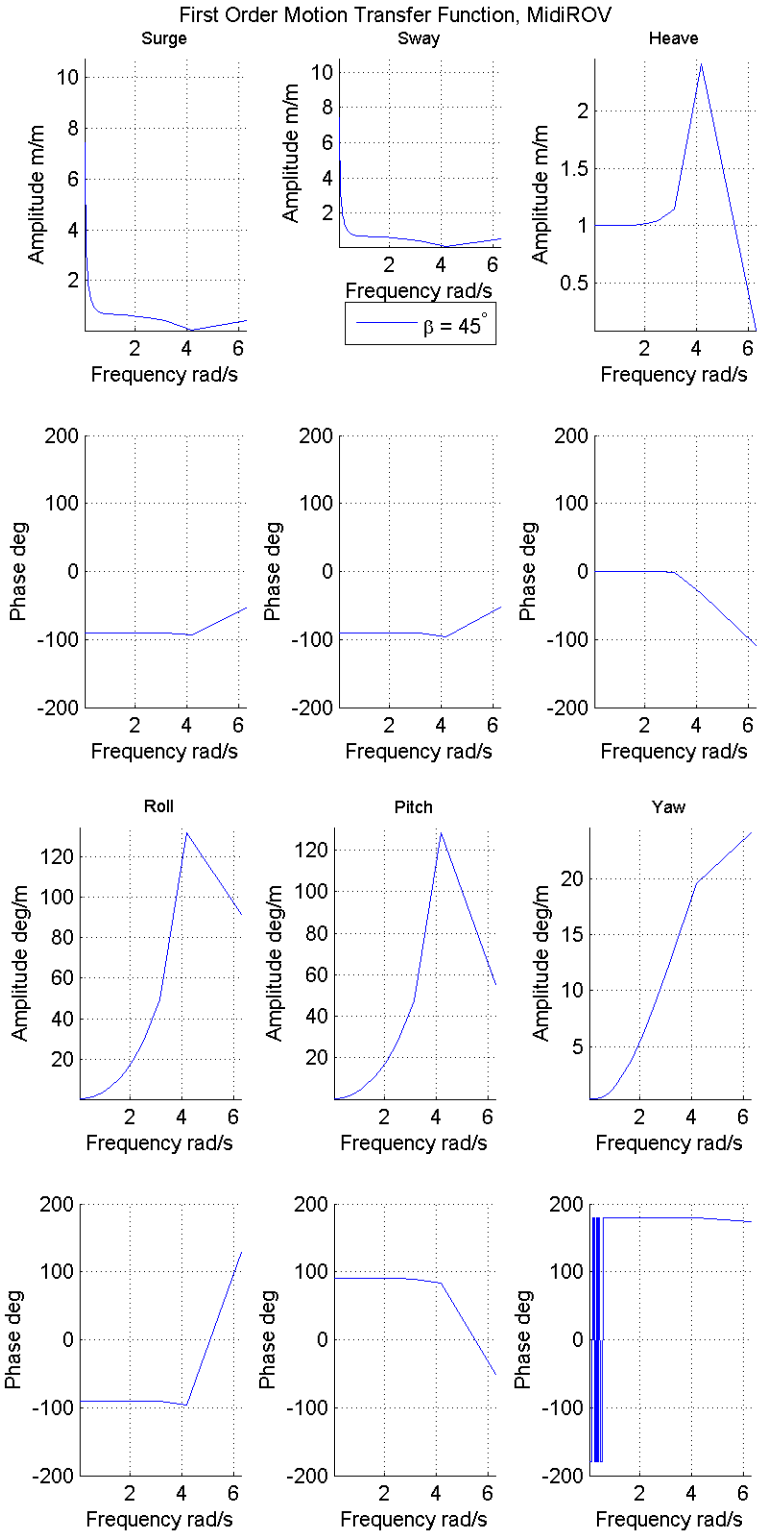

Figure C.13: The first order motion transfer function for 45 °, MidiROV.

MiniROV

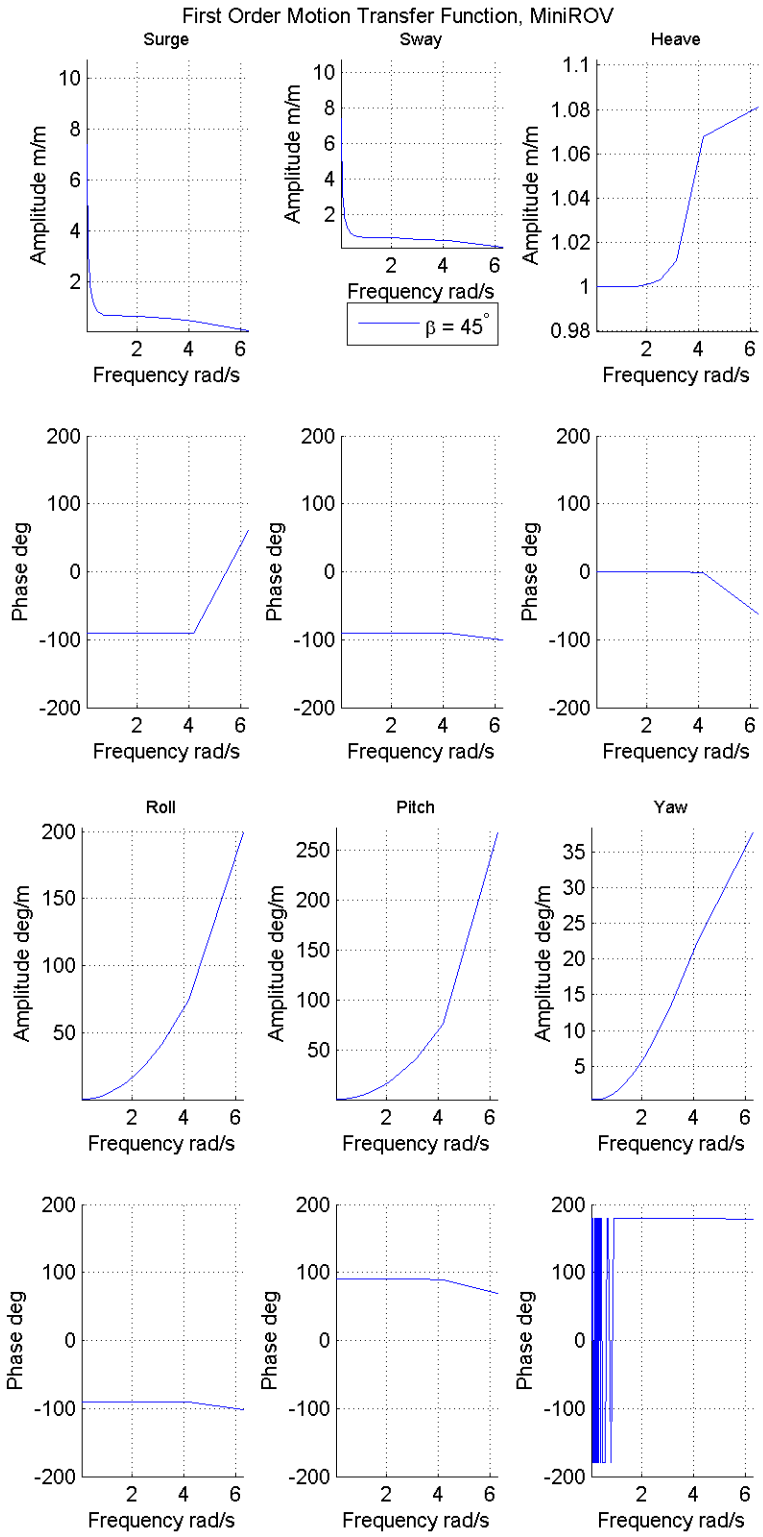

Figure C.14: The first order motion transfer function for 45 °, MiniROV.

C.3.3 90 °

MidiROV

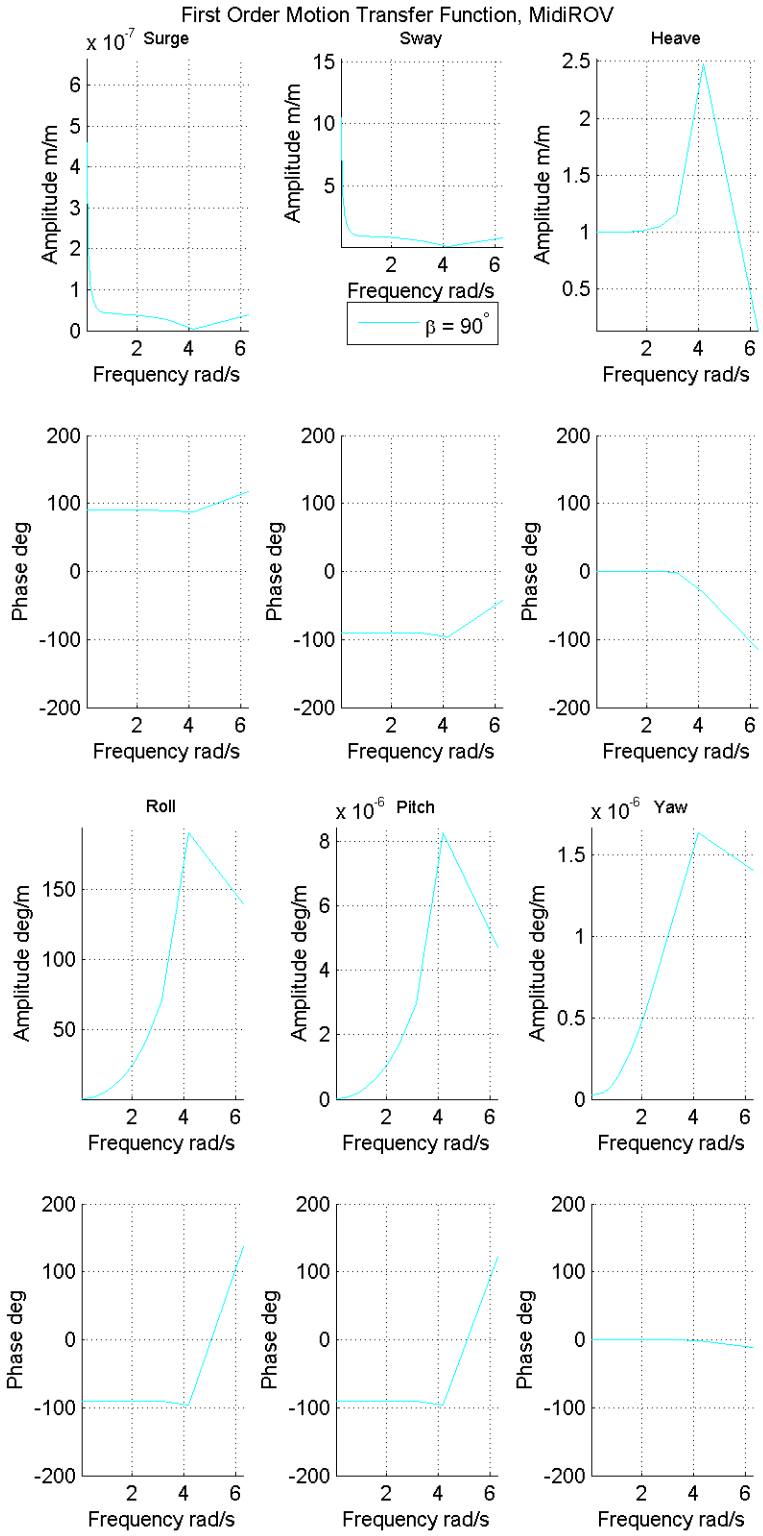

Figure C.15: The first order motion transfer function for 90 °, MidiROV.

MiniROV

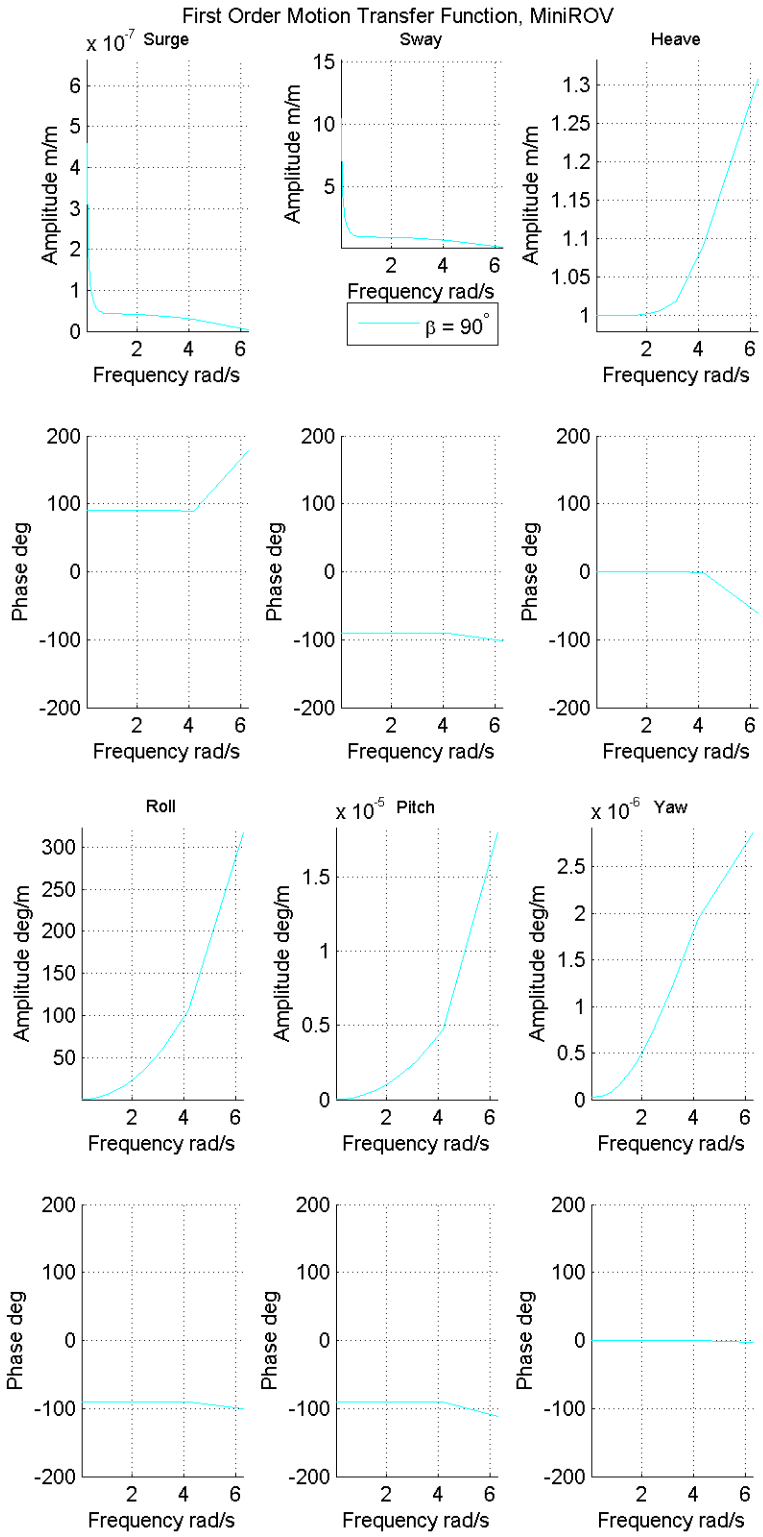

Figure C.16: The first order motion transfer function for 90 °, MiniROV.

C.3.4 135 °

MidiROV

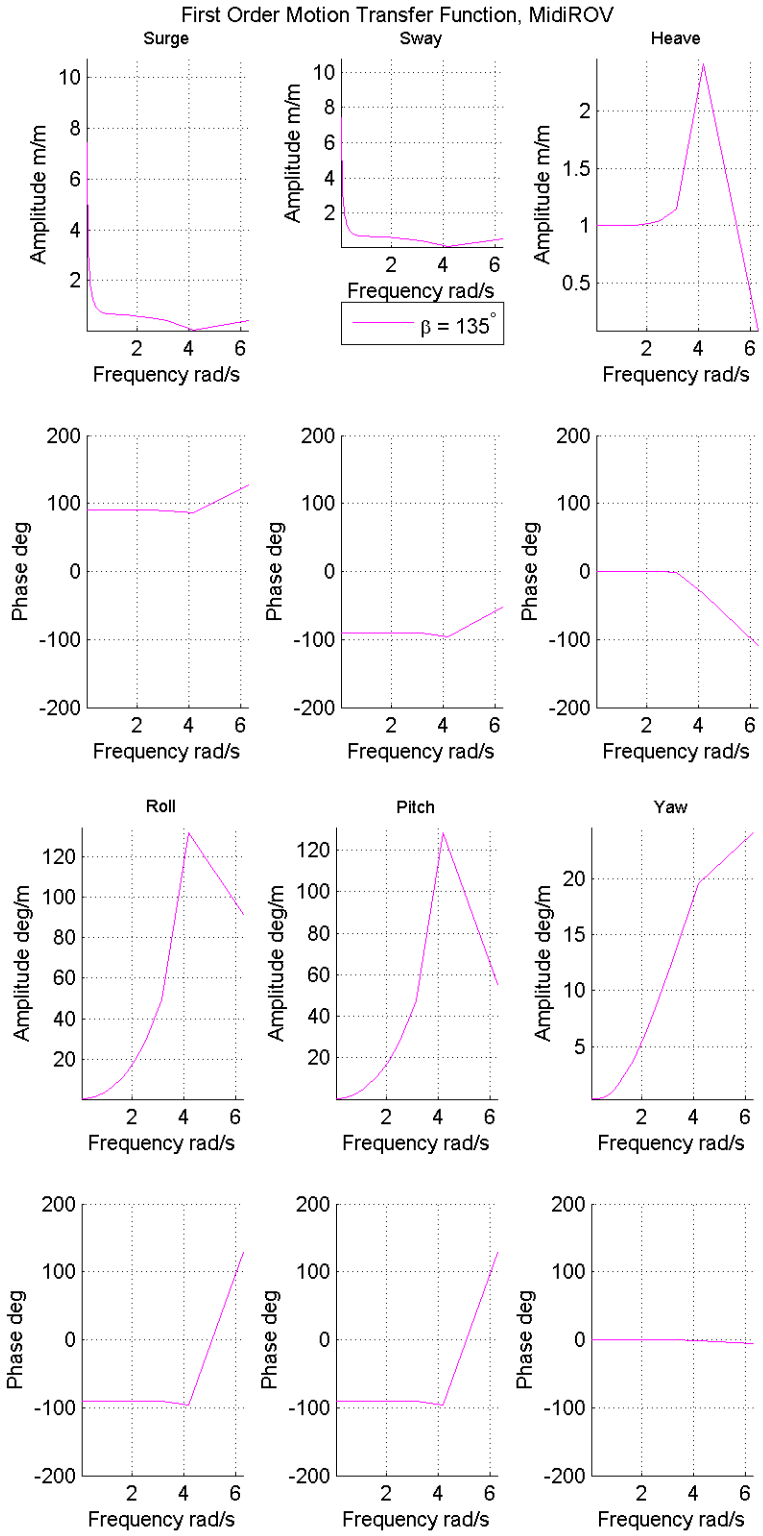

Figure C.17: The first order motion transfer function for 135 °, MidiROV.

MiniROV

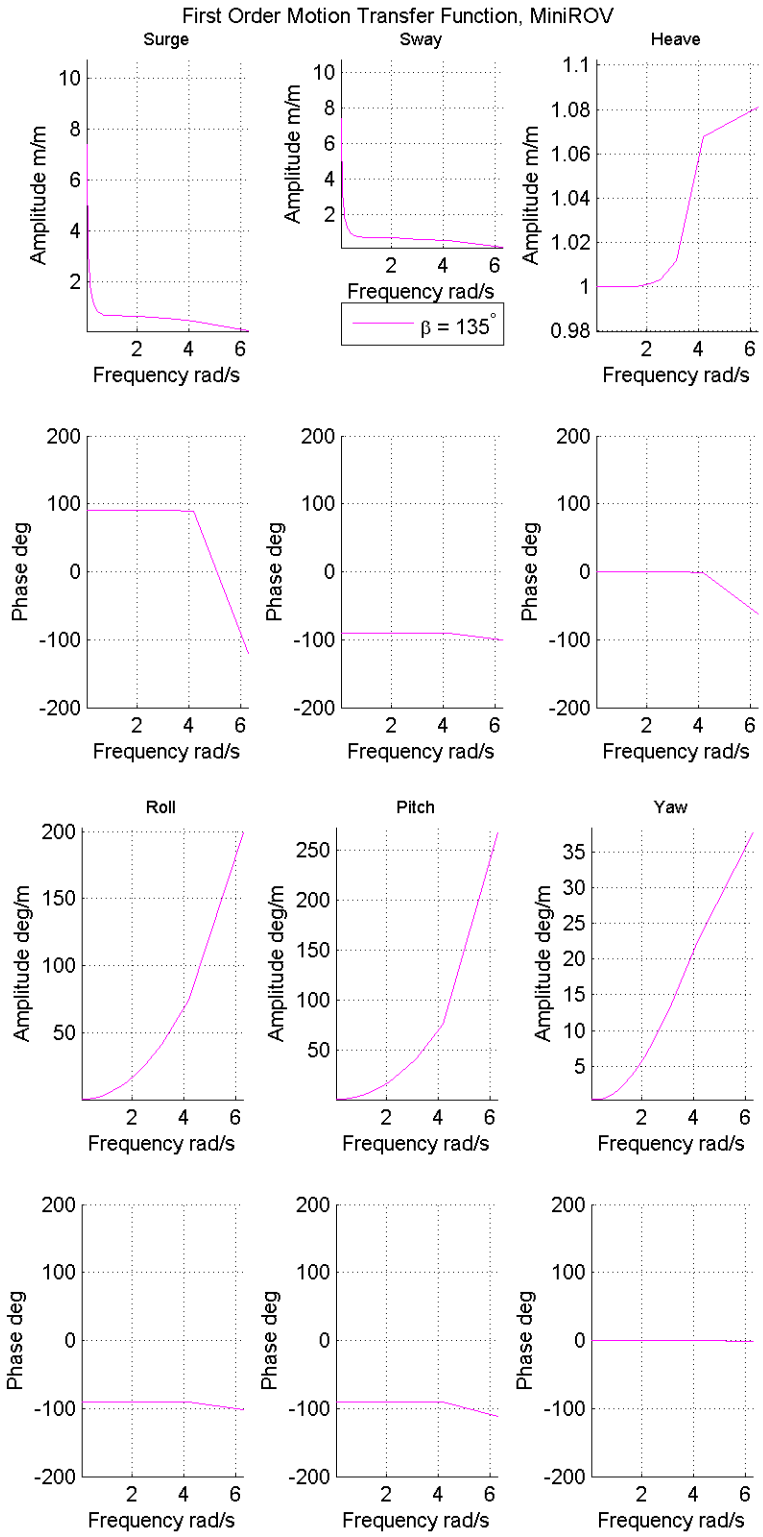

Figure C.18: The first order motion transfer function for 135 °, MiniROV.

C.3.5 180 °

MidiROV

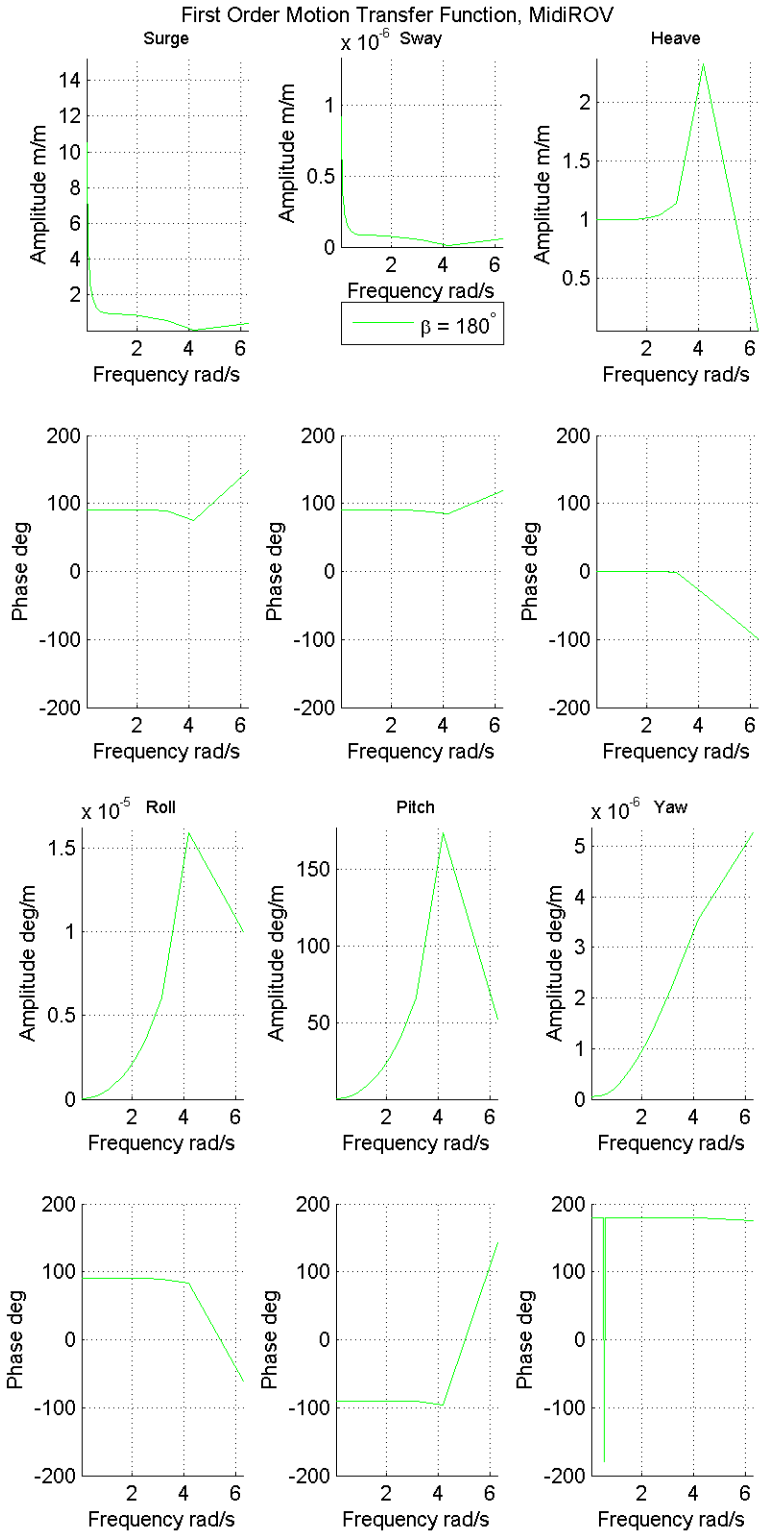

Figure C.19: The first order motion transfer function for 180 °, MidiROV.

MiniROV

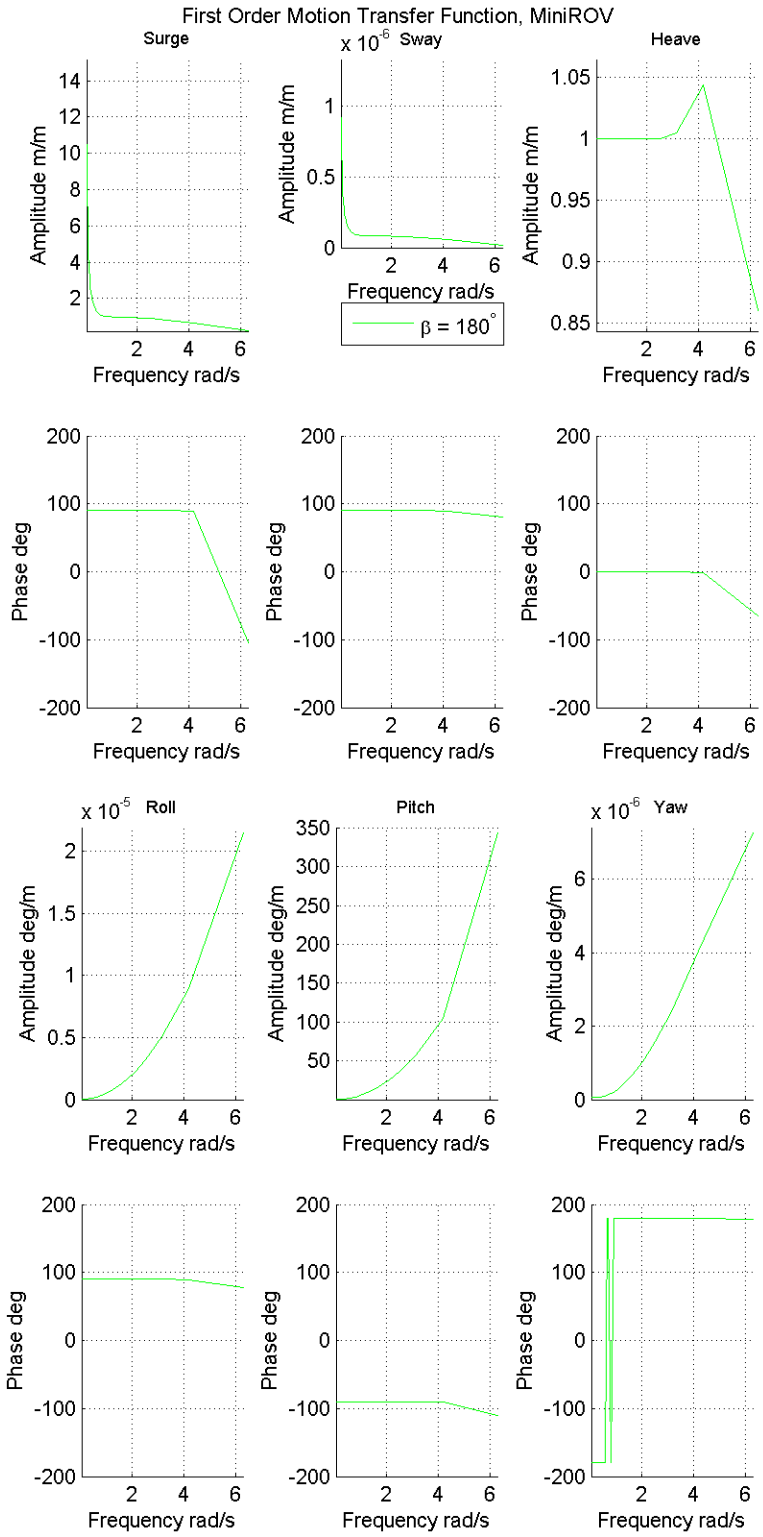

Figure C.20: The first order motion transfer function for 180 °, MiniROV.

Appendix D

SIMO Results

D.1 ROV Position Performance at Depth 20 m

Case 1

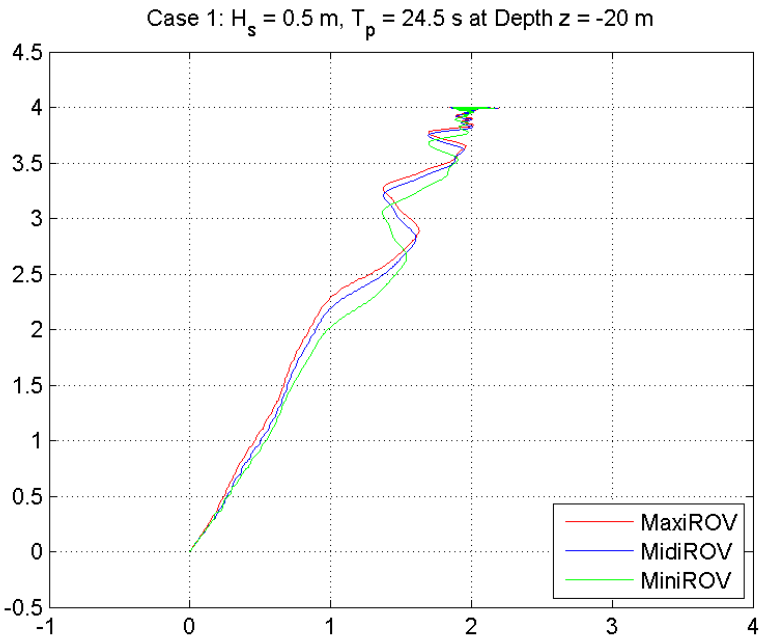

Figure D.1: XY position of ROVs, Case 1 at depth 20 m.

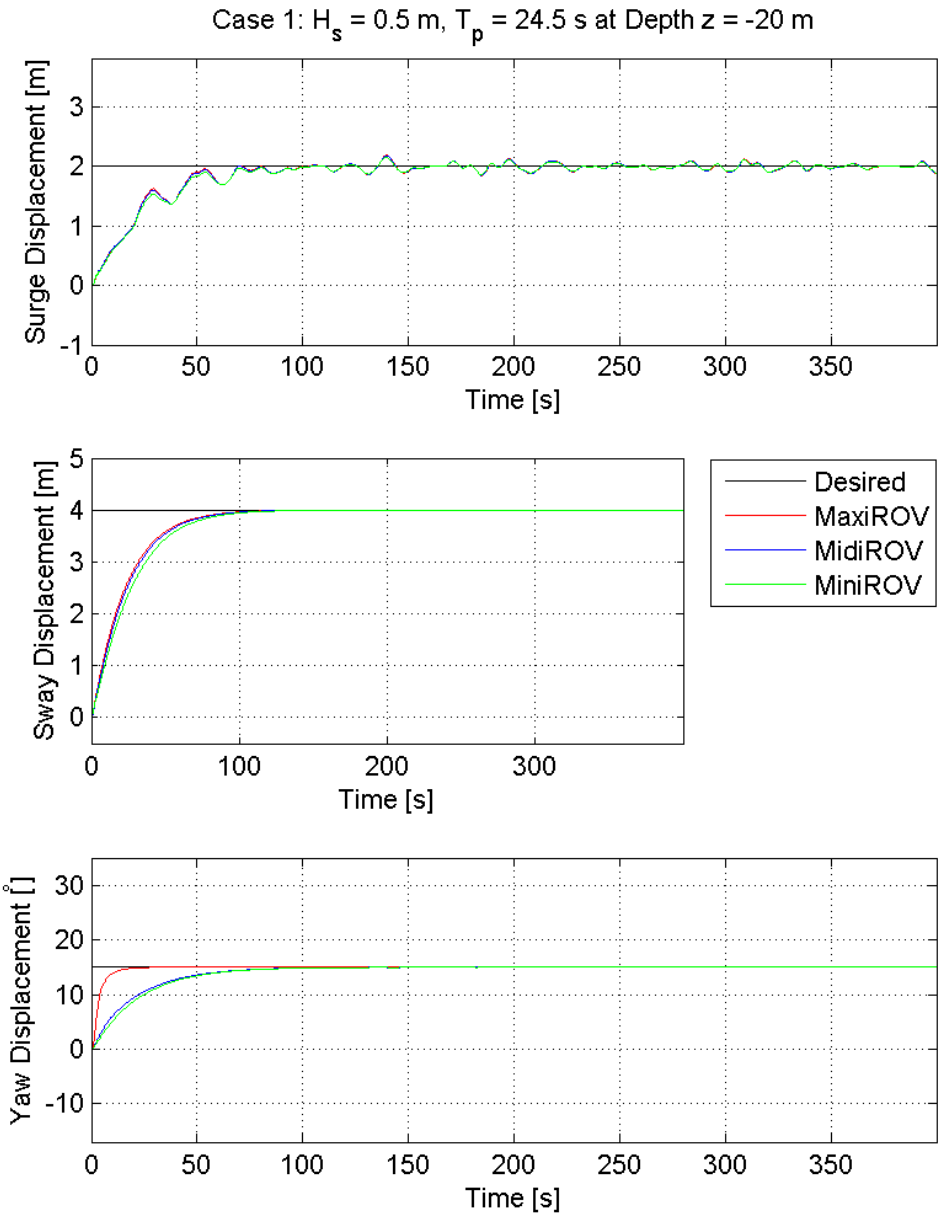

Figure D.2: Position of ROVs, Case 1 at depth 20 m.

Case 2

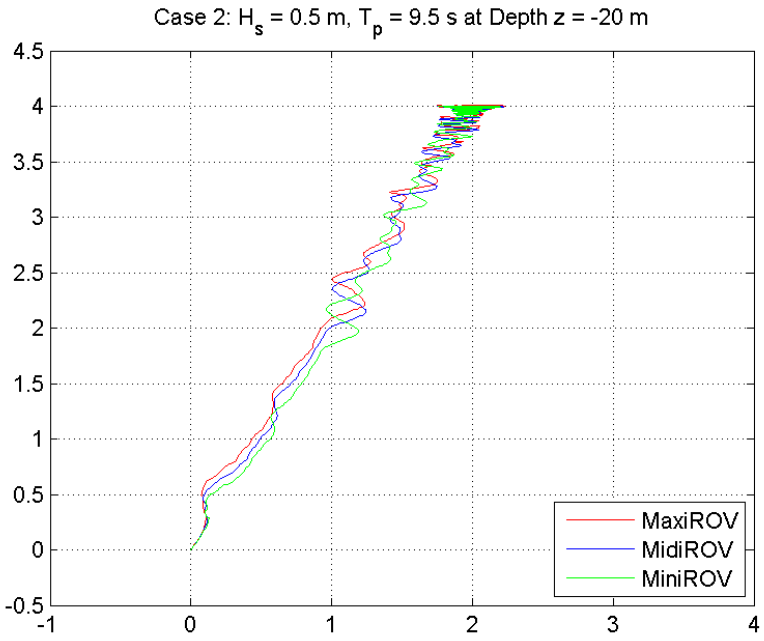

Figure D.3: XY position of ROVs, Case 2 at depth 20 m.

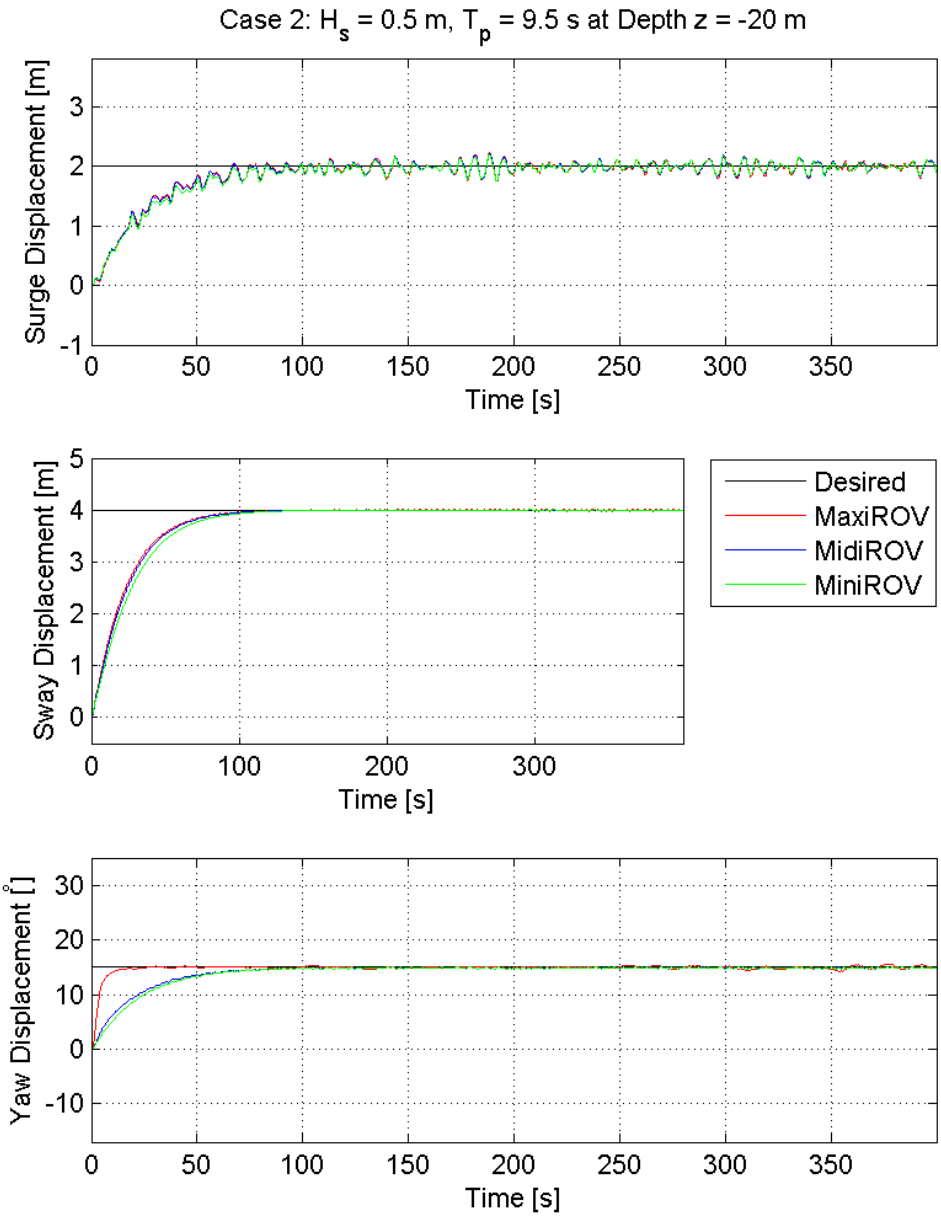

Figure D.4: Position of ROVs, Case 2 at depth 20 m.

Case 3

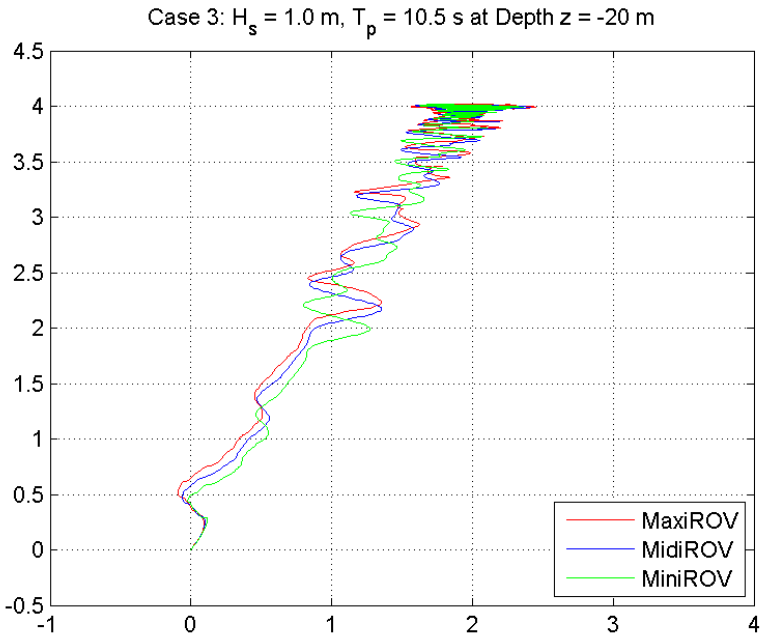

Figure D.5: XY position of ROVs, Case 3 at depth 20 m.

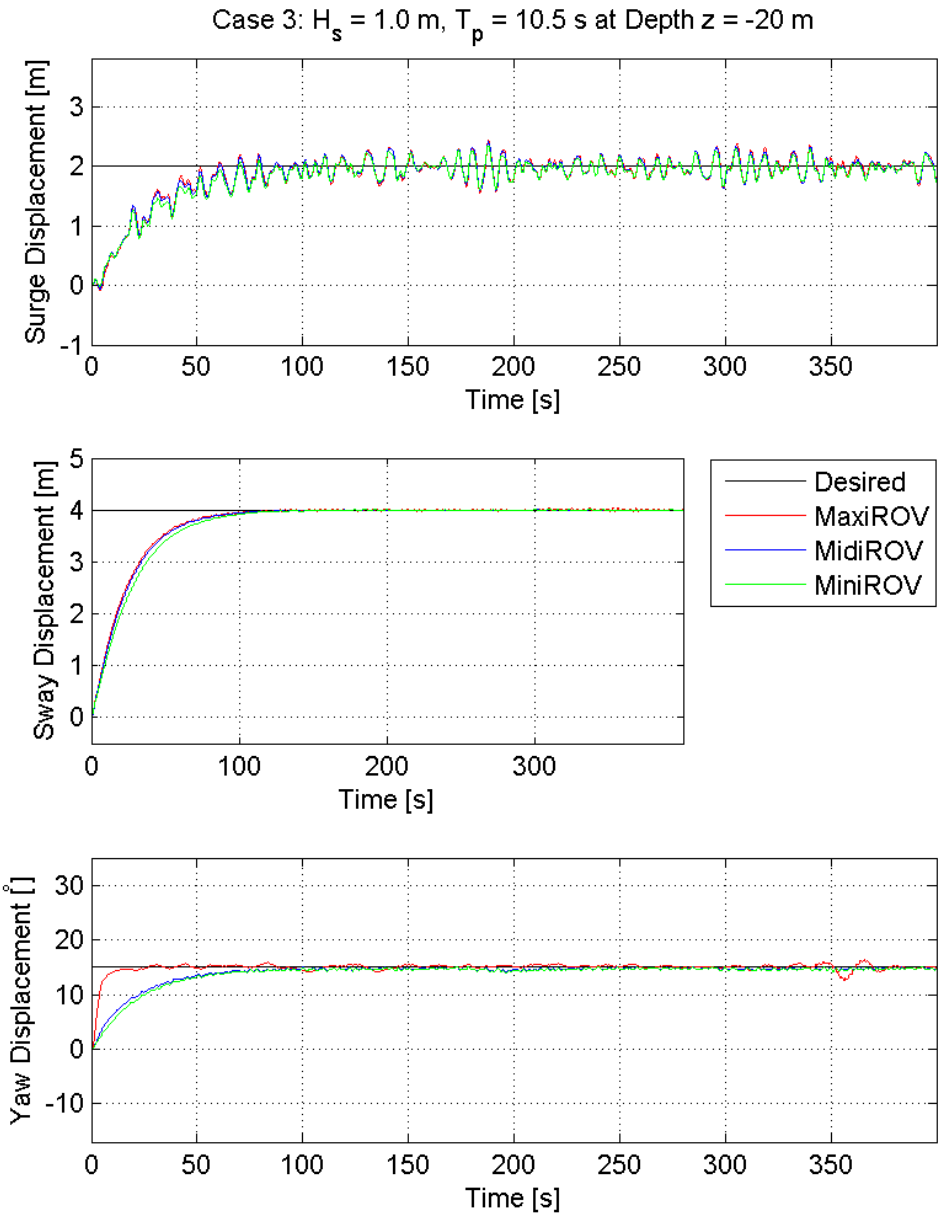

Figure D.6: Position of ROVs, Case 3 at depth 20 m.

Case 4

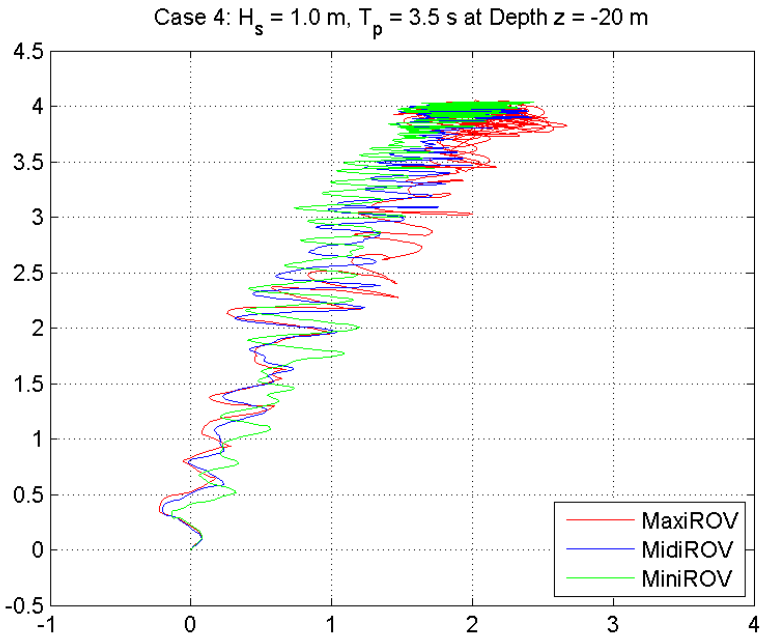

Figure D.7: XY position of ROVs, Case 4 at depth 20 m.

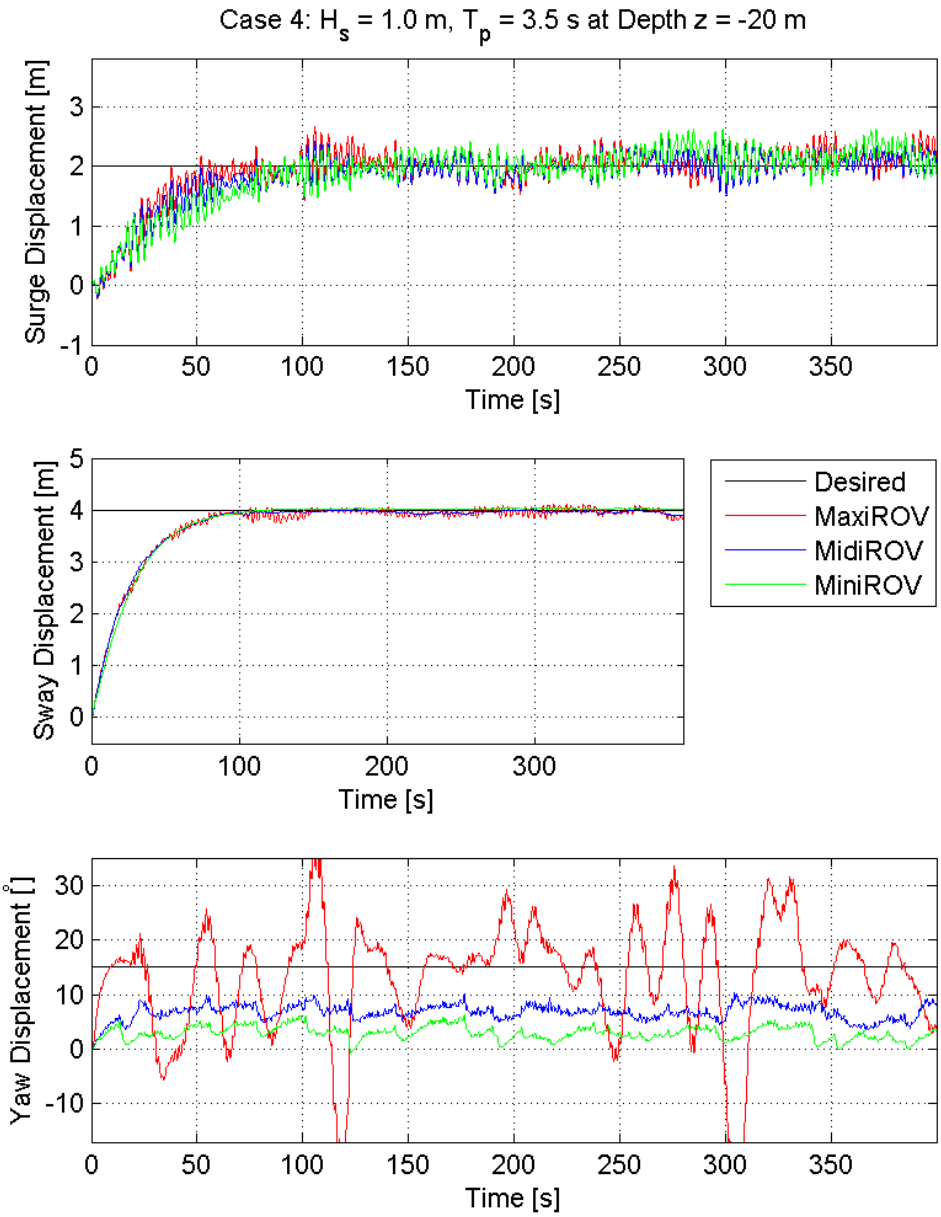

Figure D.8: Position of ROVs, Case 4 at depth 20 m.

Case 5

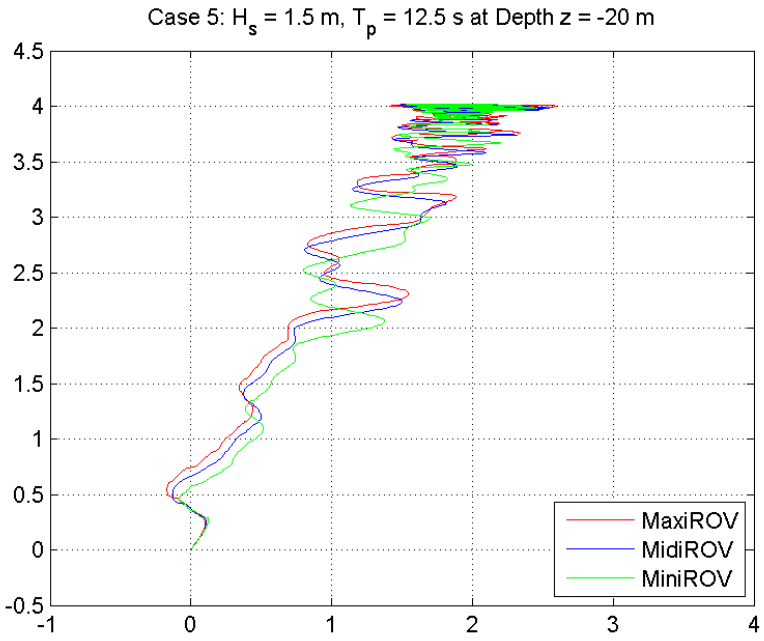

Figure D.9: XY position of ROVs, Case 5 at depth 20 m.

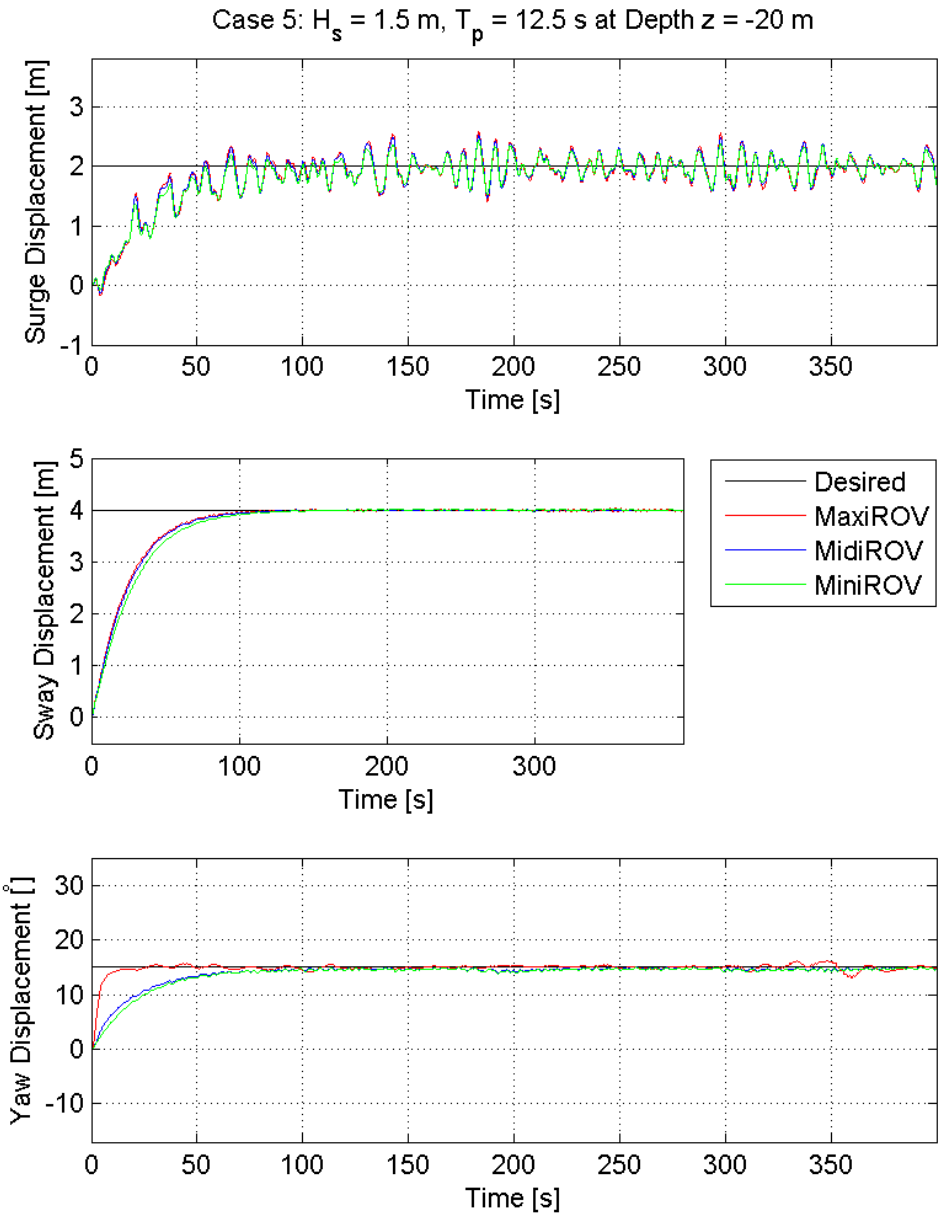

Figure D.10: Position of ROVs, Case 5 at depth 20 m.

Case 6

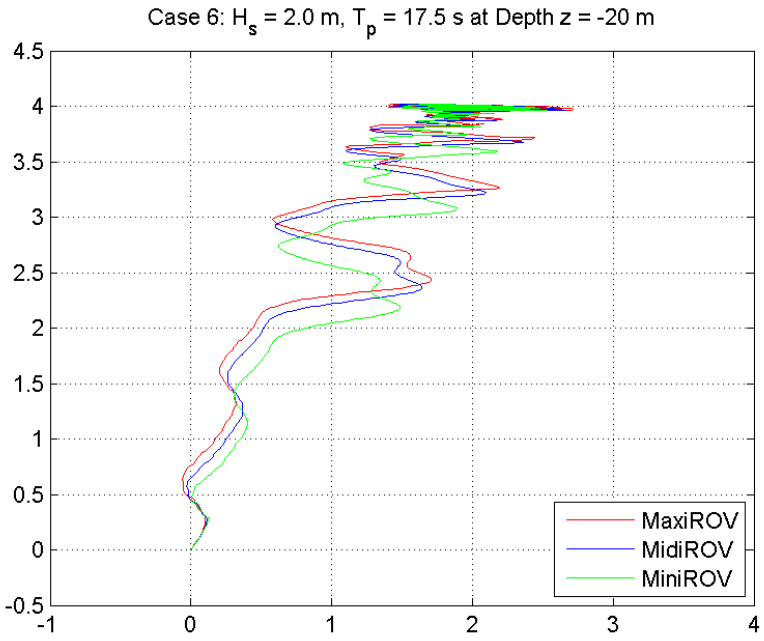

Figure D.11: XY position of ROVs, Case 6 at depth 20 m.

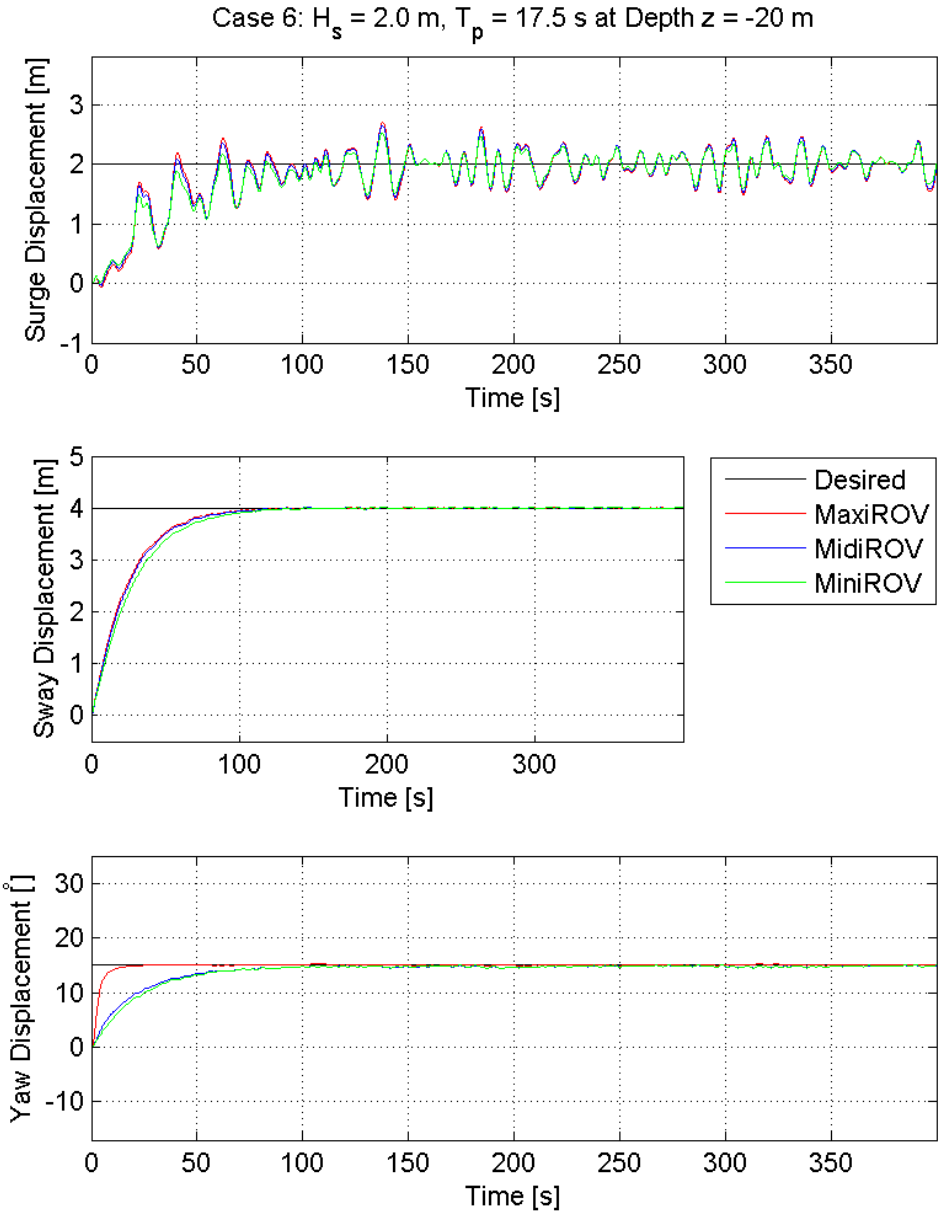

Figure D.12: Position of ROVs, Case 6 at depth 20 m.

Case 7

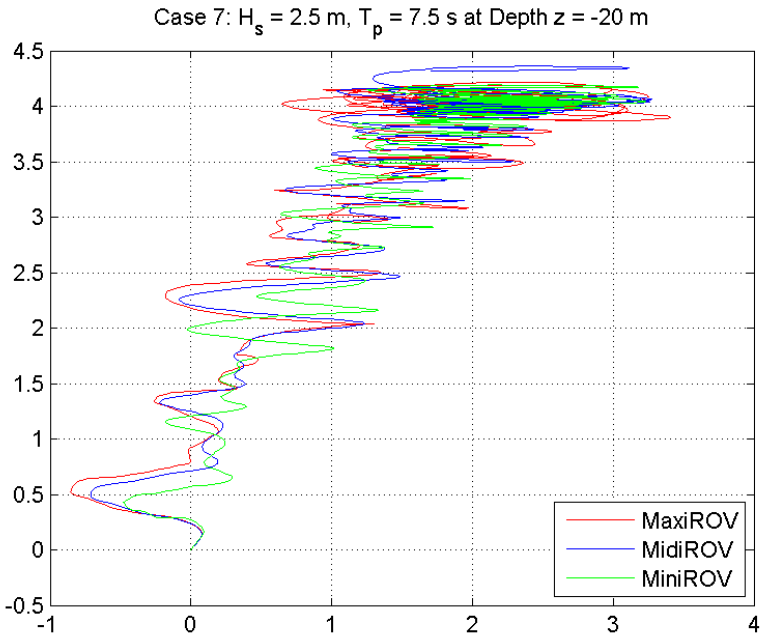

Figure D.13: XY position of ROVs, Case 7 at depth 20 m.

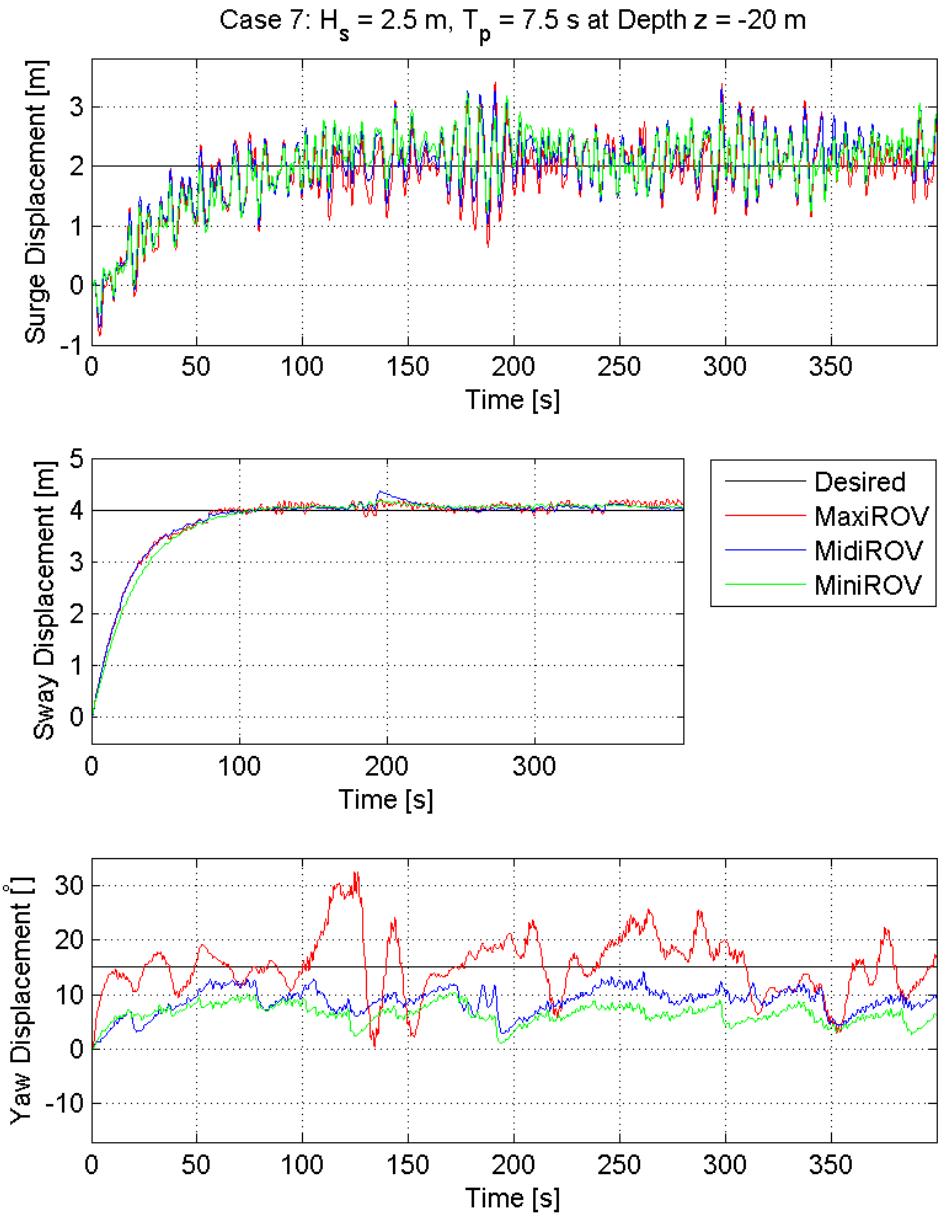

Figure D.14: Position of ROVs, Case 7 at depth 20 m.

Case 8

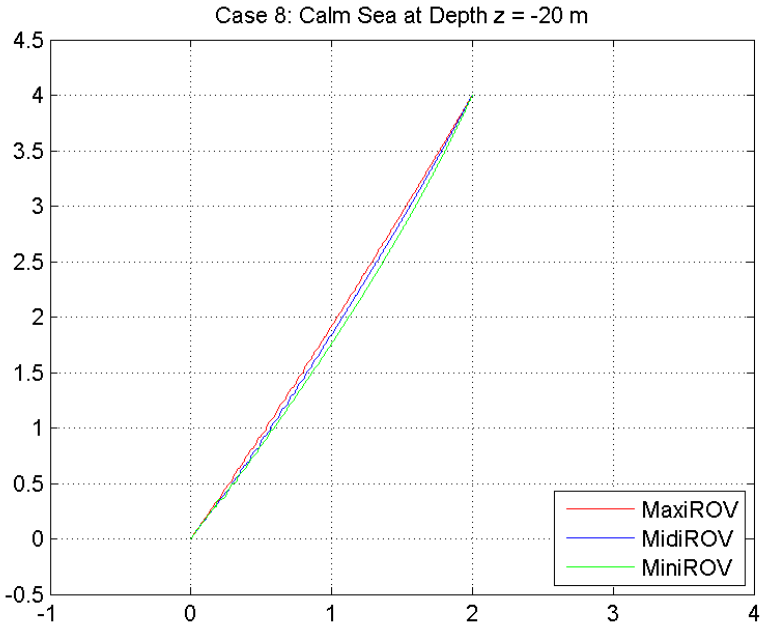

Figure D.15: XY position of ROVs, Case 8 at depth 20 m.

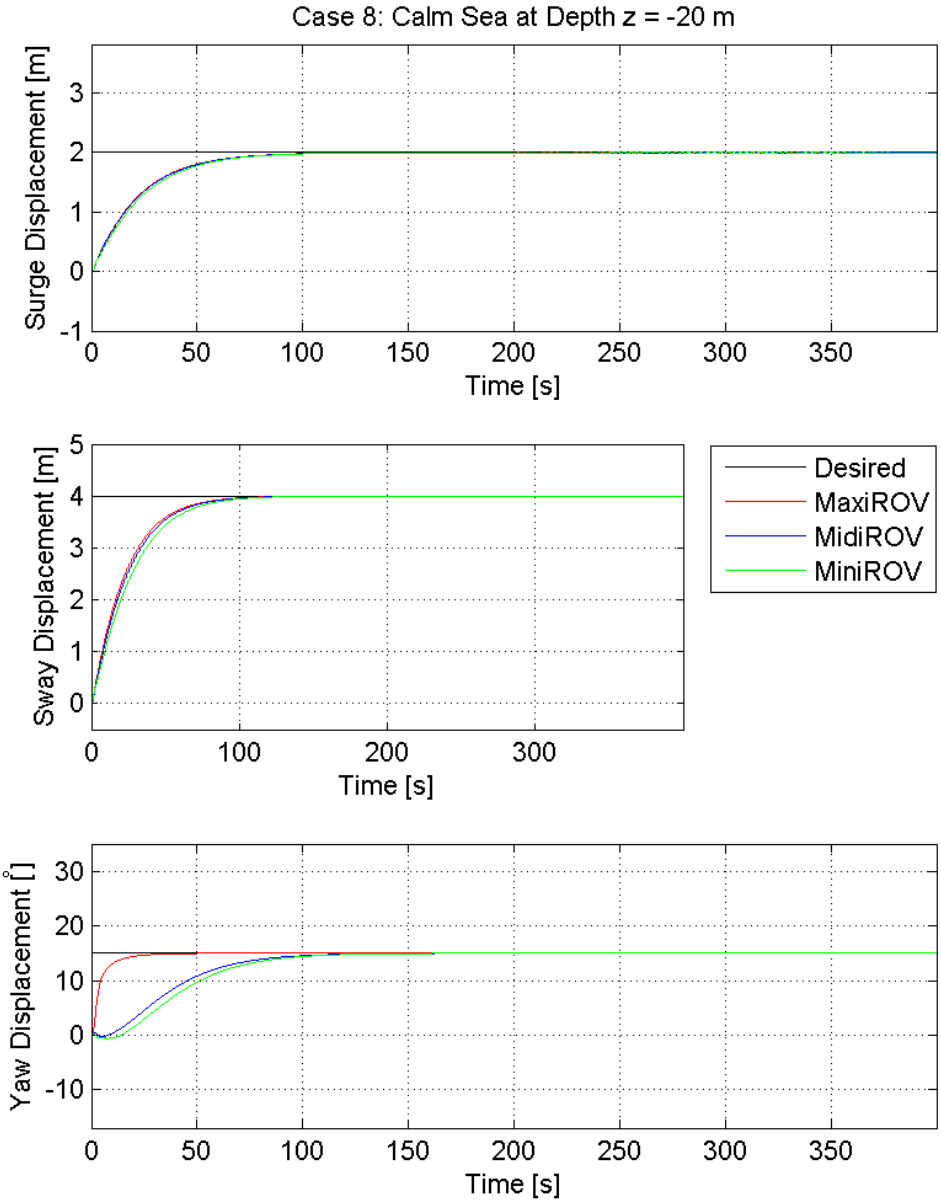

Figure D.16: Position of ROVs, Case 8 at depth 20 m.

Appendix E

Zip File

The appended zip-file includes the following files:

E.1 GeniE Models

MaxiROV.JS

MidiROV.JS

MiniROV.JS

MAXIROVT1.FEM

MIDIROVT1.FEM

MINIROVT1.FEM

E.2 Wadam Analysis Result Files

WADAM1.LIS (Wadam results)

WAMIT_5S.OUT (The results converted in to WAMIT result file)

E.3 SIMO Task

SimulationMaxiMidiMini.stask

sysMaxi.TXT

sysMidi.TXT

sysMini.TXT

E.4 Ecxel Spreadsheets

SeawatchMai-Now2011.xls

Observations.xlsx

Calculations.xlsx

E.5 Matlab

ReadResults.m

ReadResultsStab.m

PlotResults.m

AddedMassandPotDampRet.m

ReadResultsW.m

PlotResultsW.m

mtit.m